DESIGN, SYNTHESIS AND CHARACTERIZATION OF ORTHOGONAL BODIPY TRIMERS AND PROGRESS TOWARDS A SINGLET OXYGEN PROBE

A THESIS SUBMITTED TO

THE GRADUATE SCHOOL OF ENGINEERING AND SCIENCE

OF BILKENT UNIVERSITY

IN PARTIAL FULFILLMENT OF THE REQUIREMENTS FOR

THE DEGREE OF

MASTER OF SCIENCE

IN

CHEMISTRY

By

José Luis Bila

August, 2015

DESIGN, SYNTHESIS AND CHARACTERIZATION OF ORTHOGONAL BODIPY TRIMERS AND PROGRESS TOWARDS A SINGLET OXYGEN PROBE

By José Luis Bila

August, 2015

We certify that we have read this thesis and that in our opinion it is fully adequate, in scope and in quality, as a thesis for the degree of Master of Science.

_____

Prof. Dr. Engin U. Akkaya (Advisor)

_____

Assoc. Prof. Dr. Dönüş Tuncel

_____

Assist. Prof. Dr. Fazlı Sözmen

Approved for the Graduate School of Engineering and Science:

_____

Prof. Dr. Levent Onural

Director of the Graduate School

Abstract

DESIGN, SYNTHESIS AND CHARACTERIZATION OF ORTHOGONAL BODIPY TRIMERS AND PROGRESS TOWARDS A SINGLET OXYGEN PROBE

José Luis Bila

M. Sc. in Department of Chemistry

Supervisor: Prof. Dr. Engin Umut Akkaya

August, 2015

Several methods of fighting cancer have been proposed over the years after it was discovered. Photodynamic therapy (PDT) has been part of these methods for many years therefore; too much financial effort has been spent on this field. Since PDT relays on three important components namely: Sensitizer, molecular oxygen and light, our group has worked and published several photosensitizers derived from BODIPY over the years. In this thesis two different ideas to be used in PDT are introduced. First, Heavy atom free orthogonal BODIPY trimmers are introduced for the first time in literature and they are believed to work according to DS-TR principle. Effective singlet oxygen productions were obtained up to 0.53 quantum yields. The second topic is the use of BODIPY and 1,3-DiphenylIsobenzofuran hybrids as a singlet oxygen sensor. This sensor is meant to work based on PeT and ICT mechanisms. No further experimental methods were applied to this molecule after synthesis however; we intend to use it for in-vivo singlet oxygen experiments in the future.

Keywords: Photodynamic therapy, singlet oxygen sensor, DS-TR, BODIPY trimmers, orthogonal

ÖZET

TRİMER DİK BODIPY YAPILARININ DİZAYN, SENTEZ VE KARAKTERİZASYONU VE SİNGLET OKSİJEN ALGILAYICISININ GELİŞİMİ

José Luis Bila

Bilkent Kimya Bölümü

Danışman: Prof. Dr. Engin Umut Akkaya

Ağustos, 2015

Kanserin keşfinden sonra, kanserle mücadele için bir çok metod geliştirilmiştir. Fotodinamik terapi de bu metodlardan biri olup, bu alanda çok para harcanmıştır. Fotodinamik terapide kullanılan üç ana bileşen vardır: duyarlaştırıcı, moleküler oksijen ve ışık. Araştırma grubumuz da BODIPY tabanlı fotoduyarlaştırıcılar üzerine uzun yıllardır çalışmakta ve bu konuda bir çok yayın çıkarmaktadır. Bu çalışmada, fotodinamik terapide kullanılan iki farklı fikir tanıtılmıştır. Ilk olarak, DS-TR prensibiyle çalışılacağına inanılan, literatürde ilk defa çalışılan, ağır atom bulunmayan trimer dik BODIPY tanıtılmıştır. 0.53 quantum verimine sahip singlet oksijen üretilmiştir. Ikinci konu ise, BODIPY ve 1-3,difenilizobenzofuran hibritlerinin singlet oksijen sensörü olarak kullanılmasıdır. Sentezlenen bu sensör PeT ve ICT mekanizmalarıyla çalışmaktadır. Sensörün sentezi bitmiş olup, henüz ölçüm alınmamıştır, ancak ilerde canlı içinde singlet oksijen deneyleri yapılacaktır.

Anahtar kelimeler: Fotodinamik terapi, singlet oksijen sensor, DS-TR, Trimer BODIPY, Dik BODIPY

Dedicated to my mother…

Acknowledgement

I would like to start by thanking Prof. Dr. Engin U. Akkaya for his patience and guidance throughout my master's degree. I would like to specially thank him for all the positive insights and attitudes both in good and bad times. He has never let me down no matter what, and I believe choosing him, as my adviser was one of the best decisions I have ever made because he is one of a kind.

Secondly, I would like to direct a million thanks to Dr. Tuğba Özdemir Kütük for being my older sister, partner and guide in almost everything. I have worked with her most of the time and in almost every project I was involved she was there to carry the burden with me. I sincerely have no words to express the amount of love and gratitude I will always carry towards her.

I thank in particular my closest friends Ceren Çamur, Darika Okeeva, Tuğçe Durgut, Tuğçe Karataş, Melek Baydar Baytak, Hidayet Baytak, Dielse Inroga and Cansu Kaya, Muazzam Idris for being there when I needed them, in every birthday celebration, every unnecessary çiğköfte meal, marriage proposal and especially for their priceless friendship and invaluable love. I thank Ceren Çamur, Darika Okeeva, Dr. Fazlı Sözmen, Dr. Safacan Kölemen, Seray Ural and Bilal Uyar for working with me in other projects, which helped me learn new topics and synthetic methods in chemistry.

I would like to thank every other member of the supramolecular chemistry research group: Nisa Yeşilgül, Dr. Dilek Taşgın, Ahmet Atılgan, Veli Polat, Bilal Kılıç, Dr. Ruslan Guliyev, Deniz Yıldız, Özlem Seven, Dr. İlke Şimşek and Seylan Ayan.

I would like to express my deepest love to my family, Luis Bila and Ana Chirrizane for bringing me to the world and for taking care of my siblings and I, in every step and way they could. They struggled to watch me grow and study. I wish they were still in this world to share this happiness with me. I would like to thank my aunt Beatriz Bila for her support in most of the time of my life. She has been the mother and father I always needed. I also thank my high school teacher and friend Bahattin Akar for his financial and moral support in every step of the way to the university.

No words are there to express the deep love and gratitude I have for my fiancée, Hale Atılgan for being in every single moment of my life and academic career. We watched each other grow and she supported and guided me in every decision I took. With her I shared every dream, every hope, sorrow and the smallest burden. All I can say is: I love you with all my heart and I hope you will always be in my life until the end of the road.

LIST OF ABBREVIATIONS

AcOH	:	Acetic Acid
DCM	:	Dichloromethane
$CHCl_3$	:	Chloroform
BODIPY	:	4,4-difluoro-4-bora-3a,4a-diaza-s-indacene
DS-TR	:	Doubly substituted tetra radicalic
HOMO	:	Highest Occupied Molecular Orbital
ICT	:	Internal Charge Transfer
LUMO	:	Lowest Unoccupied Molecular Orbital
MS	:	Mass Spectroscopy
NMR	:	Nuclear Magnetic Resonance
PDT	:	Photodynamic Therapy
PET	:	Photoinduced Electron Transfer
TFA	:	Trifluoroacetic Acid
TLC	:	Thin Layer Chromotography

TABLE OF CONTENTS

LIST OF FIGURES

CHAPTER 1

1. INTRODUCTION

There are more than 100 diseases known as cancer and what these diseases have in common is their origin; all cancers are known to start due to abnormal growth of cells.[1] A normal body consists of billions and trillions of cells that grow, multiply and die each and every second in order to repair injuries. However, in an abnormal body the growth and multiplication of the cells is not controlled and instead of dying these cells continue to grow as abnormal cells invading other tissues.[2] Moreover, sometimes there is damage in the DNA (deoxyribonucleic acid) and normal cells either repair it or die but since cancer cells are not able to that there is a risk of inheriting such damages. Therefore, cancer is probably one of the most life threatening and challenging diseases the world has ever seen. The number of people carrying cancer is expected to increase in the upcoming years so, by then several treatments and diagnostic methods must be available in order to replace the nowadays-available methods (Chemotherapy and Radiotherapy) since they are very invasive and have several side effects. [3]

As mentioned above, conventional cancer treatment methods such as Chemotherapy and Radiotherapy are very well known and mostly applied all over the world however, other methods such as; Stem cell transplant, Surgery, Immunotherapy and Hormone therapy are also known. The greatest challenge with most of them is the number of side effects they carry and the great discomfort they might cause to the patients while they are being used. That is why organic chemists and biochemists play an important role on the design and synthesis of molecules that are selective towards cancer cells in order to kill or diagnose them.[4–6] Besides, Photodynamic Therapy is probably one of the best candidates for the selective treatment of

malignant cancers such as; gastrointestinal, head and neck, skin and gynecological cancers, premalignant cancers such as; actinic keratosis and non-malignant cancers such as; psoriasis, AMD-age related macular generation.[7]

In this cancer cell killing crusade, BODIPY (4,4-diflouro-4-bora-3a,4a-diaza-s-indacene) dyes have shown great promise due to their high fluorescence quantum yields and absorption coefficients, easy functionalization and synthesis and tunable absorption/fluorescence peaks. Because of the rich BODIPY chemistry, we are able to design and synthesize orthogonal BODIPY molecules and in chapter 4 we have shown three orthogonally mixed BODIPY molecule synthesis to be used on Photodynamic Therapy. The most important issue in Photodynamic Therapy is the sensitizer chosen because it must have low toxicity in the absorbance of light among other properties. Moreover, high triplet quantum yields are desired therefore the design is critical. [8–11]

In Chapter 5 we will focus on the diagnostics of the singlet oxygen production for Photodynamic Therapy. Knowing whether the singlet oxygen is being produced at the presumed rates or not required several instruments however, it is now possible to determine that with a single experiment. Two designs are presented in this chapter with different working mechanisms; Photo-induced electron transfer (PET) and Photo-induced Internal Charge Transfer (ICT). So, depending on the system performed by each designed molecule the system can switch from fluorescent OFF to ON or *vice versa* or we can expect a color change of sort.

In chapter 4 we will introduce the orthogonal BODIPY molecules synthesized for the first time by our group and they are able to provide an Inter-system Crossing smoothly without incorporating heavy atoms. A similar working concept was introduced by our group where it was named doubly substituted tetra radical state (DS-TR) of S_1 which was also shown to have a strong correlation with $S_1 - T_1$ Inter-system crossing to yield singlet oxygen ($^1O_2$).[12] The detailed studies from literature and the problem with heavy atoms will be explained in more details in the coming chapters of this thesis.

CHAPTER 2

2. BACKGROUND INFORMATION

2.1 Sensors

Any device that yields an output that can be measured by interaction of matter or energy is called *sensor*.[13] Only until the beginning of the nineties that microscopic devices were considered sensors for instance, thermometer and pH electrodes. Due to the development of technology but specially nanotechnology a new page was open to properly designed molecules to be suitable candidates for sensing purposes. Therefore, nowadays we are able to design molecular sensors; they can signal a physical output upon interaction with an analyte. A molecular sensor basically is designed to have a selective interaction with the analyte which will form a measurable type of energy that can be detected with any conventional spectroscopic technique such as UV-visible, Fluorescence or electrochemical methods such as cyclic voltammetry. The vast use of optical sensors (UV-vis, Flourescence) lies in the fact that they are cheap and easy to use. For example, calorimetric sensor involves a color change due to a shift in absorbance when interacted with an analyte. Another example is the use of fluorescence spectroscopy, which senses analyte concentrations with a fluorescent signal transduction. Usually, this type of instruments work based on photophysical mechanisms that include Photo-induced electron transfer (PET), excimer or exciplex formation, Photo-induced charge transfer (PCT), aggregation-induced emission (AIE) and Förster resonance energy transfer (FRET). Some of these mechanisms shall be discussed in the upcoming chapters.[14]

While designing molecular sensors, three different approaches can be implemented, first binding site-signaling subunit, second displacement approach and chemodosimeter designs. In order for the first design to work, the molecular sensor should contain covalently bonded binding site(s) that are selective to an analyte and this binding site should be able to trigger an electronic modulation in the optical

signaling unit in terms of fluorescence emission change. As of the second approach, there shall be non-covalent interactions between the binding site and the signaling sites. There is a destruction of the molecular ensemble upon binding of analyte, which causes a displacement of the binding moiety yielding a detectable optical change. In the chemodosimeter designs there is a reaction on the molecular probe with specific analytes for instance a cation or anion that causes fluorescence alterations. This type of design usually results in an irreversible bond formation or breaking. [15]

The design of Fluorescent molecular sensors became an attractive field after Tsiesn's Ca^{2+} probe in 1980 and was followed by several other studies worldwide. Applications such as real time imaging of biological systems/processes and medical diagnosis are very well know for fluorescent molecules. A molecular level understanding of processes in living organisms and their environment is extremely important since the detection of the rich array of analytes in these organisms is a great challenge but at the same time an opportunity for researchers to investigate biological systems *in vivo* and for biological disgnostic instrumentation development.[16–18]

2.2 Fluorescence

When a molecule absorbs light, depending on it energy electrons from singlet ground state level S_0 are elevated to an excited state S_n. On its return, the electron follows two different steps; one is the scattering of some of its energy, which is called "internal conversion" until S_1 excited state then, from this state it is ready to relax to the ground state S_0 via four competitive processes.[19]

Depending on the type of relaxation, these processes are: flourscence, collosional quenching, inter-system crossing and phosphorescence. Fluorescence is probably the most important process where there is an emission of a photon with a radiative rate constant. In collosional quenching there is energy transfer from one excited molecule to another on its ground state. When an electron passes from S1 state to the T1 and then from T1 to So these processes are called intersystem crossing and

phosphorescence consecutively. These processes are shown in the Jablosnki Diagram below

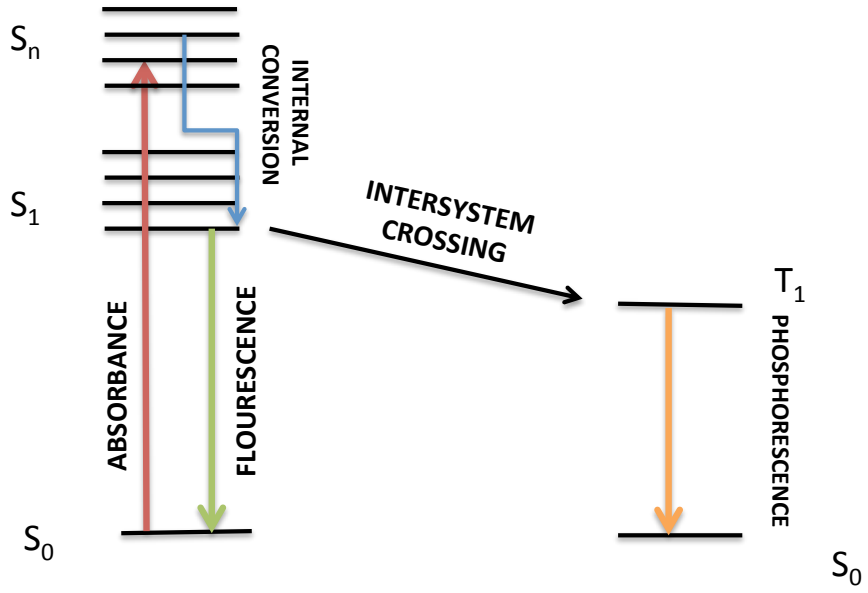

Figure 1. Jablonski diagram.

Flourophore is a molecule/chromophore that emits light. Since the total energy absorbed by a chromophore is released in various manners such as a photon, the energy absorbed by a flourophore is always greater than the emitted energy. Meaning that, the emission spectrum maximum of the flourophore is shifted to longer wavelengths as compared to absorption spectrum. Such shifts are called "Stokes shift" in honor of the man who observed this phenomenon in 1852, sir George Stokes.[20] This is illustrated below.

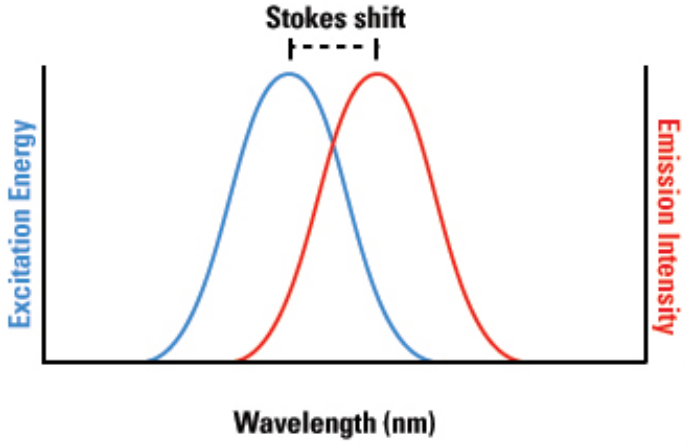

Figure 2. Stokes shift representation.

Every flourophore has its own position of emission wavelength, intensity and lifetime, which are very important observables in the fluorescence spectrum characterization because the energy difference between ground state and singlet-excited states of different molecules differs. Fluorescence and absorption processes are faster than phosphorescence since absorption occurs in 10^{-15} s, fluorescence in 10^{-9} – 10^{-12} s whereas phosphorescence may last up to hours. The reason behind this is; for phosphorescence to occur primarily intersystem crossing must occur first. Fluorescence lifetime is the average time, which molecules remain in the excited state before they return to the ground state and this depends on the design of the flourophore itself.

Since fluorescence lifetime is an intrinsic property it is considered a state function therefore, it is independent from the method of measurement, initial conditions such as excitation wavelength while it is exposed to light. Moreover, the concentration and emission intensity do not affect the fluorescence lifetime. Nevertheless, factors like temperature, polarity and presence of fluorescence quenchers affect fluorescence lifetime. Knowing that fluorescence lifetime is basically first order kinetics decay, it can be calculated as follows:

$$\mathbf{T = 1/(k_f + k_{nr})}$$

Where **T** = Flourescence lifetime

$\mathbf{K_f}$ = rate constant of the radiative process

$\mathbf{K_{nr}}$ = rate constant of the nonradiative process

Flourescence intensity is directly proportional to the quantum yield (the number of photons radiatively emitted over number of photons absorbed by a molecule) and it can be calculated as:[21]

O = photons emitted/ photons absorbed = kf/(kf+knr)

The higher the quantum yields the brighter the fluorescence. It is possible to control fluorescence intensity by properly designing fluorescence switch on/off using PET, ICT and ET mechanisms.[22,23]

2.2.1 Photo-induced electron transfer (PeT)

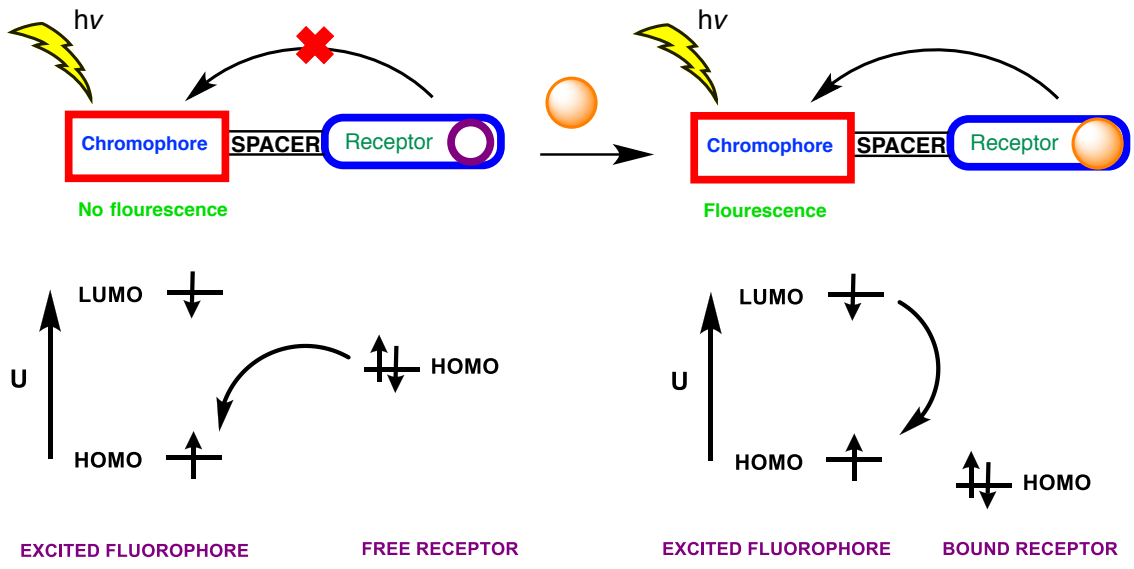

Figure 3 - Schematic and molecular orbital representation of PeT working mechanism.

In photo-induced electron transfer system, there are three units: fluorophore (signaling unit), receptor for recognition of an analyte, and spacer between these two parts. There is no conjugation between fluorophore and receptor in a PeT system; however, they are close enough for electronic interaction by spacer.

As it is seen Figure 22, in a PeT system, firstly, an electron is excited from highest occupied molecular orbital (HOMO) of the fluorophore to its lowest unoccupied

molecular orbital (LUMO) upon irradiation. If there is a receptor whose function is to accept or donate the electrons is linked to fluorophore without any conjugation and has its lone pair electrons occuring at separate orbital as it is seen in the figure above. When the energy of the receptor's orbital is between the HOMO and LUMO of the fluorophore, an electron transfer occurs from HOMO of the receptor to the holes in the HOMO of the fluorophore which is created after the excitation process, which causes decrease in emission intensity and the quenching of the fluorophore. This phenomenon is known as photo-induced electron transfer (PeT). However, when there is an analyte such as a metal cation, it binds to the receptor and that decreases the energy of HOMO of the receptor due to stabilization, then PeT is prevented and quenching is finished.

There is another mechanism of PeT process which is called "oxidative PeT". In this process, in the absence of an analyte, emission occurs normally. However, when there is an analyte such as metal cation, the energy of LUMO of the receptor decreases and takes places between HOMO and LUMO of the fluorophore. After the excitation of fluorophore, electron transfer occurs from LUMO of the excited molecule (fluorophore) to LUMO of the receptor instead of HOMO of the fluorophore during the relaxation process as it is seen in Figure 23. Compared to conventional PeT process, now firstly fluorophores are strongly fluorescent at the initial state (there are also some exceptions, e.g., Nagano *et al.*)[ ] and upon binding, they becomes weakly or non-fluorescent due to the electron transfer between the LUMOs.[24,25]

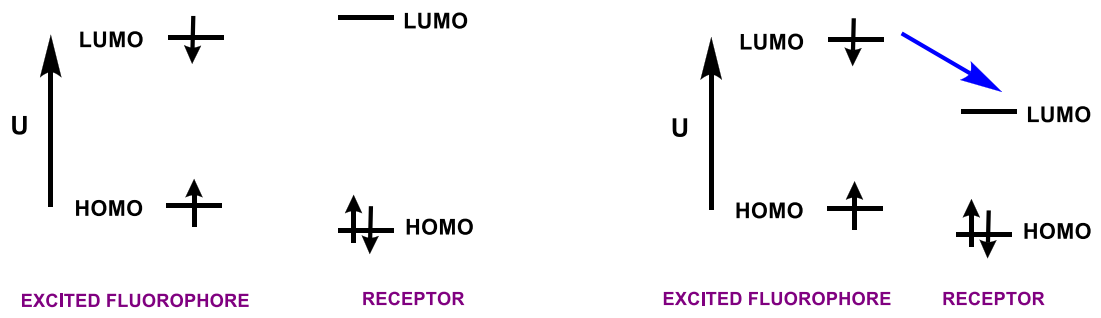

Figure 4. Schematic representation of reverse PeT.

There are many fluorescent chemosensors work via PeT mechanism. Acceptance moiety can change from crown ether to cryptand as it is seen in Figure 5. There has been reported many PeT sensors for recognition of specific metals such as zinc, sodium, magnesium, calcium ions. [26]

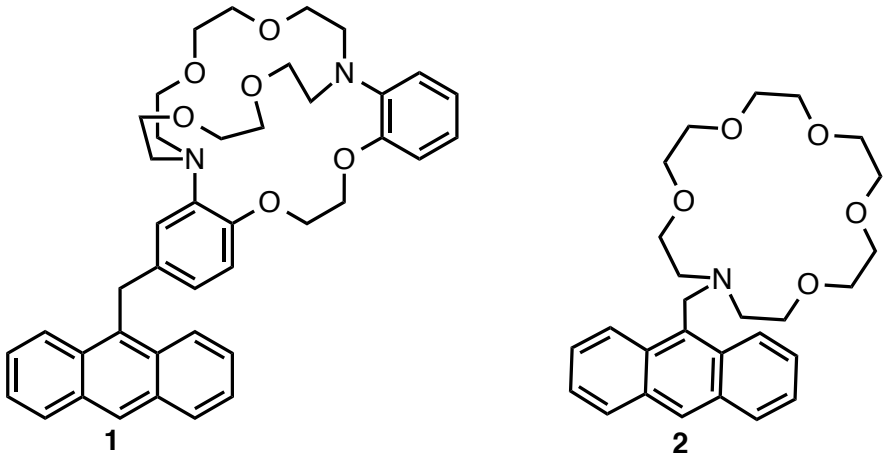

Figure 5. Some examples of PeT based sensors.

2.2.2 Internal Charge Transfer (ICT)

In internal charge transfer (ICT) system, there are two units: fluorophore and receptor. Unlike PeT process, there is no spacer in ICT, which means the fluorophore is directly attached to the receptor, in other words, there is a conjugation between the receptor and the π-electron system fluorophore moiety. Therefore, there is orbital overlapping in this conjugated system which causes the internal charge transfer. When an analyte is binded to the receptor, it causes excited state dipole and affects emission spectrum.

There are two types of stokes shift in the emission spectrum: blue shift and red shift depending on the interaction of analytes with receptor, which is an electron withdrawing or donating group as it is seen in Figure 25. If there is an electron donating group binding to the fluorophore, the electron donating ability of the electron donor group will decrease which causes the decrease in conjugation and blue-shift in the absorption spectrum of the fluorophore. To understand the changes in emission spectrum, one can use excited state of molecules. For example, there is a

positive charge on amine groups at the excited state. Due to the interaction between the positively charged groups, there will be destabilization of excited state. Hence, energy gap between HOMO and LUMO increases.

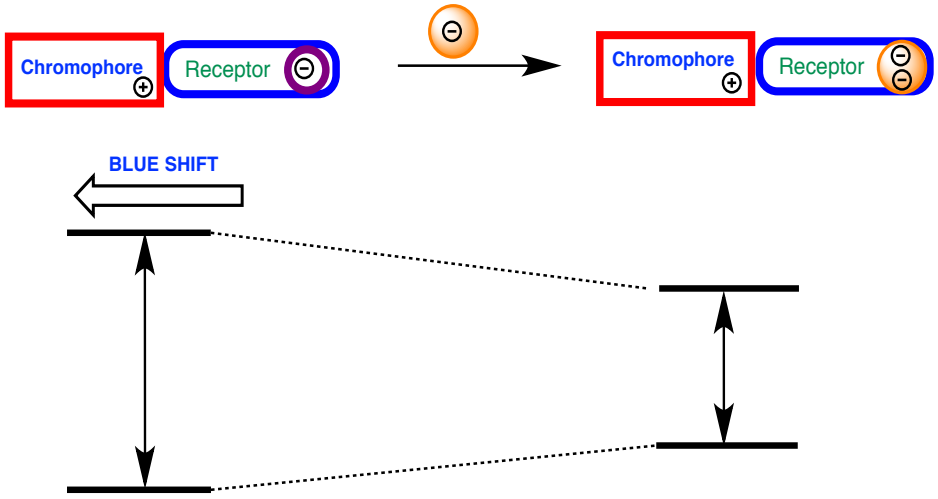

Figure 6. Representation of ICT working mechanism for blue shift.

On the other hand, if there is a withdrawing group binding to the fluorophore such as carbonyl groups, the interaction between the cation and withdrawing group increases the electron witdrawing ability of the acceptor. This interaction between the cation and negatively charged acceptor group stabilize excited state, which results in decrease in energy gap of HOMO and LUMO and red-shifted absorption.

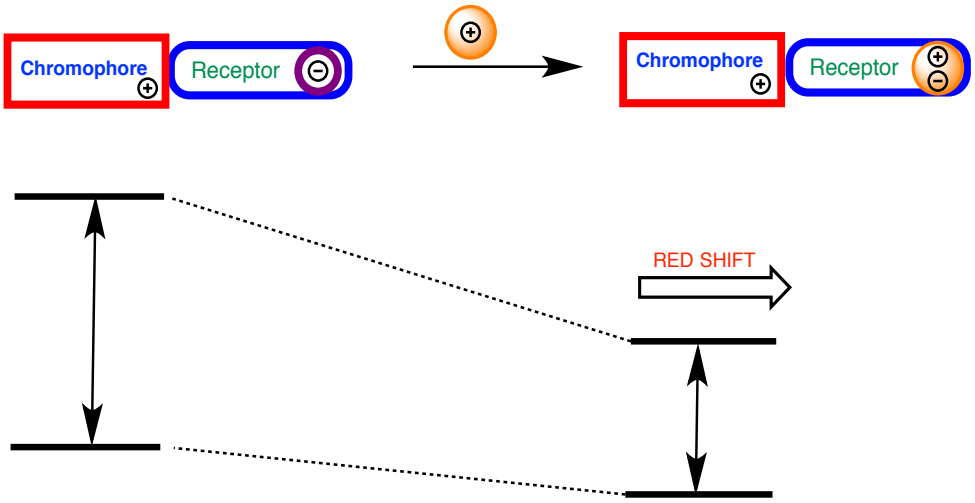

Figure 7. Representation of ICT working mechanism for red shift

There are many examples of ICT based sensor in the literature. For instance, compound **22**[ ] (figure 26) is a good example of ICT-based probe for Hg (II) ions. In this molecule, dithia-dioxa-aza macrocycle is the receptor part and in the literature it is known as Hg (II) selective ligand. Due to the interaction of positively charged groups that causes blocking of ICT process upon coordination of Hg (II) ions to the nitrogen donor atoms, blue shift is observed. In addition, when there is no Hg (II) ions in the environment, fluorescence is highly quenched because of ICT process from crown moiety to BODIPY core. On the other hand, with a Hg (II) ions, strong fluorescence intensity with a large blue shift will be observed.[27–29]

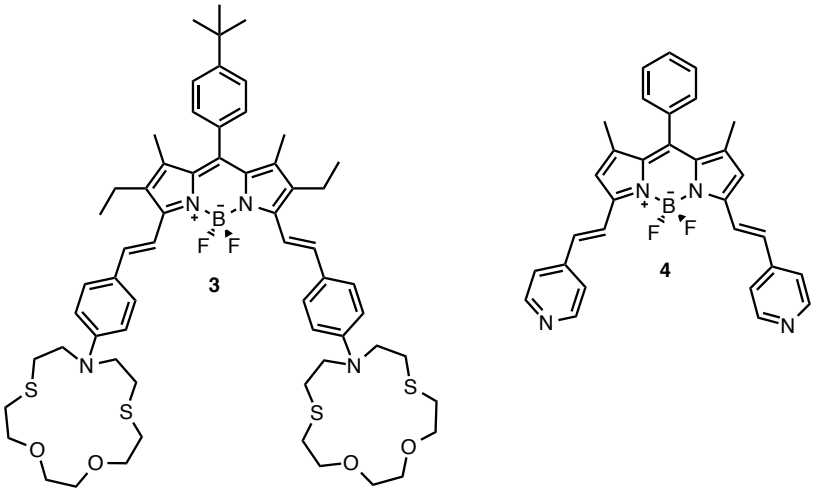

Figure 8.. Examples of ICT sensors.

2.3 Photodynamic Therapy (PDT)

2.3.1 History of PDT

. The use of photoactive molecules started has been with us for too long for instance, back in time photoactive molecules were used for the treatment of vitiligo as the holy book of India (*Atharava-veda*) describes it however, it was first realized by Herodotes more than two hundred years ago. Oscar Raab first observed the toxic effects of acridine red molecule on different bacteria in the presence of light and after doing the control experiments he then concluded that a flourophore must be present in order to have light-induce toxicity. With this contribution to scientific literature, several groups nowadays are working on the crusade of finding cancer cure using light-induced molecules, which started with Tappeiner and Jesionek using eosin dye to treat skin cancer for the first time in history.

Following the same course of research, Teppeiner and Jodbauer in 1904 found out that oxygen is a critical component for photodynamic therapy nevertheless no mechanism was proposed until 1979 when electron spin resonance was used to monitor the generation of singlet oxygen. Meyer-Betz performed the first human trial of PDT on himself and he described apses and severe pain. Whereas, the first clinical applications were done at the Rosewell Park Cancer Institute back in 1978. In 1980, FDA approved photophrin (a mixture of haematoporphryn derivatives) as a

photosensitizer and from there on, several other molecules have been proposed to be used as PDT agents.[30]

2.3.2 Working mechanism

Singlet oxygen must be generated in order for PDT to work as desired. Three main components are required for PDT namely; Photosensitizer (flourophore), Light and Oxygen. First the flourophore must be excited from its ground state to the first excited state by appropriate photon energy. There is a relaxation on the viabrational states then there are two possibilities of relaxation; one is intersystem crossing and the other is relaxing to the ground state where we will have fluorescence. In PDT we require the relaxation through intersystem crossing because in this case there is a spin conversion and the energy can be later transferred to molecular oxygen in order to produce singlet oxygen. However, if we have the intersystem crossing and no oxygen present then a relaxation with phosphorescence is observed.[30] This phenomenon is described on the Jablonski diagram for singlet oxygen production below:

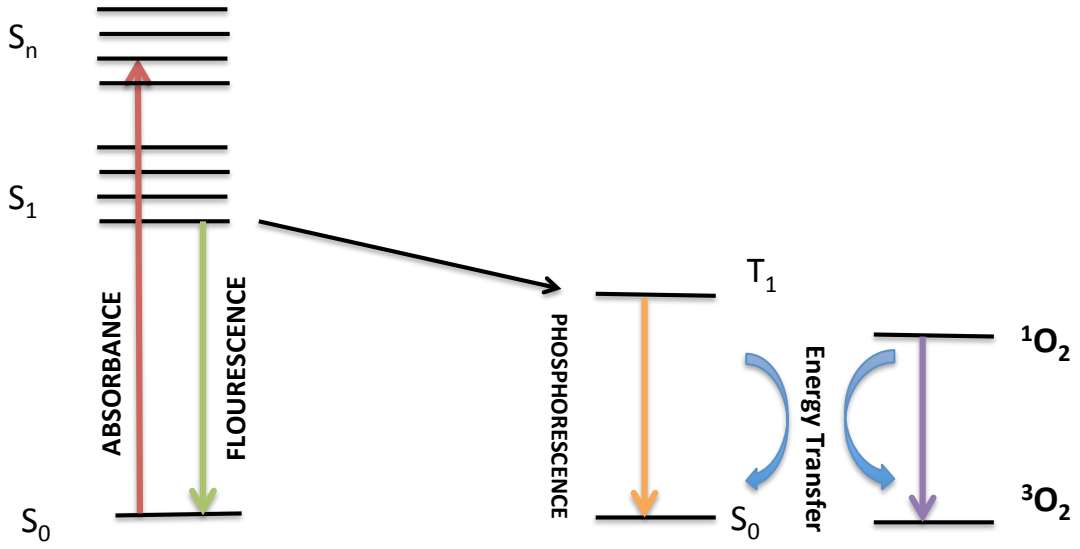

Figure 9. Jablosnki diagram for singlet oxygen production.

Singlet oxygen can lead to formation of reactive oxidative species or oxidative damage of cells because it has a short lifetime of about 0.6 us and diffusion distance of 0.1 um. Therefore, only cellular structures on the vicinity of the photosensitizer

can be damaged and these reasons have been the *moto* for the synthesis of localized and more target oriented photosensitizers. [31]

2.3.3 Oxidative damage of singlet oxygen

Two mechanisms rule the cytotoxicity mediated by the photosensitizer. When the photosensitizer reacts directly with the biomolecule and forms unstable radicals it is called type-I reaction. After the radicals are formed, they react with other substrates or molecular oxygen to for singlet oxygen. On the other hand, when energy is transferred directly to the photosensitizer and produces singlet oxygen it is called type-II reaction. The differentiation between the two mechanisms is difficult therefore it is usually assumed that they occur simultaneously.

After singlet oxygen is produced it immediately reacts with biomolecules in the vicinity provoking an oxidative stress since it is a powerful oxidant. Lipid peroxidation alters the membrane structure, integrity and its fluidity so lipid radicals are then formed causing another cytotoxic danger to the cells. Free amino and thiol groups are other targets of singlet oxygen and with this there is a disruption of the proper folding and functioning of the aminoacids. Another damage is caused to mithocondrial membrane permeability through oxidation of disulfide histidine amino acids and membrane proteins, which leads to more labile membrane, that permits the passage of mithocondrial constituents and ends up with cell death. Dioxyribose sugars and bases are easy targets for chemical reactions with singlet oxygen for instance thymine. In case of such modifications, DNA strands may break and after accumulation of such damages cell death is triggered.[32–34]

2.3.4 Requirements for photosensitizers

In order for a photosensitizer to be successfully used in PDT it must bear several properties for instance; photostability, easy synthesis, absorption coefficients ranging between 600 to 900 nm known as the therapeutic window. The reason for this is, the penetration depth of light is high at this range. Neither dark toxicity nor reactivity is required in the presence of light. An amphiphilic character is also required for safe cell penetration. In addition, high quantum triplet yields are required therefore an

effective ISC and long triplet lifetimes are desired.[35] Nevertheless, these are not easy requirements for example to decrease dark toxicity one should embed targeting moieties and depending on the photosensitizers it might be very difficult to do so. Although photofrin has low absorption coefficients and a rather complicated structure, it is the most widely used photosensitizer in medicine. As a consequence, scientists are have been looking for alternatives. Foscan was developed in order to diminish the high drug/light exposure and long-term photosensitivity presented by photofrin. Other photosensitizers such as rose Bengal, methylene blue, eosin B, phtalocyanine and BODIPY derivatives have been developed and employed over the years of research. [36,37]

On the other hand, the efficiency of PDT is determined by the light source used. The penetration depth of blue light is quite limited but that of red light and near-IR can be more useful in tissue penetrations. Wavelengths outside the therapeutic window are not useful because for instance; if we use longer wavelengths, the energy will not be enough to penetrate the tissues and water and other molecules can absorb the incoming light causing no PDT reactions at all. Whereas when shorter wavelengths are used, the energy is so high that can damage tissues on its way to the required target. As result, light dose, light delivery and time of exposure are important factors for clinical efficacy.[35,37,38]

2.4 Photosensitizer families in literature[39]

2.4.1 Phenothiazines

Methylene blue is one of the mostly used photosensitizer for PDT applications. It takes part of phenothiazolium family and with εmax of approximately 82,000 M−1 cm−1 it absorbs at 666 nm. Besides, it targets melanoma cells and a positive PDT action was observed in melanoma cell cultures. In clinical PDT treatments methylene blue is used for basal cell carcinoma and Kaposi's sarcoma whereas in vitro it is used for testing adenocarcinoma, HeLa cervical tumor cells and bladder carcinoma. On the other hand, toluidine blue which asorbs at 596 nm and 630 nm with εmax 51,000 M−1 cm−1 of approximately is known to be undergoing phase two trials to treat

chronic periodontitis.[40–42]

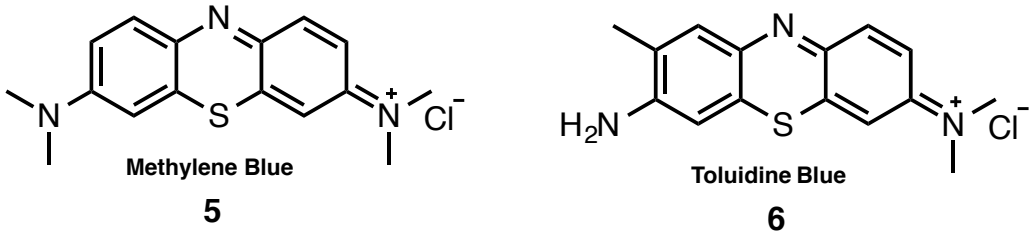

Figure 10. Examples of phenothiazines sensitizers.[43]

2.4.2 Xanthenes

Water soluble rose Bengal is a xanthene photosensitizer and it absorbs at 549 nm and it has an ε_{max} of approx.100,000 In addition, it is used in the treatment of cancinoma and metastitatic melanoma. Another effective Xanthene sensitizer is 4,5-Dibromorhodamine with $\varepsilon_{max} \sim 100{,}000\ M^{-1}\ cm^{-1}$ and absorbs light at 514 nm. Moreover, it was investigated for PDT on graft-versus-host disease and it can destroy lymphocytes via apoptosis.[44,45]

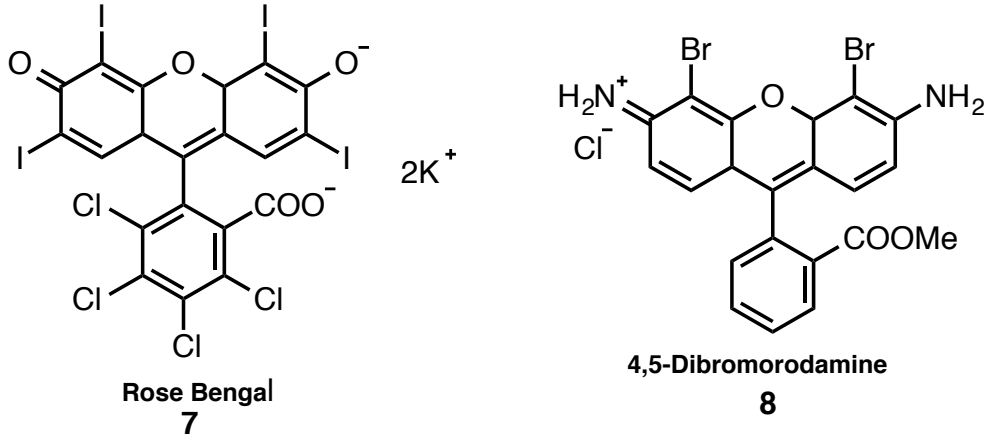

Figure 11. Examples of xanthene sensitizers.

2.4.3 Phtalocyanines

As mentioned before in the previous chapters, the use of heavy metals enhances ISC and in the case of phtalocyanines, a metal complex formation is required. They absorb light in the range of 670 – 700 nm with $\varepsilon_{max} \sim 200{,}000\ M^{-1}\ cm^{-1}$. For instance, aluminum phthalocyanine tetrasulfonate is one typical example of this class

of sensitizers. Another example is Photosens with an absorption at 676 nm and in Russia it is used to treat stomach, oral, breast and lip cancer. Nevertheless, skin photoxicity may occur for many weeks as a side effect. Silicon phtalocyanine absorbs light at 675 nm and has completed phase I trials.[46–49] In these trials it was able to treat actinic keratosis, skin cance, micosis *e.t.c.*

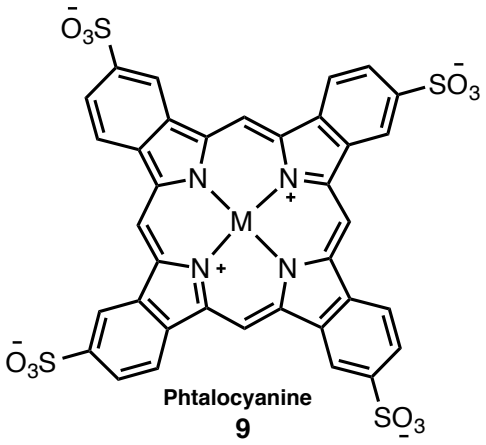

Phtalocyanine

9

Figure 12. Example of phtalocyanine sensitizer.

2.4.4 Anthraquinones

Naturally occurring anthraquinone derivative **"*Hypericin*"** absorbs light at 590 nm with εmax ~ 44,000 M−1 cm−1 generates reactive oxygen species that target cancer cells. Although several clinical trials have been performed to treat squamous cell carcinoma and basal cell carcinoma, the results were unsatisfactory.[50–54]

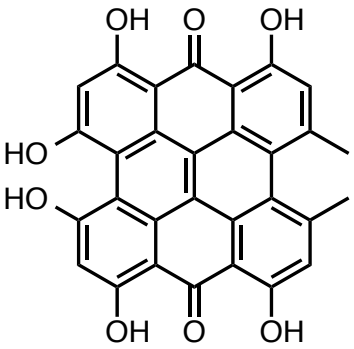

Hypericin

10

Figure 13. Example of anthraquinone sensitizer.

2.4.5 Cyanines

Merocyanine 540 is a cyanine that targets leukemia and lymphoma cells. It was investigated for PDT in vitro to treat neuroblastoma and leukemia with considerable results. Besides, it absorbs at 556 nm with $\varepsilon_{max} \sim 110{,}000\ M^{-1}\ cm^{-1}$ which is almost within the therapeutic window.[50,55,56]

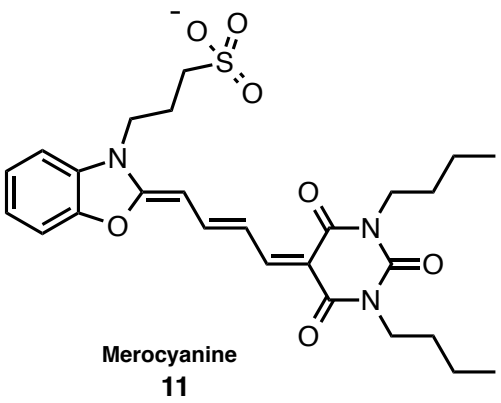

Figure 14. Example of cyanine sensitizer.

2.4.6 Curcuminoids

Curcumin absorbs at 420 nm with $\varepsilon_{max} \sim 55{,}000\ M^{-1}\ cm^{-1}$. It can be isolated from rhizomas of curcuma longa L and it is also a component of turmeric (a cooking spice). In PDT it was used as a disinfectant in oral surgery. This sensitizer upon PDT action destroys bacteria.

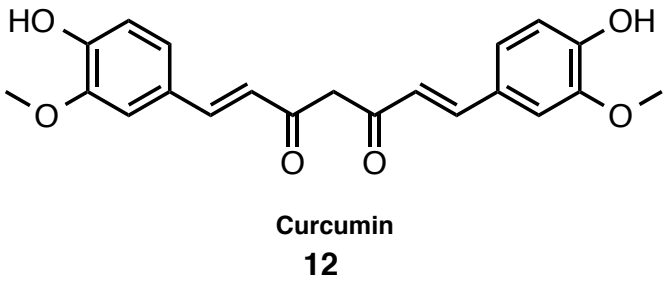

Figure 15. Example of curcuminoid sensitizer.

As listed below several non-porphyrin sensitizers have been proposed and FDA approved.[39,50,57,58]

2.5 Triplet Photosensitization in PDT

After intersystem crossing ($S_1 \rightarrow Tn$ ($n \geq 1$)) takes place, the triplet state of a photosensitizer is populated by non-radiative electrons. Therefore, strong absorption is required in order to have a powerful triplet photosensitizer, as this is one of the most important requirements in PDT process. To trigger photophysical and photochemical processes long-lived triplet excited state is required because it acts as triplet energy donor. Triplet excited states play an important role not only in PDT applications but also photocatalytic organic reactions and triplet-triplet anhilation upconversion. Another use is in the phosphorescence imaging, sensing and electroluminescence.[59–63]

Pauli exclusion principle states that electrons have opposite spins while in their singlet excited state whereas in the triplet excited state they have parallel spins.[64,65] As result, during the ISC a quantum mechanically forbidden process takes place because there must be a reversion of spins making triplet excited state less probably to observe. Much effort has been spent to increase the probability of triplet excited state existence within several years and several different results were published. For instance, Spin orbit coupling is one of the processes required because it favors ISC. During this process, there is a coupling between electron spin and orbital angular momentum and total angular momentum and energy are conserved.[66–71]

2.5.1 Incorporation of Heavy Atoms

Large atomic number decorated photosensitizers are known to be very effective in the induction of ISC because, when an electron moves around a largely positive nucleus it accelerates then the spin (μ_S) and angular (μ_L) momentum increase. Therefore, the spin orbit coupling becomes more probable.

It is also possible to calculate the probability of getting SOC, as it is directly proportional to the fourth power of the nuclear charge (Z). As illustrated below:

$$H_{SO} = \frac{e^2 Z^4}{2a_o m^2 c^2 n^3} \; L.S$$

Equation 1. Calculation of SOC probability.

Therefore, the atomic number of the photosensitizer increases, the higher the chances for ISC to occur. Heavy atoms have been the perfect candidates to increase the SOC in photosensitizers because the majority of the existing organic dyes have low triplet quantum yields. Although this incorporation has been successful in many cases, several drawbacks were later presented for instance; incorporation of Br, I, Ir, Rh, Pt, Ru and Os usually lead to *dark toxicity.* While heavy atoms such as transition metal complexes might seem safer than halogens, their absorption coefficients in the visible region are very small so they have a restricted use. Thus, organic photosensitizers such as Rose Bengal, eosin blue and BODIPY have been extensively employed in the research of PDT due to the easy incorporation of iodine and Bromine.[72–77] Moreover, they have high absorption coefficients within the visible region, which is highly desired. Molecules are given below:

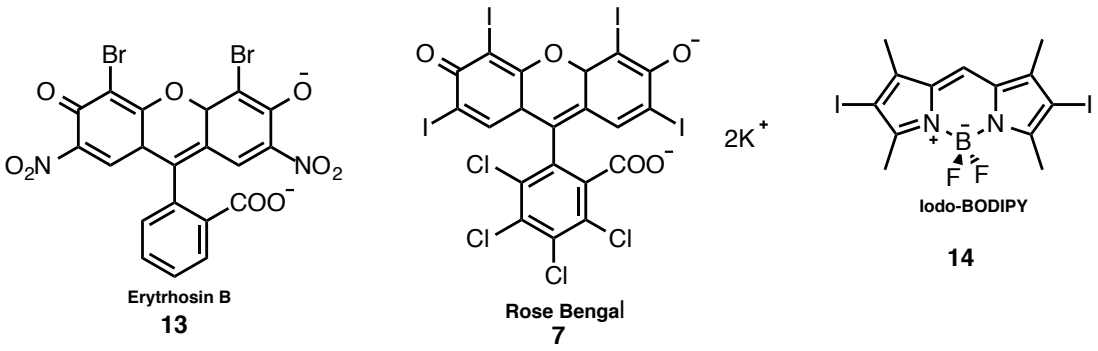

Figure 16. Halogenated sensitizers for PDT.

BODIPY chromophore is a highly remarkable sensitizer with high triplet quantum yields. In addition, they have high resistance to photobleaching, inert, reduced dark toxicity and insensitive to the environment. As result, they have been chosen as ideal candidates for future PDT clinical applications.

Negano *et al.* reported the first application of BODIPY molecule as a PDT agent in 2005 where **2,6-Diiodo-BODIPY** was investigated for singlet oxygen generation on

the heavy atom class. When low fluorescence quantum yields (about 2%) were observed it was considered a successful task since this indicated the high efficiency of ISC. Then, cancer cell studies in vitro were also performed and branded fruitful.

Akkaya and coworkers also reported near-IR absorbing and water-soluble BODIPY derivatives such as di-styryl bromo-substituted BODIPY derivative. This molecules has a red-shifted absorption maximum and due to the oligoethylene glycol groups, the water solubility is increased. In the cancer cell experiments, cell membrane damage is observed via fluorescence microscopy which proves the cytotoxic effect of the sensitizer.[50,78–82]

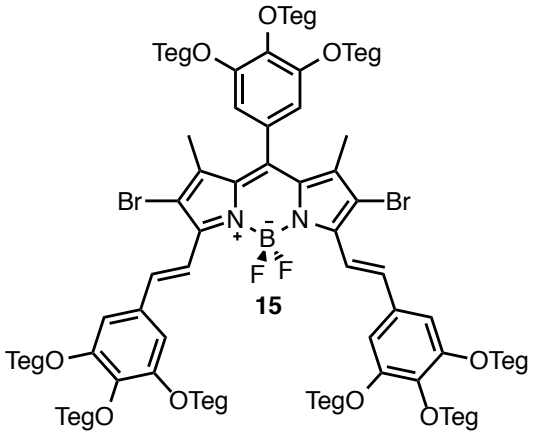

Teg: Triethylene glycol

Figure 17. Di-styryl bromo-substituted BODIPY molecule.

2.5.2 Heavy Atom Free Photosensitization

As stated before, heavy atoms in most cases result in dark toxicity so since this in an undesired phenomenon, scientists have struggled with finding new heavy atom free photosensitizers. Within these attempts, various well known processes can be employed for example; designing chromophores with low *lying n-π** transitions, the use of *spin convertors* and *exciton coupling*. In PDT, low levels of toxicity are required when compared to chemotherapy and other convectional methods even at cellular and organ levels. In this thesis, heavy atom free designed BODIPY molecules are presented and some information the other possible mechanisms are explained below.

2.5.3 Low-Lying n-π* Transition based chromophore design

In order for the Spin Orbit Coupling to take place the energy difference between singlet and triplet excited states has to be close enough. In some cases when the electronic configuration of the singlet and triplet excited states are similar, the energy difference may appear to be twice of the electron exchange integral (J). Nevertheless the energy gap between singlet and triplet excited states of the n-π* is much smaller. El-Sayed generalized that; organic molecules with an extended conjugation undergo π-π* transitions that decrease triplet quantum yields. According to him, S_1 (n-π*) → T_1 (π-π*) is an allowed transition because the energy gap is small and the angular momentum is conserved whereas S_1 (π-π*) → T_1 (π-π*) is a forbidden process. According to the equation below, rate constant is directly proportional to the probability of getting SOC and inversely proportional to the energy gap between singlet and triplet excited states.

$$k_{ISC} \propto \langle T_1|H_{SO}|S_1\rangle^2 / (\Delta E_{S_1\text{-}T_1})^2$$

This proves that the smaller the energy gap, the higher the probability of o more effective ISC. One typical example of excited states with low-lying n-π* is benzophenone.

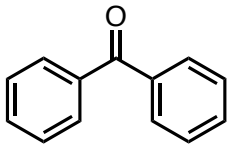

Benzophenone
16

Figure 18. An example of excited states with low-lying n-p* orbitals.

Charge transfer mediated ISC was reported in a theoretical study by Dede *et al.* where quinolizinium flourophore was investigated and concluded that quinolizinium flourophore has an ISC at its deprotonated form and none at its protonated form. The reason for this presumed to be the aminophenyl moiety that transfers charge to the benzoquinolizinium ring and there is an n-π* type of charge transfer. When the quinolizinium is protonated on the other hand, π-π* was detected resulting in low triplet quantum yields which is in accordance with the El-Sayed's rule.[50,83–86]

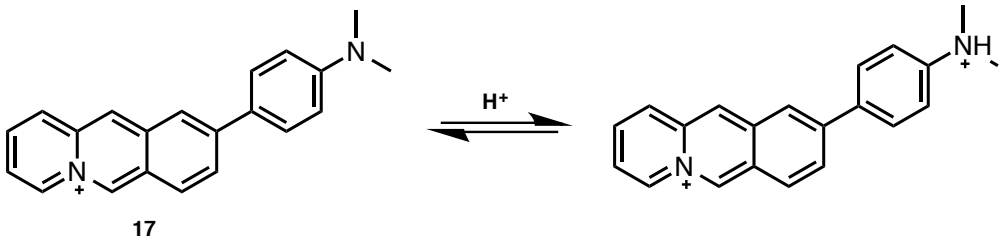

17

Figure 19. An example of p-p* sensitizer.

2.5.4 Exciton Coupling

When two identical chromophores linked together but with no π-conjugation are excited, two delocalized ecited states for each chomophore are observed meaning that they are actually being excited separately. In this case, only when one of the singlet exciton states is close enough to the triplet excited state that ISC takes place.

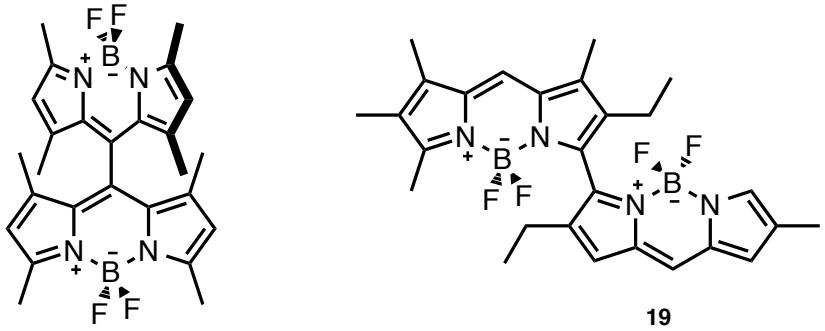

18 19

Figure 20. Examples of sensitizers with exciton coupling states.

Flamigni *et al.* investigated an example of heavy atom free photosensitizer employing exciton coupling, where they synthesized dimeric BODIPY derivative and the absorption spectra of the dimer and monomer are different. The monomer typically shows ground state to singlet excited state excitation behavior with an absorption peak at 530 nm whereas; the dimeric form two different peaks are observed at 381 nm and 534 nm. This results in higher singlet oxygen generation rate due to the more effective ISC. [87–92]

2.5.5 Spin Convertors

The selection rules on highly populated triplet excited states are very challenging since sensitizers should be synthesized taking them into consideration.

Inserting an energy acceptor that has an intrinsic character or also known as spin convertor to a sensitizer, may increase the probability for high triplet quantum yields. Moieties such as C_{60} are very prised because they can be easily coupled with chromophores by a covalent bond and a more effective singlet oxygen production can be observed.

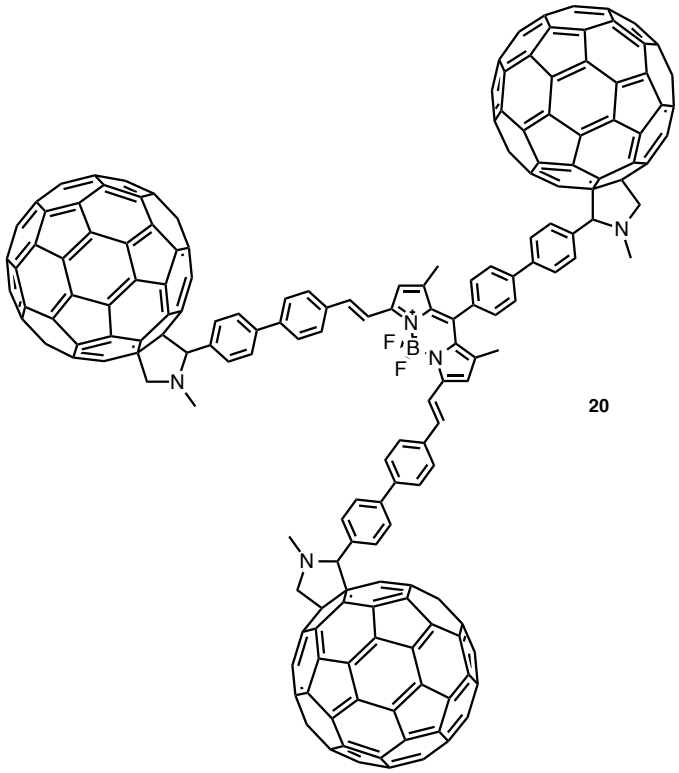

20

Figure 21. An example of sensitizer with spin convertor.

Zhao and coworkers used fullerene (C_{60}) as a spin converter. In their work they combined BODIPY sensitizer with fullerene moiety enhancing an intrinsic ISC property. On the other hand, it would not be possible to achieve such triplet quantum yields without the incorporation of fullerene and this is considered a good sensitizer because it has its absorption peak at the UV region. Besides, fullerene has an additional absorption peak at 700 nm as result it is suitable for intramolecular energy transfer processes and it acts like an *antenna*. The singlet excited state of the BODIPY molecule has 1.93 eV and the fullerene molecule has low lying singlet excited state at 1.72 eV therefore, upon excitation the electron passes from the high

singlet excited state to the low lying singlet excited state. At this stage there is an intrinsic intersystem crossing which then results in easy triplet-to-triplet excited state transition.[50,93–97]

2.6 BODIPY

In 1968 Treibs and Kreuzer discovered BODIPY dyes and today they have a significantly popular area due to their wide applications. BODIPY has several uses in applications such as; solar cells, bimolecular labeling, molecular logic gates, drug delivery *e.t.c*. In addition, compared to other sensitizers, high molar extinction coefficients, high fluorescence quantum yields and depending on the design they may have high triplet quantum yields as well. The absorbance is within the therapeutic window and pH and solvent polarity do not affect them as much therefore, they tend to maintain their physical structure. Easy functionalization from 1 to 8 positions is probably one of the strongest suits of BODIPY because it can be modified for almost any function and solubility. Akkaya, Burgess, Negano, Rurack and Ziessel research groups have played an important role on investigating these modifications.[36]

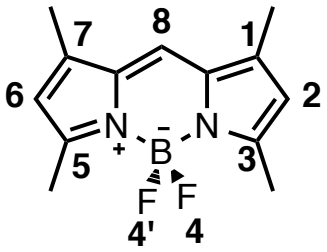

Figure 22. BODIPY molecule.

2.6.1 BODIPY Applications

As mentioned before, several applications are depicted from literature as shown below.

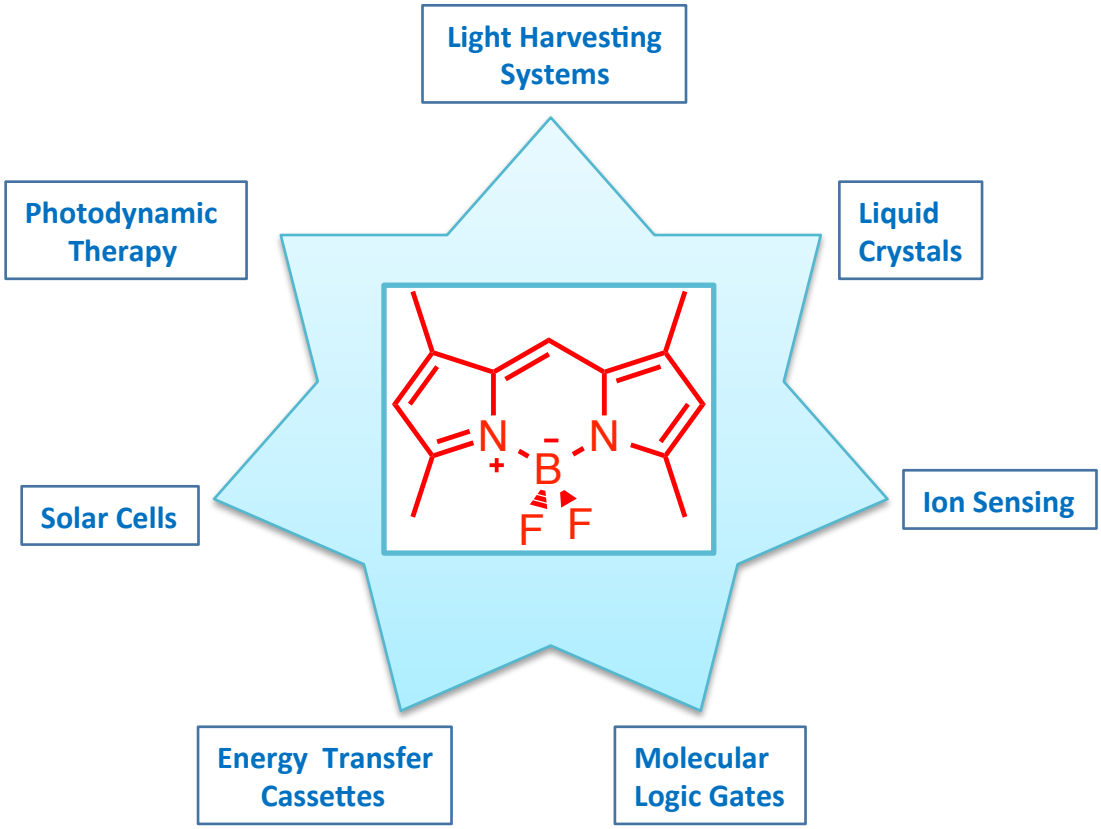

Figure 23. Applications of BODIPY molecule.

Daub and Rurack first employed BODIPY as a chemosensor in 1997 and from that moment forward, various examples were presented in the literature. PET and ICT based sensors such as compound 21. It is a proton sensor because dimethyl amino group is a strong electron donor and when the molecule is excited weak fluorescence will be present whereas upon reaction with proton the PET is blocked and strong fluorescence is allowed. Some metal sensors such as compound 21 - 25 are also available. For instance, they sense cadmium and zinc metals. [98–107]

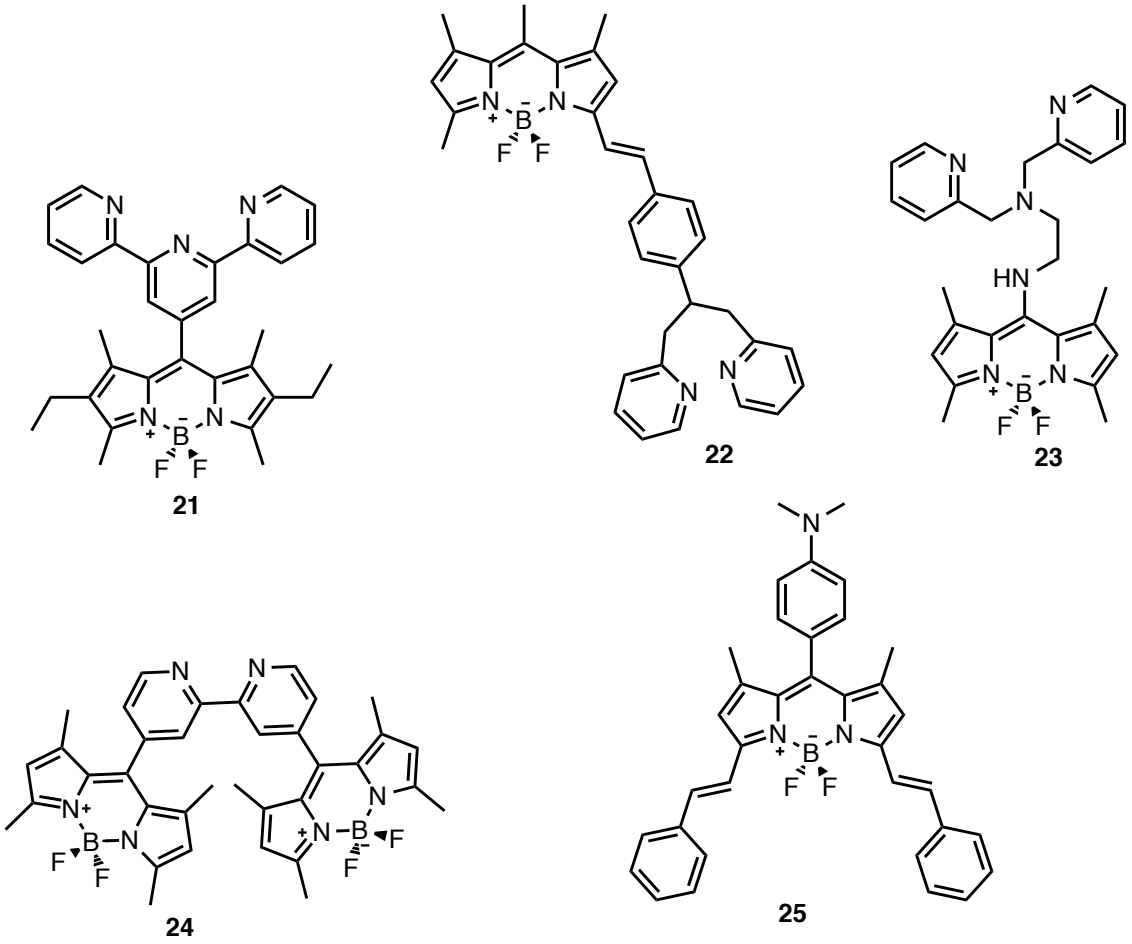

Figure 24. Examples of BODIPY PeT sensors.

In PDT, there is usually the need of heavy atoms to facilitate the ISC. In addition, water -soluble groups can be attached to in increase hydrophilicity for example compound 22 and 23. Akkaya et al. developed water soluble compound 20 to be used in PDT and Negano et al synthesized compound 21 with fluorescence quantum yields of around 0.02, which is consistent with the required because it has high triplet quantum yields.[11,108–111]

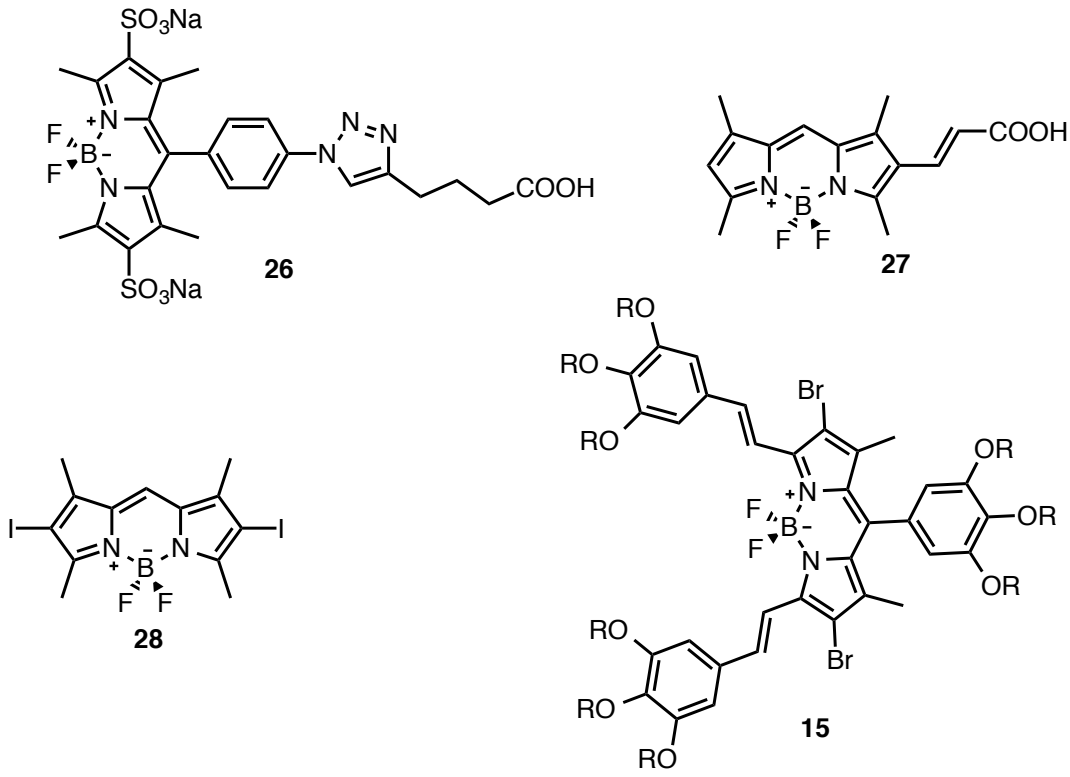

Figure 25. Water soluble BODIPY based molecules.

CHAPTER 3

3. EXPERIMENTAL PROCEDURES

3.1 Methods and materials

All commercial chemicals were purchased from Merck, Sigma-Aldrich and ABCR and were used without any further purification. Merck TLC Silica gel 60 $F_{254.}$ was used to monitor the reactions. Merck Silica Gel 60 (particle size: 0.040-0.063 mm, 230-400 mesh ASTM) was used for the column chromatography. All ^{1}H NMR and ^{13}C NMR spectra were recorded on Bruker DPX-400 in $CDCl_3$ and DMSO with tetramethylsilane as internal standard. Chemical shifts were given in parts per million and the coupling constants (*J*) were in Hz. Mass spectra were recorded on Agilent Technologies 6224 TOF LC/MS. The absorption spectra were recorded on Varian Cary-100 spectrophotometer and Varian Cary 5000 UV-VIS-NIR absorption spectrophotometer. For fluorescence measurements Varian Eclipse Spectrofluometer was used. 1,3-Diphenylisobenzofuran (commercial) was used as a singlet oxygen trap in organic medium.

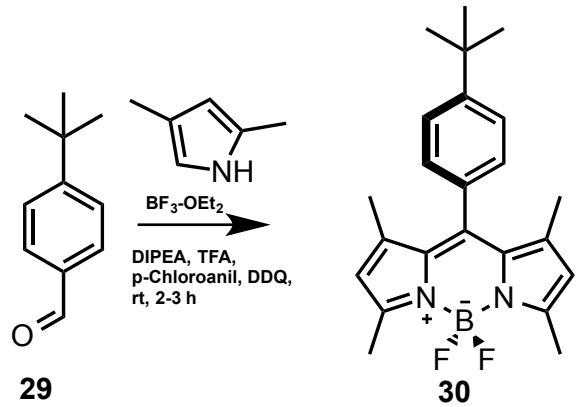

Figure 26. Symthesis of compound 30.

3.2 Synthesis of (30)[112]

To a 500 mL round-bottomed flask containing 250 mL argon-degassed dichloromethane, 2,4-dimethylpyrrole (1.05 mL, 10.26 mmol), 4-*tert*-butylbenzaldehyde (0.773 mL, 4.623 mmol) were added. Then, trifluoroacetic acid

(400 μL) was added to the reaction mixture and left to stirr overnight. Then, p-chloranil (1.36 g, 5.5 mmol) was added and mixed for 1 additional hour. After that, TEA (3.5 mL) was added and mixed for 1 additional hour and $BF_3.OEt_2$ (3.5 mL) was added and the reaction mixture was left to stir at room temperature for 1h. When the starting material was consumed, water (100 mL) was added and the reaction mixture was extracted with DCM (3x100 mL), evaporated and dried over Na_2SO_4. The product was purified by silica gel column chromatography using DCM:Hexane (1:1) as the eluant and the compound was obtained as purple redish solid (1.49 g, 85 %). 1H NMR (CD2Cl2, 250 MHz): δ = 7.42 (d, 2H), 7.11 (d, 2H), 5.91 (s, 2H), 2.42 (s, 6H), 1.30 (s, 6H), 1.27 (s, 9H). 13C NMR (CD2Cl2, 62.5MHz): δ=155.7, 153.2, 144.2, 143.4, 132.2, 128.2, 126.5, 121.8, 35.5, 31.8, 15.0, 14.8. ESI-HRMS ($M-H^+$) calculated 380.2344, found 380.2297, Δ= 12.48 ppm

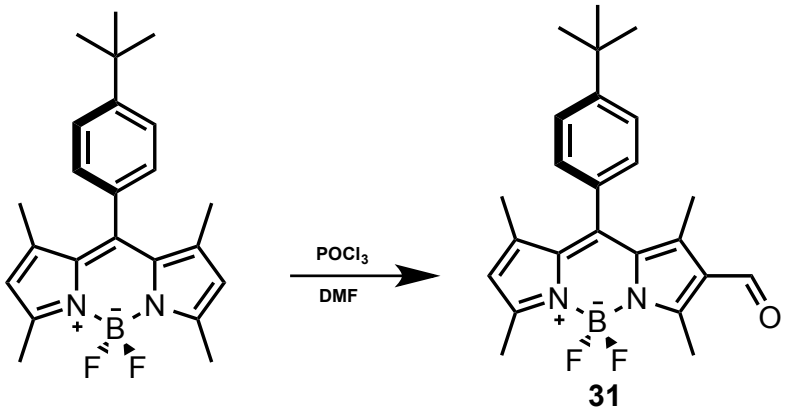

31

Figure 27. Symthesis of compound 31.

3.3 Synthesis of (31):

1 mL of DMF and 1 mL of $POCl_3$ was stirred in an ice bath for 5 min under argon. Then it was warmed to room temperature and waited for 30 minutes. To this mixture compound **(30)** (300 mg, 0.789 mmol) was added in dichloroethane (60 mL). The temperature was raised to 50^0C and stirred for 2 hours. The reaction was then cooled to room temperature and poured to an ice cold NaHCO3 solution (150 mL)This mixture was extracted with DCM (3x100 mL) and dried over Na_2SO_4. Solvent was evaporated in *vacuo* and purified by silica gel column chromatography using DCM:MeOH (98:2) as the eluent. Product **31** was obtained as an orange solid (289.9

mg, 90% yield). ^{1}H NMR (400 MHz, $CDCl_3$) δ 10.02 (s, 1H), 7.55 (dd, *J* = 6.5, 1.8 Hz, 2H), 7.19 (dd, *J* = 6.4, 1.8 Hz, 2H), 6.16 (s, 1H), 2.83 (s, 3H), 2.62 (s, 3H), 1.66 (s, 3H), 1.44 (s, 3H), 1.39 (s, 9H). ^{13}C NMR (100 MHz, $CDCl_3$) δ 185.87, 161.32, 156.27, 153.20, 147.35, 144.10, 142.96, 134.21, 131.06, 127.31, 126.25, 123.85, 34.86, 31.34, 15.02, 14.72, 13.00, 11.43. MS (TOF-ESI): m/z: Calcd: 408.2293 $[M-H]^+$, Found: 408.2267 $[M-H]^+$, Δ= 6.51 ppm.

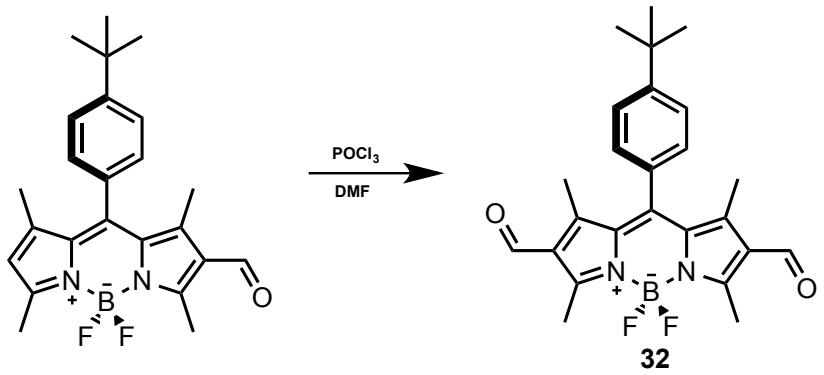

32

Figure 28. Symthesis of compound 32

3.4 Synthesis of (32):

1 mL of DMF and 1 mL of $POCl_3$ was stirred in an ice bath for 5 min under argon. Then it was warmed to room temperature and waited for 30 minutes. To this mixture compound **(31)** (200 mg, 0.490 mmol) was added in dichloroethane (60 mL). The temperature was raised to 50^0C and stirred for 2 hours. The reaction was then cooled to room temperature and poured to an ice cold NaHCO3 solution (150 mL)This mixture was extracted with DCM (3x100 mL) and dried over Na_2SO_4. Solvent was evaporated in *vacuo* and purified by silica gel column chromatography using DCM:MeOH (98:2) as the eluent. Product **32** was obtained as an orange solid (171 mg, 80% yield). ^{1}H NMR (400 MHz, $CDCl_3$) δ 10.07 (s, 2H), 7.61 (d, *J* = 8.3 Hz, 2H), 7.22 (d, *J* = 8.4 Hz, 2H), 2.89 (s, 6H), 1.73 (s, 6H), 1.41 (s, 9H). ^{13}C NMR (100 MHz, $CDCl_3$) δ 185.62, 160.51, 153.99, 148.42, 147.86, 132.03, 130.47, 128.02, 127.02, 126.88, 34.98, 31.32, 13.73, 11.95. MS (TOF-ESI): m/z: Calcd: 481.21045 $[M-H]^+$, Found: 481.17248 $[M-H]^+$, Δ= 74.13 ppm.

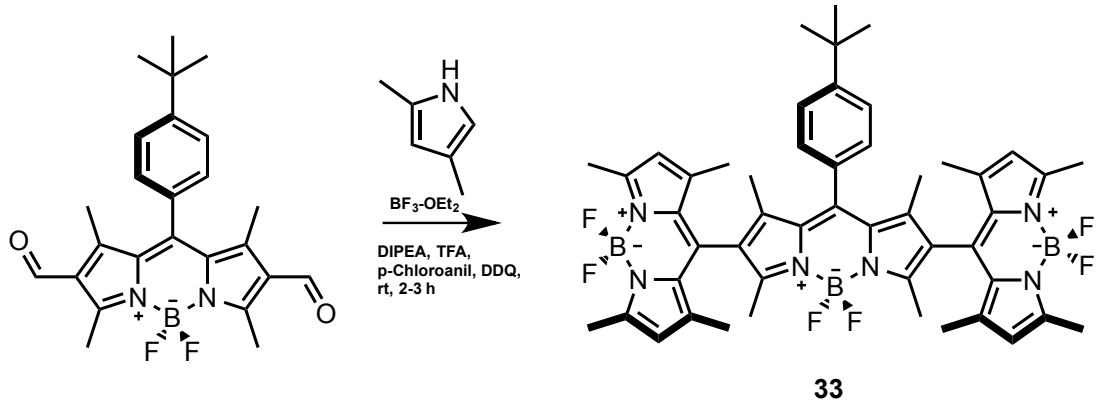

Figure 29. Symthesis of compound 33.

3.5 Synthesis of (33):

To a 500 mL round-bottomed flask containing 250 mL argon-degassed dichloromethane, 2,4-dimethylpyrrole (2.10 mL, 20.5 mmol), 4-*tert*-butylbenzaldehyde (200 mg, 0.458 mmol) were added. Then, trifluoroacetic acid (500 μL) was added to the reaction mixture and left to stirr overnight. Then, p-chloranil (2.72 g, 11 mmol) was added and mixed for 1 additional hour. After that, TEA (5 mL) was added and mixed for 1 additional hour and $BF_3.OEt_2$ (5 mL) was added and the reaction mixture was left to stir at room temperature for 1h. When the starting material was consumed, water (100 mL) was added and the reaction mixture was extracted with DCM (3x100 mL), evaporated and dried over Na_2SO_4. The product was purified by silica gel column chromatography using DCM:Hexane (1:1) as the eluant and the compound was obtained as purple redish solid (160 mg, 40 %). ^{1}H NMR (400 MHz, $CDCl_3$) δ 7.54 (d, *J* = 8.2 Hz, 2H), 7.21 (d, *J* = 8.2 Hz, 2H), 6.03 (s, 4H), 2.56 (s, 12H), 2.48 (s, 6H), 1.79 (s, 12H), 1.34 (s, 9H), 1.30 (s, 6H). ^{13}C NMR (100 MHz, $CDCl_3$) δ 156.00, 153.63, 153.45, 143.98, 142.31, 140.78, 132.91, 131.74, 131.04, 127.23, 126.89, 126.41, 121.34, 53.38, 34.84, 31.56, 31.26, 22.63, 14.61, 14.25, 14.08, 12.95, 12.39. ESI-HRMS ($M-H^+$) calculated 869.46295, found 869.44414, Δ= 21.63 ppm

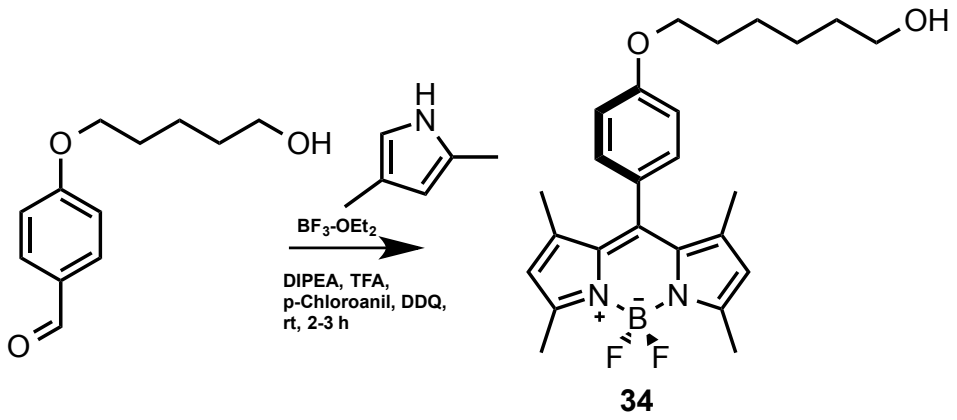

Figure 30. Symthesis of compound 34.

3.6 Synthesis of (34):

To a 500 mL round-bottomed flask containing 250 mL argon-degassed dichloromethane, 2,4-dimethylpyrrole (1.05 mL, 10.26 mmol), 4-((5-hydroxypentyl)oxy)benzaldehyde (300 mg, 1.44 mmol) were added. Then, trifluoroacetic acid (400 μL) was added to the reaction mixture and left to stirr overnight. Then, p-chloranil (1.36 g, 5.5 mmol) was added and mixed for 1 additional hour. After that, TEA (3.5 mL) was added and mixed for 1 additional hour and $BF_3.OEt_2$ (3.5 mL) was added and the reaction mixture was left to stir at room temperature for 1h. When the starting material was consumed, water (100 mL) was added and the reaction mixture was extracted with DCM (3x100 mL), evaporated and dried over Na_2SO_4. The product was purified by silica gel column chromatography using DCM:Hexane (1:1) as the eluant and the compound was obtained as purple redish solid (0.380 g, 60 %). ^{1}H NMR (400 MHz, $CDCl_3$) δ 7.19 – 7.14 (m, 2H), 7.04 – 7.00 (m, 2H), 5.99 (s, 2H), 4.19 (t, J = 6.0 Hz, 2H), 3.91 (t, J = 5.9 Hz, 2H), 2.56 (s, 6H), 2.10 (dq, J = 12.1, 6.0 Hz, 2H), 1.44 (s, 6H). ^{13}C NMR (100 MHz, $CDCl_3$) δ 159.40, 155.27, 143.17, 141.81, 131.83, 130.41, 129.24, 127.18, 121.12, 115.06, 65.62, 60.20, 32.00, 14.58. ESI-HRMS ($M-H^+$) calculated 438.24102 , found 438.241662, Δ= 6.0 ppm

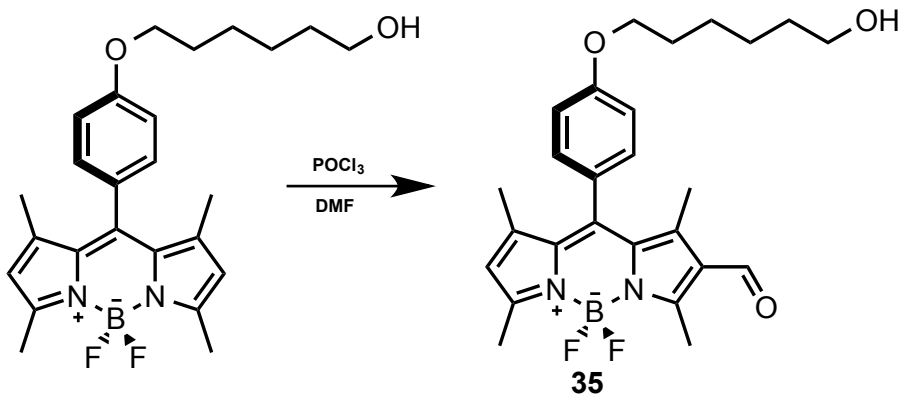

Figure 31. Symthesis of compound 35

3.7 Synthesis of (35):

1 mL of DMF and 1 mL of $POCl_3$ was stirred in an ice bath for 5 min under argon. Then it was warmed to room temperature and waited for 30 minutes. To this mixture compound **(34)** (200 mg, 0.469 mmol) was added in dichloroethane (60 mL). The temperature was raised to 50^0C and stirred for 2 hours. The reaction was then cooled to room temperature and poured to an ice cold NaHCO3 solution (150 mL)This mixture was extracted with DCM (3x100 mL) and dried over Na_2SO_4. Solvent was evaporated in *vacuo* and purified by silica gel column chromatography using DCM:MeOH (98:2) as the eluent. Product **35** was obtained as (385 mg, 82% yield). ^{1}H NMR (400 MHz, $CDCl_3$) δ 10.03 (s, 1H), 7.19 (d, *J* = 8.6 Hz, 2H), 7.07 (d, *J* = 8.6 Hz, 2H), 6.17 (s, 1H), 4.21 (t, *J* = 5.9 Hz, 2H), 3.81 (t, *J* = 6.3 Hz, 2H), 2.83 (s, 3H), 2.63 (s, 3H), 2.31 (dd, *J* = 12.0, 5.9 Hz, 2H), 1.73 (s, 3H), 1.50 (s, 3H). ^{13}C NMR (100 MHz, $CDCl_3$) δ 185.91, 161.45, 159.74, 156.39, 147.31, 143.66, 142.86, 134.47, 129.10, 126.37, 123.93, 115.42, 64.53, 41.39, 32.20, 15.11, 12.99, 11.81. MS (TOF-ESI): m/z: Calcd: 546.1621 $[M-Br]^-$, Found: 546.16003 $[M-Br]^-$, Δ= 3.79 ppm.

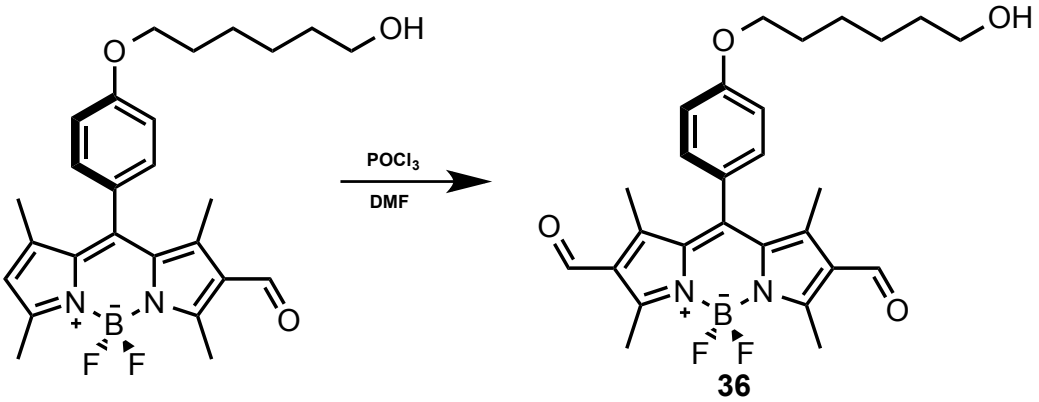

36

Figure 32. Synthesis of compound 36.

3.8 Synthesis of (36):

1 mL of DMF and 1 mL of $POCl_3$ was stirred in an ice bath for 5 min under argon. Then it was warmed to room temperature and waited for 30 minutes. To this mixture compound **(35)** (200 mg, 0.440 mmol) was added in dichloroethane (60 mL). The temperature was raised to 50^0C and stirred for 2 hours. The reaction was then cooled to room temperature and poured to an ice cold NaHCO3 solution (150 mL)This mixture was extracted with DCM (3x100 mL) and dried over Na_2SO_4. Solvent was evaporated in *vacuo* and purified by silica gel column chromatography using DCM:MeOH (98:2) as the eluent. Product **36** was obtained as (174.6 mg, 80% yield). ^{1}H NMR (400 MHz, $CDCl_3$) δ 10.08 (s, 2H), 7.23 – 7.19 (m, 2H), 7.14 – 7.10 (m, 2H), 4.24 (t, *J* = 5.9 Hz, 2H), 3.82 (t, *J* = 6.2 Hz, 2H), 2.90 (s, 6H), 2.33 (dd, *J* = 12.1, 6.1 Hz, 2H), 1.80 (s, 6H). ^{13}C NMR (100 MHz, $CDCl_3$) δ 185.63, 160.59, 160.21, 148.32, 147.46, 132.28, 128.86, 128.05, 125.67, 115.81, 64.63, 41.31, 32.15, 13.72, 12.33.

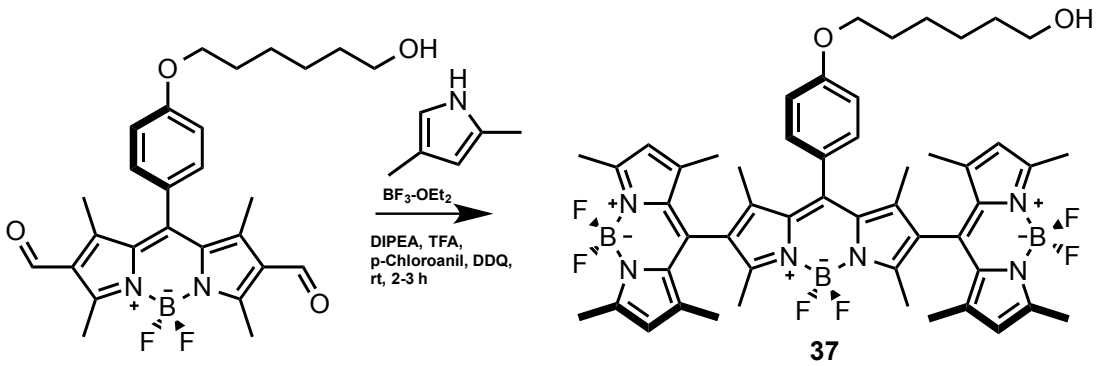

Figure 33. Synthesis of compound 37.

3.9 Synthesis of (37):

To a 500 mL round-bottomed flask containing 250 mL argon-degassed dichloromethane, 2,4-dimethylpyrrole (2.10 mL, 20.5 mmol), Compound **36** (200 mg, 0.415 mmol) were added. Then, trifluoroacetic acid (500 µL) was added to the reaction mixture and left to stirr overnight. Then, p-chloranil (2.72 g, 11 mmol) was added and mixed for 1 additional hour. After that, TEA (5 mL) was added and mixed for 1 additional hour and $BF_3.OEt_2$ (5 mL) was added and the reaction mixture was left to stir at room temperature for 1h. When the starting material was consumed, water (100 mL) was added and the reaction mixture was extracted with DCM (3x100 mL), evaporated and dried over Na_2SO_4. The product was purified by silica gel column chromatography using DCM:Hexane (1:1) as the eluent (218 g, 56 %). ^{1}H NMR (400 MHz, $CDCl_3$) δ 7.18 (d, *J* = 8.5 Hz, 2H), 7.04 (d, *J* = 8.5 Hz, 2H), 6.03 (s, 4H), 4.02 (t, *J* = 6.4 Hz, 2H), 3.56 (t, *J* = 6.6 Hz, 2H), 2.56 (s, 12H), 2.47 (s, 6H), 1.84 (d, *J* = 6.8 Hz, 2H), 1.78 (s, 12H), 1.35 (s, 6H). ^{13}C NMR (100 MHz, $CDCl_3$) δ 160.21, 156.03, 153.65, 143.77, 142.31, 140.67, 132.89, 132.15, 131.70, 128.93, 126.90, 125.83, 121.38, 115.55, 32.43, 31.58, 28.99, 26.62, 25.37, 14.65, 14.28, 12.95, 12.66. ESI-HRMS ($M-H^+$) calculated929.48358, found 929.4435, Δ= 43.06 ppm

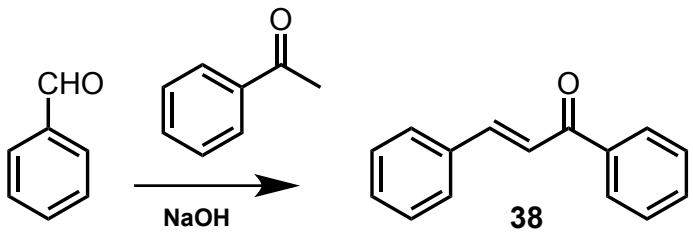

Figure 34. Synthesis of compound 38.

3.10 Synthesis of (38):

An aqueous solution of sodium hydroxide (30%, 30 mL) was added to a solution of methanol (30 mL) and acetophenone (5.0 mmol). After the solution had been cooled to room temperature, benzaldehyde (6.0 mmol) was added. The mixture was stirred at room temperature overnight and was then poured into water (100 mL), ice (100 g), and conc. hydrochloric acid until pH was ca. 2. The obtained solid was removed by filtration, dissolved in dichloromethane (50 mL), and washed with an aqueous solution of sodium bicarbonate (10%, 30 mL). The organic layer was dried with sodium sulfate, and the solution was concentrated and the product recrystallized from ethanol.[113] (998 mg, 96 %). ^{1}H NMR (400 MHz, $CDCl_3$) δ 8.05 (d, J = 8.3 Hz, 2H), 7.84 (d, J = 15.7 Hz, 1H), 7.67 (d, J = 5.4 Hz, 2H), 7.61 (d, J = 7.4 Hz, 1H), 7.58 (s, 1H), 7.53 (t, J = 7.5 Hz, 3H), 7.44 (d, J = 2.3 Hz, 1H). ESI-HRMS ($M-H^+$) calculated 209.09609, found 209.09693, Δ= 4.01ppm

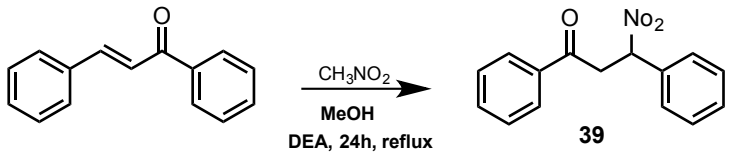

Figure 35. Synthesis of compound 39.

3.11 Synthesis of (39):

The mixture of **38** (1.0 g, 4.8 mmol), nitromethane (1.3 ml, 24 mmol) and Et2NH (2.49 ml, 24 mmol) was heated at 60^{o}C in a round bottom flask and monitored by TLC until all the starting material had finished. Then the reaction mixture was cooled to room temperature and diluted with 30 ml of EtOAc and washed with brine (3 x 20 ml). Solvent was removed in vacuo to give 3 (1.16 g; 90% yield) as a pale yellow solid. ^{1}H NMR (400 MHz, $CDCl_3$) δ 7.94 (d, *J* = 8.4 Hz, 2H), 7.60 (t, *J* = 7.4 Hz, 1H), 7.48 (t, *J* = 7.6 Hz, 2H), 7.35 (d, *J* = 7.4 Hz, 2H), 7.30 (s, 2H), 7.28 (s, 1H), 4.86 (dd, *J* = 12.5, 6.6 Hz, 1H), 4.72 (dd, *J* = 12.5, 8.0 Hz, 1H), 3.48 (t, *J* = 6.8 Hz, 1H).

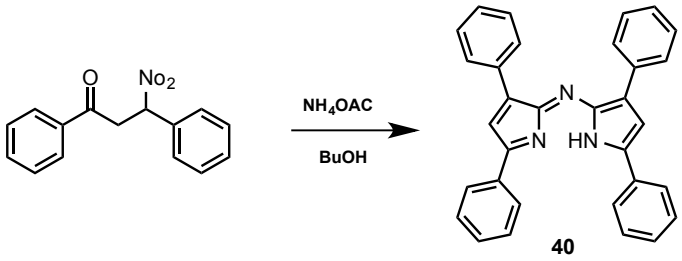

Figure 36. Synthesis of compound 40.

3.12 Synthesis of (40):

Compound **39** (50 mg, 0.19 mmol) was dissolved in butanol (10.0 ml), and the solution was added to NH4OAc (0.9 g, 11.7 mmol). Then the mixture was stirred at reflux for almost 3 hours. The dark blue residue was dissolved in DCM (50 ml) and washed with water (50 ml), 1M NaOH (50 ml x 2) and then water (50 ml). DCM was removed in vacuo and the resulting solid was purified with flash column chromatography (silica gel/$CHCl_3$) to give 4 (20 mg; 47% yield) as a blue-black

solid. ^{1}H NMR (400 MHz, $CDCl_3$) δ 8.09 (d, *J* = 7.0 Hz, 3H), 7.98 (d, *J* = 7.0 Hz, 3H), 7.58 (s, 1H), 7.56 (d, *J* = 7.5 Hz, 3H), 7.50 (d, *J* = 7.0 Hz, 2H), 7.47 (s, 1H), 7.44 (d, *J* = 7.1 Hz, 3H), 7.39 (d, *J* = 7.0 Hz, 3H), 7.28 (s, 2H), 7.23 (s, 1H).

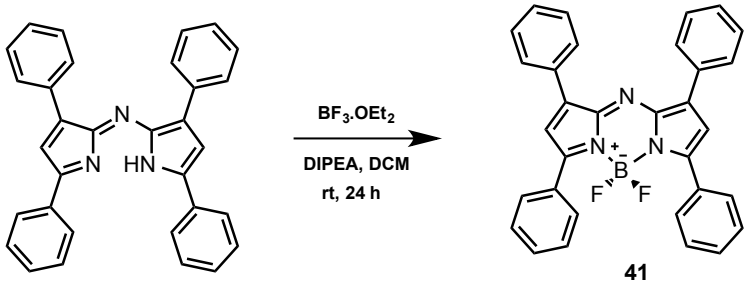

Figure 37. Synthesis of compound 41.

3.13 Synthesis of (41):

A round bottom flask was charged with a magnetic stirring bar, compound **40** (42 mg, 0.09 mmol), Et3N (0.15 ml, 1.07 mmol), and BF_3-OEt_2 (0.15 ml, 1.22 mmol), were added, sealed and heated to 80^{o}C. TLC monitored the progress of the reaction, and after compound 40 was consumed, the mixture was brought to room temperature, diluted with DCM (70 ml) and washed with 1M HCl (50 ml), and brine (50 ml). DCM was removed in vacuo and the product was purified on a flash column chromatography ($CHCl_3$) to give 1 (41 mg; 90% yield) as a metallic-black solid. ^{1}H NMR (400 MHz, $CDCl_3$) δ 8.11 (d, *J* = 1.5 Hz, 3H), 8.07 (d, *J* = 2.4 Hz, 3H), 7.52 (s, 1H), 7.51 (d, *J* = 2.8 Hz, 3H), 7.50 (s, 2H), 7.48 (d, *J* = 2.0 Hz, 3H), 7.46 (s, 2H), 7.06 (s, 2H). ESI-HRMS ($M\text{-}H^+$) calculated 496.19112, found496.19166, Δ= 9.42 ppm

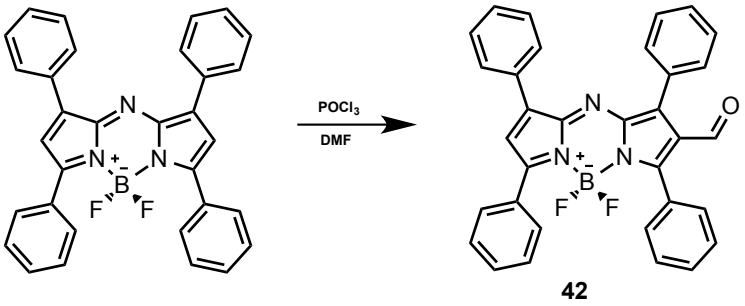

Figure 38. Synthesis of compound 42.

3.14 Synthesis of (42):

1 mL of DMF and 1 mL of $POCl_3$ was stirred in an ice bath for 5 min under argon. Then it was warmed to room temperature and waited for 30 minutes. To this mixture compound **(41)** (200 mg, 0.402 mmol) was added in dichloroethane (60 mL). The temperature was raised to 50^0C and stirred for 2 hours. The reaction was then cooled to room temperature and poured to an ice cold NaHCO3 solution (150 mL)This mixture was extracted with DCM (3x100 mL) and dried over Na_2SO_4. Solvent was evaporated in *vacuo* and purified by silica gel column chromatography using DCM:MeOH (98:2) as the eluent. Product **3** was obtained as (167 mg, 79% yield). ^{1}H NMR (400 MHz, $CDCl_3$) δ 9.80 (s, 1H), 8.10 (s, 2H), 8.08 (s, 3H), 7.88 (dd, J = 6.6, 2.9 Hz, 2H), 7.75 (d, J = 7.6 Hz, 2H), 7.55 (s, 4H), 7.53 (d, J = 2.4 Hz, 4H), 7.45 (d, J = 7.4 Hz, 4H), 7.24 (s, 1H). ESI-HRMS ($M\text{-}H^+$) calculated 525.19331, found 525.19646, Δ= 6.08 ppm

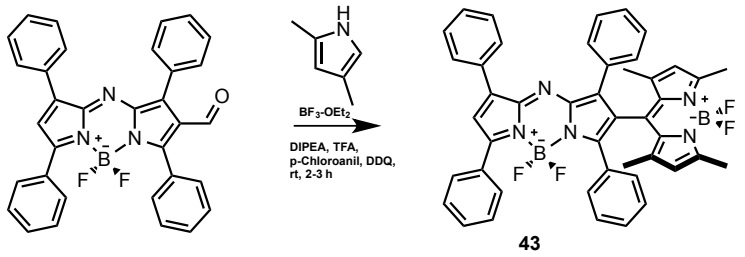

Figure 39. Synthesis of compound 43.

3.15 Synthesis of (43):

To a 500 mL round-bottomed flask containing 250 mL argon-degassed dichloromethane, 2,4-dimethylpyrrole (1.10 mL, 10.5 mmol), **compound 42** (200 mg, 0.381 mmol) were added. Then, trifluoroacetic acid (300 μL) was added to the reaction mixture and left to stirr overnight. Then, p-chloranil (1.36 g, 5.5 mmol) was added and mixed for 1 additional hour. After that, TEA (5 mL) was added and mixed for 1 additional hour and $BF_3.OEt_2$ (5 mL) was (90 mg, 32 %). ^{1}H NMR (400 MHz, $CDCl_3$) δ 8.14 (dd, *J* = 6.5, 3.1 Hz, 2H), 8.07 (dd, *J* = 7.9, 1.7 Hz, 2H), 7.78 (dd, *J* = 6.5, 3.0 Hz, 2H), 7.62 (d, *J* = 8.2 Hz, 2H), 7.49 – 7.45 (m, 4H), 7.42 – 7.36 (m, 4H), 7.37 – 7.30 (m, 3H), 7.28 (s, 1H), 7.18 (s, 1H), 5.96 (s, 2H), 2.52 (s, 3H), 1.99 (s, 3H).). ESI-HRMS ($M-H^+$) calculated 741.30873, found 741.29781, Δ= 14.74 ppm

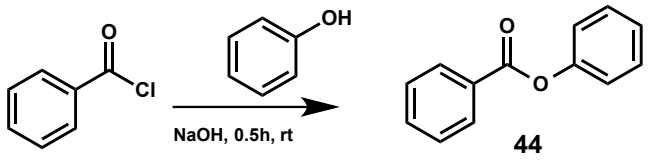

Figure 40. Synthesis of compound 44.

3.16 Synthesis of (44):

Phenol (9.41 g, 100 mmol) and sodium hydroxide (10%, 100 mL) solution were mixed. Then benzoyl chloride **(**14.1 g, 1.21 mol**)** was added and the reaction mixture was stirred at room temperature for half an hour. The product was recrystallized from ethanol and used as crude in the next step. ^{1}H NMR (400 MHz, DMSO) δ 8.27 – 8.23 (m, 2H), 7.70 – 7.65 (m, 1H), 7.55 (q, *J* = 7.5 Hz, 2H), 7.47 (t, *J* = 7.7 Hz, 2H), 7.34 – 7.30 (m, 1H), 7.26 (dd, *J* = 7.6, 1.0 Hz, 2H).^{13}C NMR (100 MHz, $CDCl_3$) δ 165.19, 151.02, 133.57, 130.19, 129.49, 128.57, 125.88, 121.73.

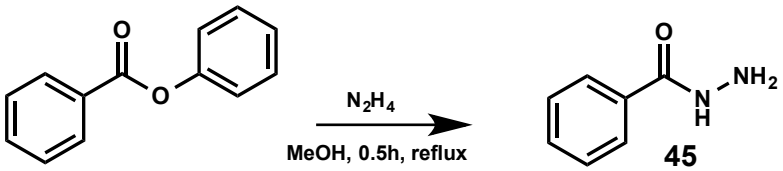

Figure 41. Synthesis of compound 45.

3.17 Synthesis of (45):

To phenyl benzoate (1.00 g, 5.00 mmol) in methanol, hydrazine hydrate (0.32 g, 1.00 mmol) was added and left to reflux for half an hour. The precipitate formed was washed with distilled water and recrystallized from ethanol to afford (129 mg ,95%) ^{1}H NMR (400 MHz, DMSO) δ 9.77 (s, 1H), 7.81 (d, *J* = 8.2 Hz, 2H), 7.48 (dd, *J* = 18.6, 6.9 Hz, 3H), 4.48 (s, 2H). ^{13}C NMR (100 MHz, DMSO) δ 166.33, 133.79, 131.49, 128.75, 127.40. ESI-HRMS ($M-H^+$) calculated 137.07094, found 137.07002, Δ= 6.85 ppm

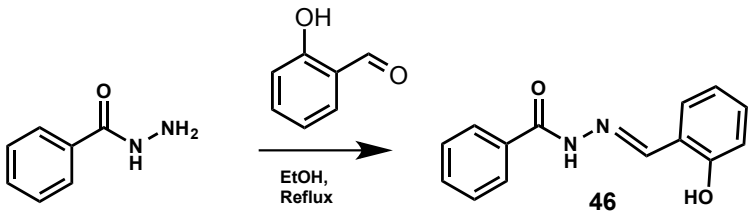

Figure 42. Synthesis of compound 46.

3.18 Synthesis of (46):

To a solution of the compound **45** (76 mg, 0.558 mmol), salicylaldehyde (68,14 mg, 0.558 mmol) in 10 ml ethanol was added and stirred for 3 hours. Then left to cool while it recrystallized to form (134 mg, 100%). ^{1}H NMR (400 MHz, DMSO) δ 12.13 (s, 1H), 11.32 (s, 1H), 8.64 (s, 1H), 7.94 (d, *J* = 7.2 Hz, 2H), 7.64 – 7.52 (m, 4H), 7.31 (t, *J* = 7.8 Hz, 1H), 6.94 (t, *J* = 7.5 Hz, 2H). ^{13}C NMR (100 MHz, DMSO) δ 163.30, 157.97, 148.85, 133.30, 132.43, 131.85, 130.05, 129.01, 128.10, 119.81, 119.14, 116.90. ESI-HRMS ($M-H^+$) calculated 323.15254, found 241.09577 , Δ= 5.74 ppm

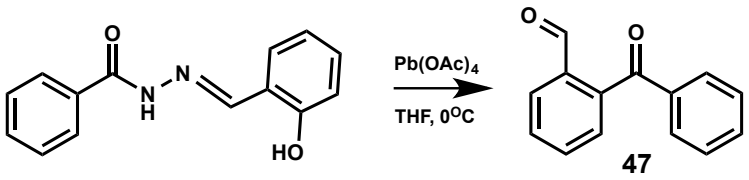

Figure 43. Synthesis of compound 47.

3.19 Synthesis of (47):

At room temperature compound **46** (100 mg, 0.416 mmol) was dissolved in THF (2 ml) at 0^0C, lead tetraacatate (186.21 mg, 0.420 mmol) was gradually added to the solution. The resulting mixture was stirred at 0^OC for 4 hours. Then the solvent was removed under reduced pressure and the organic layer was washed with saturated solution of $NaHCO_3$ and brine and dried over Na_2SO_4. The resulting compound was purified with column chromatography to yield (56.8 mg, 30%). ^{1}H NMR (400 MHz, $CDCl_3$) δ 10.01 (s, 1H), 8.02 – 7.98 (m, 1H), 7.80 – 7.77 (m, 2H), 7.66 (dd, J = 6.1, 2.9 Hz, 2H), 7.61 – 7.54 (m, 2H), 7.49 – 7.43 (m, 3H). ^{13}C NMR ($CDCl_3$, 100 MHz, δ ppm) 196.50, 190.63, 141.28, 137.03, 135.40, 133.65, 133.38, 130.64, 130.19, 129.91, 128.85, 128.66. ESI-HRMS ($M\text{-}H^+$) calculated 211.07571, found 211.07526, Δ= 0.45 ppm

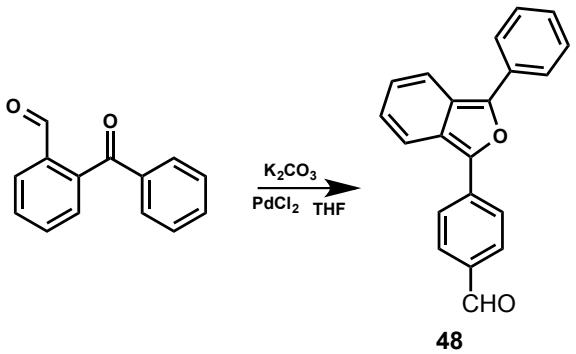

Figure 44. Synthesis of compound 48.

3.20 Synthesis of (48):

$PdCl_2$ (1.18 mg, 0.007 mmol), PPh_3 (1.73 mg, 0.007 mmol), 4-formyl benzeneboronic acid (100 mg, 0.667 mmol) and compound 47 (70.1 mg, 0.333 mmol) were mixed in a round bottom flask. Then dry THF (5 mL) was added under argon. The reacton was monitored by TLC. After the reaction was complete, 4 M HCl (1 mL) was added and mixed for 1 additional hour. Concentrated NaHCO3 was added and extracted with dichloromethane (3x50 mL) and dried ove $NaSO_4$. The product was purified as a sligthly yellow compound (15 mg, 8.72 %).^{1}H NMR (400 MHz, $CDCl_3$) δ 10.09 (s, 1H), 7.99 (t, *J* = 1.8 Hz, 1H), 7.98 (d, *J* = 1.9 Hz, 1H), 7.83 (dd, *J* = 8.4, 1.4 Hz, 1H), 7.79 (t, *J* = 1.7 Hz, 1H), 7.78 (d, *J* = 1.6 Hz, 1H), 7.68 (d, *J* = 1.5 Hz, 1H), 7.67 – 7.65 (m, 1H), 7.54 – 7.48 (m, 3H), 7.47 – 7.44 (m, 1H).

^{13}C NMR ($CDCl_3$, 100 MHz, δ ppm) 191.88, 147,22, 135.25, 132,39, 130.26, 130.05, 130.03, 129,01, 129.00, 128.46, 128.27, 128.26, 127.70, 127,69, 127.37, 127.36. ESI-HRMS ($M-H^+$) calculated 299.10744, found 299.10632, Δ= 1.12 ppm

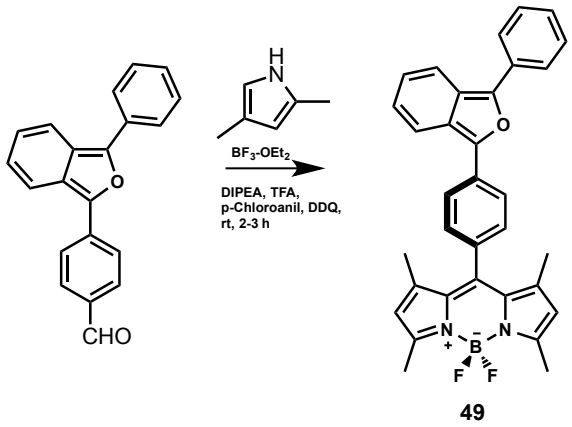

Figure 45. Synthesis of compound 49.

3.21 Synthesis of (49):

To a 500 mL round-bottomed flask containing 250 mL argon-degassed dichloromethane, 2,4-dimethylpyrrole (2.10 mL, 20.5 mmol), compound **48** (20 mg, 0.067 mmol) were added. Then, trifluoroacetic acid (400 µL) was added to the reaction mixture and left to stirr overnight. Then, p-chloranil (2.72 g, 11 mmol) was added and mixed for 1 additional hour. After that, TEA (5 mL) was added and mixed

for 1 additional hour and $BF_3.OEt_2$ (5 mL) was added and the reaction mixture was left to stir at room temperature for 1h. When the starting material was consumed, water (100 mL) was added and the reaction mixture was extracted with DCM (3x100 mL), evaporated and dried over Na_2SO_4. The product was purified by silica gel column chromatography using DCM:Hexane (1:1) to obtatin (2.77 mg, 8%). ^1H NMR (400 MHz, $CDCl_3$) δ 7.79 (d, *J* = 1.7 Hz, 1H), 7.77 (t, *J* = 1.6 Hz, 1H), 7.72 (t, *J* = 1.5 Hz, 1H), 7.71 – 7.69 (m, 1H), 7.54 – 7.48 (m, 2H), 7.43 (dd, *J* = 5.0, 3.7 Hz, 1H), 7.41 – 7.36 (m, 1H), 6.02 (s, 2H), 2.60 (s, 6H), 1.48 (s, 6H).

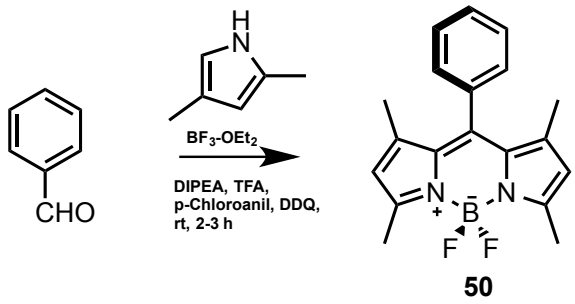

Figure 46. Synthesis of compound 50.

3.22 Synthesis of (50):

To a 500 mL round-bottomed flask containing 250 mL argon-degassed dichloromethane, 2,4-dimethylpyrrole (2.10 mL, 20.5 mmol), benzaldehyde (200 mg, 1.88 mmol) were added. Then, trifluoroacetic acid (400 µL) was added to the reaction mixture and left to stirr overnight. Then, p-chloranil (2.72 g, 11 mmol) was added and mixed for 1 additional hour. After that, TEA (5 mL) was added and mixed for 1 additional hour and $BF_3.OEt_2$ (5 mL) was added and the reaction mixture was left to stir at room temperature for 1h. When the starting material was consumed, water (100 mL) was added and the reaction mixture was extracted with DCM (3x100 mL), evaporated and dried over Na_2SO_4. The product was purified by silica gel column chromatography using DCM:Hexane (1:1) as the eluant and the compound was obtained as purple redish solid (317 mg, 52 %). 1H NMR (400 MHz, CDCl3) δ 7.48-7.50 (m, 3H), 7.29-7.32 (m, 2H), 2.58 (s, 6H), 2.33 (q, J= 15.0 Hz, 4H),1.32 (s, 6H), 1.02 (t, J= 7.4 Hz, 6H). 13C NMR (100 MHz, CDCl3) δ 153.6, 140.2, 138.3,

135.8, 132.7, 131.6, 130.8, 129.3, 129.0, 128.7, 128.2, 17.0, 14.6, 12.4, 11.6 ppm. ESI-HRMS (M-Na+) calculated 402.21639 found 402.22312, Δ= 16.74 ppm

--

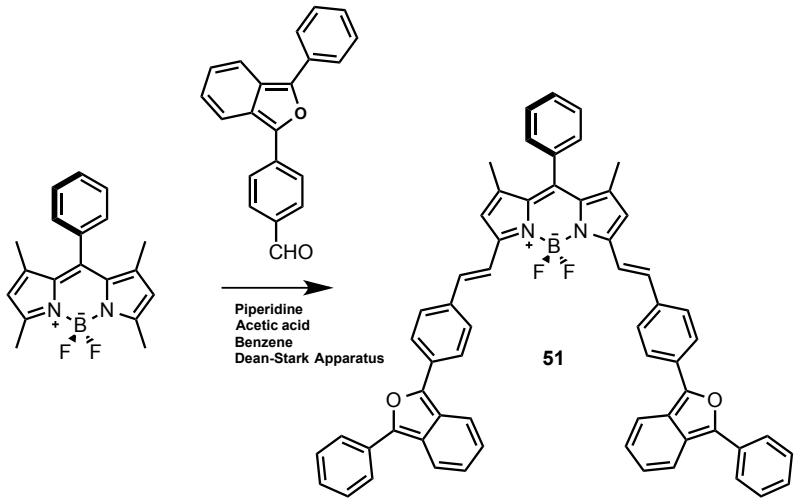

Figure 47. Synthesis of compound 51.

3.23 Synthesis of (51):

Compound **(50)** (38.9 mg, 0.120 mmol) and compound (**48**) (72 mg, 0.241 mmol) were added to a 100 mL round-bottomed flask containing 50 mL benzene and to this solution, piperidine (270 µL, 2.73 mmol) and acetic acid (220 µL, 3.84 mmol) were added. The mixture was heated under reflux at 100 oC overnight by using a Dean Stark trap and it is monitored by TLC. When all the starting material had been consumed, the mixture was cooled to room temperature and the solvent was evaporated. Water (100 mL) was added to the residue and the product was extracted with the DCM (3 x100 mL). The organic phace dried over Na2SO4, evaporated. The residue was purified by silica gel column chromatography using 92:8 (EtOAc: MeOH) solution as the eluant and the compound was obtained as blue solid.

CHAPTER 4

4. Heavy Atom free sensitizers for PDT

4.1 Introduction

Fighting cancer is one of the biggest challenges mankind has ever faced. Finding solutions has not been easy since the time cancer was first discovered. Several solutions have been proposed so far however, the convectional solutions are not safe because they are invasive and have many side effects. Therefore, better solutions are still in search and a lot of money has been spent in this crusade. From the solutions presented in literature, photodynamic therapy is one of the most selective and least invasive methods of fighting cancer.

As stated before in this thesis, three main components are required for photodynamic therapy to work namely; light, oxygen and sensitizer. The most important and most difficult component to manufacture is the sensitizer because there are several constraints on the design of organic molecules to be used in photodynamic therapy. Besides, the sensitizer has to have high triplet quantum yields because the energy responsible for phosphorescence of the sensitizer is transferred to the triplet oxygen, which then yields singlet oxygen.

On the other hand, the hardest challenge is to design these sensitizers to have high triplet quantum yields without any side effects. For instance, several methods to increase triplet quantum yields have been proposed such as; heavy atom incorporation on the sensitizer or known as heavy atom effect, exciton-coupling *e.t.c.* Taking into consideration how the heavy atoms apply to the sensitizer, it is clear that they are favorable and easy to incorporate. However, heavy atoms can cause dark toxicity. So, heavy atom free sensitizers are an alternative to new sensitizers in PDT.

4.2 Objectives

In this project our mission was to synthesize heavy atom free BODIPY cores that are assembled orthogonally to each other. Considering the previous example in literature published by our research group, bis-BODIPY cores are radically different than the parent BODIPY chromophore when it comes to $S_0 \rightarrow S_1$ excitation characteristics. 8,8' and 8,2' bis-BODIPY chromophore combinations were presented in literature and proved to be very efficient for PDT applications. While orthogonal BODIPY molecules are described as linear combination of doubly substituted (DS) configurations, which yield four electrons in four singly occupied orbitals also known as tetra-radical (TR) state, parent BODIPY molecules have a simple HOMO-LUMO substitution. Consequently, DS-TR has a significant effect and correlation with intersystem-crossing since in such molecules, high triplet quantum yields were observed characterized by a strong phosphorescence peak at 1270 nm and also with high singlet oxygen quantum yields. These results lead to a new path in the research of heavy atom free sensitizers with remarkable singlet oxygen effiencies. Moreover, use of cell cultures and trap molecules was also used to prove the production of singlet oxygen generation with BODIPY dimers.

Unfortunately, DS-TR singlet states are destabilized with π- extension so; it is not viable to design photosensitizers with Near-IR absorption. On the other hand, this is desirable since sensitizers should be in the therapeutic window. Nevertheless, with the development of technology, it is possible that in the future such molecules will still be useful even though they are outside the therapeutic window. The easy modifications and substitutions of the BODIPY molecules will make it possible incorporate other moieties to the sensitizers to help achieve elevated triplet quantum yields.

4.3 Synthesis

Akkaya and co-workers synthesized orthogonal BODIPY through formylation reaction (Vilsmeier reaction) of the parent BODIPY. The BODIPY framework was constructed on the formyl group at position 6 of parent BODIPY. In their experiments, they obtained an orange colored compound and no detectable fluorescence. They also synthesized other symmetrical orthogonal BODIPY dyes composed of 8,8' BODIPY dimers. A single absorbance peak was observed at 506 nm so; there is no big difference between the parent BODIPY.[15]

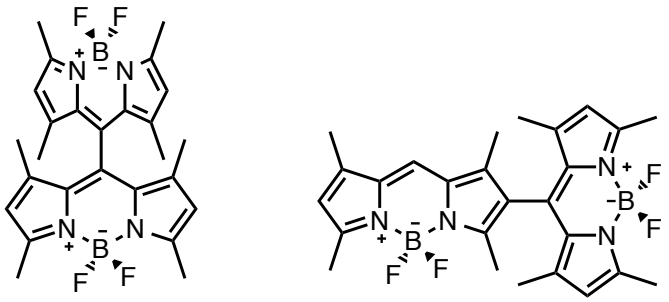

52 53

Figure 48. BODIPY dimers.

In our Project, a similar pathway to the first synthesis was implemented. First 8-Phenyl BODIPY was synthesized and using 2,4-dimethyl pyrrole and then followed by formylation with phosphoryl chloride in DMF. This reaction was straightforward and high yields were obtained up to 80%. The next step was to formylate the second site of the BODIPY since double formylation was required at positions 2 and 6. After both sides were formylated, a BODIPY network was formed and a trimer BODIPY was obtained at consideably high yields. **Compund 33** and **37.** This is illustrated in figure 49.

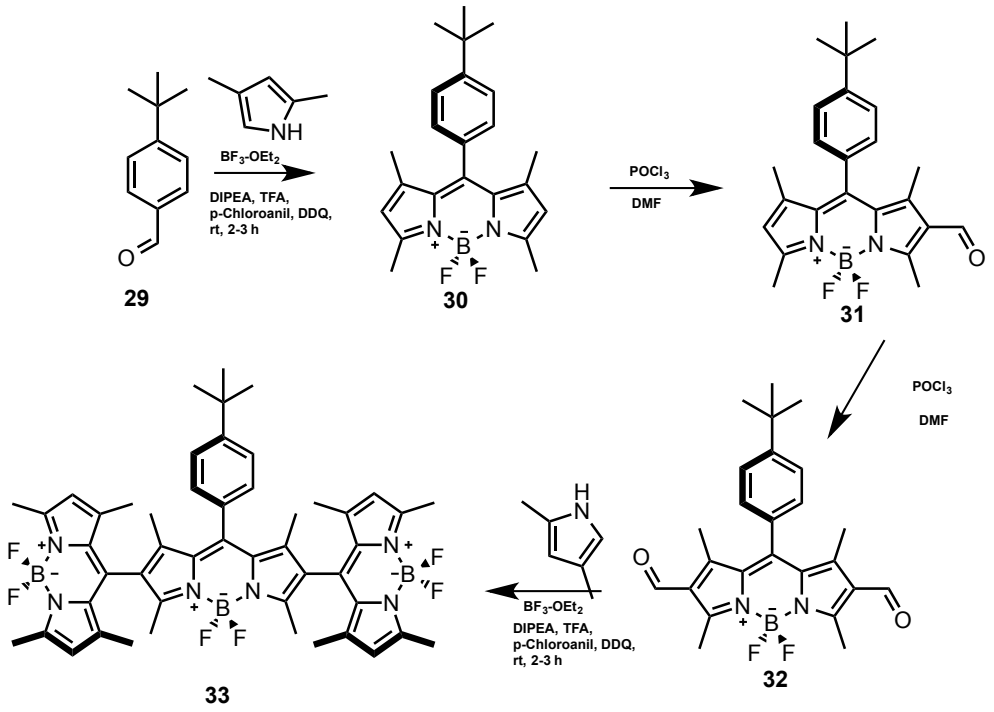

Figure 49. Schematic representation for the synthesis of compound **33**.

A different procedure was followed for the synthesis of compound **43**. An aldol condesation took part at first and the followed by a Michael addition. Both reactions had considerably good yields and were easily purified. After an aza-BODIPY was formed a formylation was done and proceeded to a final BODIPY framework formation.

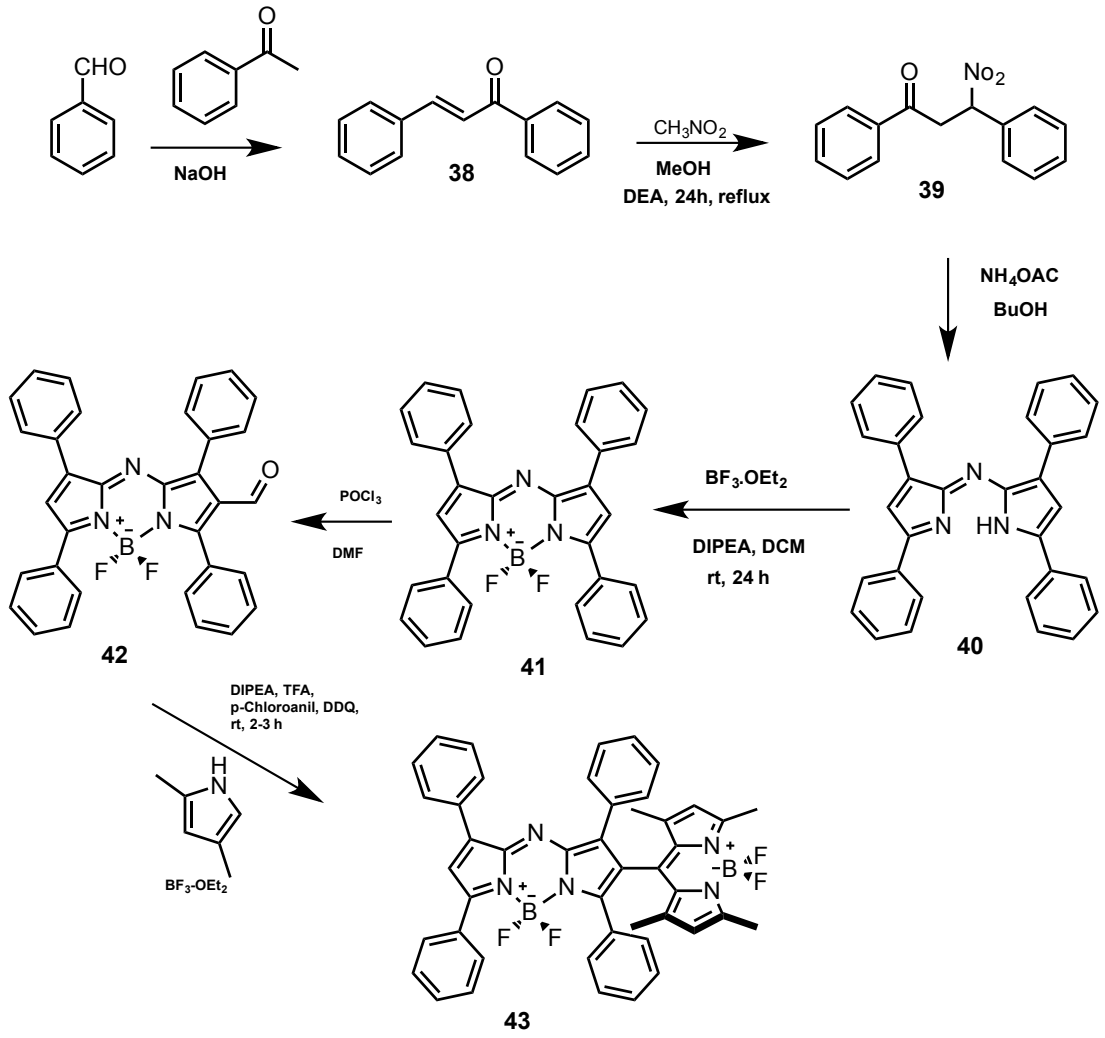

Figure 50. Schematic representation for the synthesis pf compound **43**.

After obtaining compound 33, we performed the PDT experiments. The experiments were performed in organic medium using 1,3-diphenylisobenzofuran (DPBF), a well-known universal scavenger compound because it can trap singlet oxygen easily and can be followed by UV-vis. experiments. It absorbs at 414 nm with a broad range of organic solvents and a decrease in the absorbance maximum is observed upon reaction with singlet oxygen.

We first bubbled molecular oxygen in dichloromethane for 5 min and performed a control experiment where we intended to check if DPBF was affected by the intensity of light we used. If it were affected then we would observe a decrease on the absorption peak only in the presence of light. Since we do not expect singlet

oxygen to be produced in the absence of sensitizer, we were fortunate to not observe any decrease on the absorbance of DPBF at 414 nm.

We performed another control experiment of the sensitizer to check its photo-stability. If the sensitizer is not stable enough then we would observe a decrease on the sensitizers absorbance peak. In this experiment we also bubbled molecular oxygen in dichloromethane for 5 min. However, no decrease was observed on the sensitizer, which was the desired.

4.4 Results and discussion

During the Photodynamic therapy experiments we withdrew the light since we should perform them in the dark. For the excitation of compound **33** we used an external light at 510 nm corresponding to the absorption of the sensitizer for 45 min in 5 min intervals. A clearly perfect decrease on the absorbance of the scavenger with time and number of excitation is observed proving the formation of $^1O_2$ as observed in figure 51.

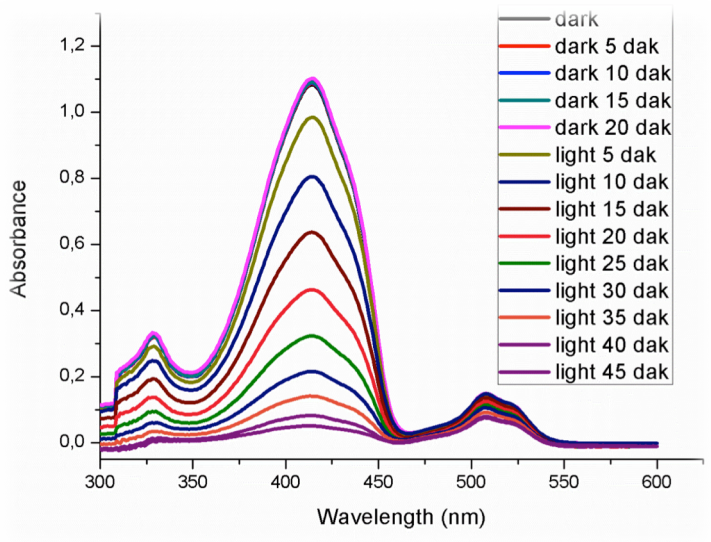

Figure 51. Singlet oxygen generation experiment in DCM solution. Decrease in Absorbance spectrum of trap molecule (DPBF) in the presence of 5.0 μM compound **(33).**

The reason we observe a decrease on DPBF absorbance peak is clearly observable on the reaction below. Figure 52 After reacting with singlet oxygen through a [4+2] cycloaddition DPBF an endoperoxide is formed then due to its instability, it transforms the benzofuran molecule into a carboxylic group. As result, the conjugation is broken and the absorbance maximum of the DPBF decreases since no absorbance is observed for compound **60** in the UV-vis. region.

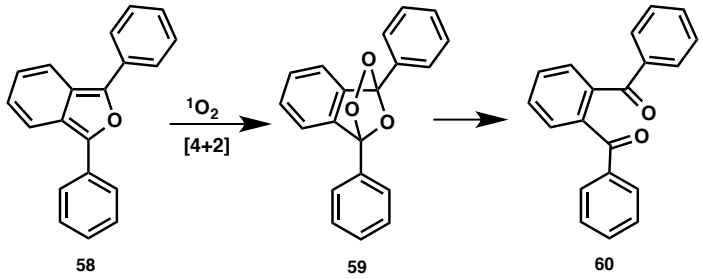

Figure 52. Reaction of singlet oxygen with DPBF.

A quasi-linear was abotained for the decrease in absorbace of DPBF when plotted at constant wavelenght with change in time. This was once again to prove that compound 33 as given in figure 53 produced singlet oxygen.

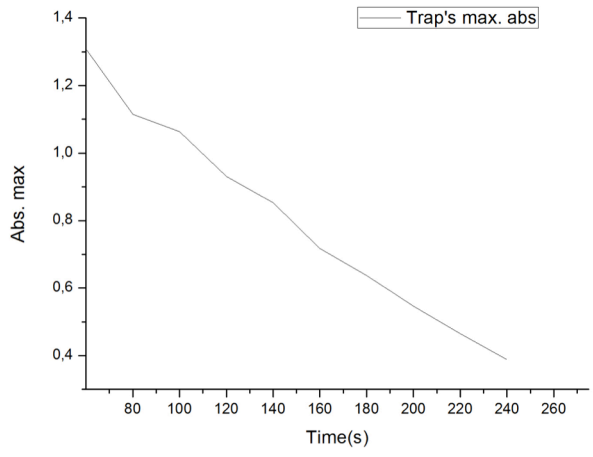

Figure 53. Absorbance decrease of DPBF at 414 nm with time in dichloromethane in the presence of BODIPY photosensitizer **33**.

A similar procedure was followed for compound **37** and the results obtained are reported in figure 54.

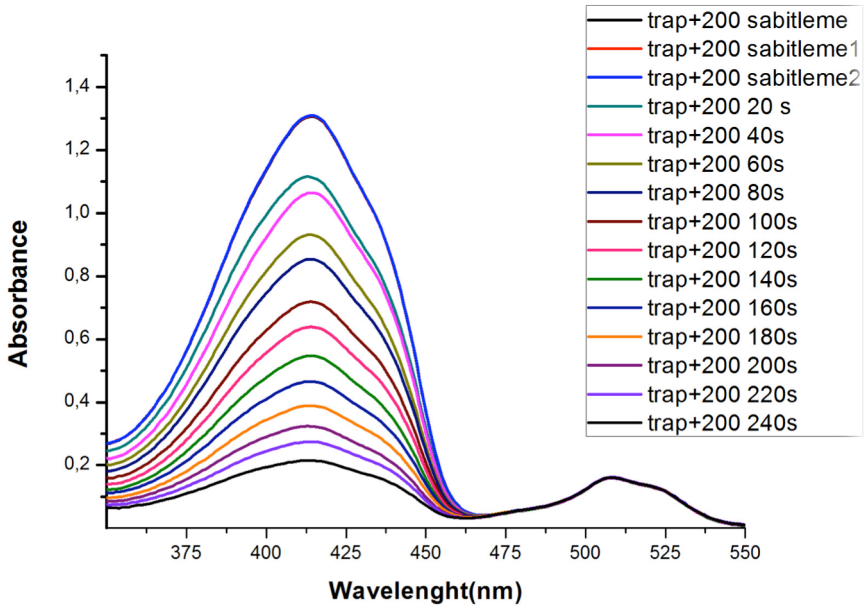

Figure 54. Singlet oxygen generation experiment in DCM solution. Decrease in Absorbance spectrum of trap molecule (DPBF) in the presence of 5.0 µM compound **(37).**

When sensitizer is excited at its absorption wavelenght and there is enough enhancement for intersystem crossing to ocur, then the electron can relax from its triplet excited state to deliver phosphorescence. The phosphorescence energy is transferred to the molecular oxygen already present in the medium and with a small rearrangement it is in the molecular diagrams as shown in figure 55.

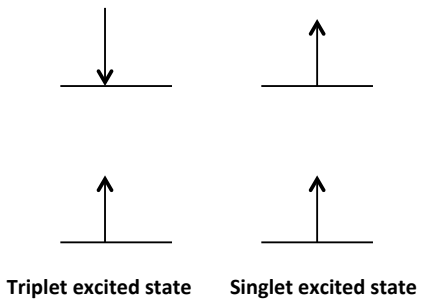

Figure 55. molecular orbitals of triplet and singlet excited states.

A relaxation from singlet excited state to triplet excited state is also possible in phosphorescence means. The phosphorescence energy released in this relaxation is exactly at 1275 nm. Therefore, phosphorescence spectroscopy is another instrument viable to prove the production of singlet oxygen.

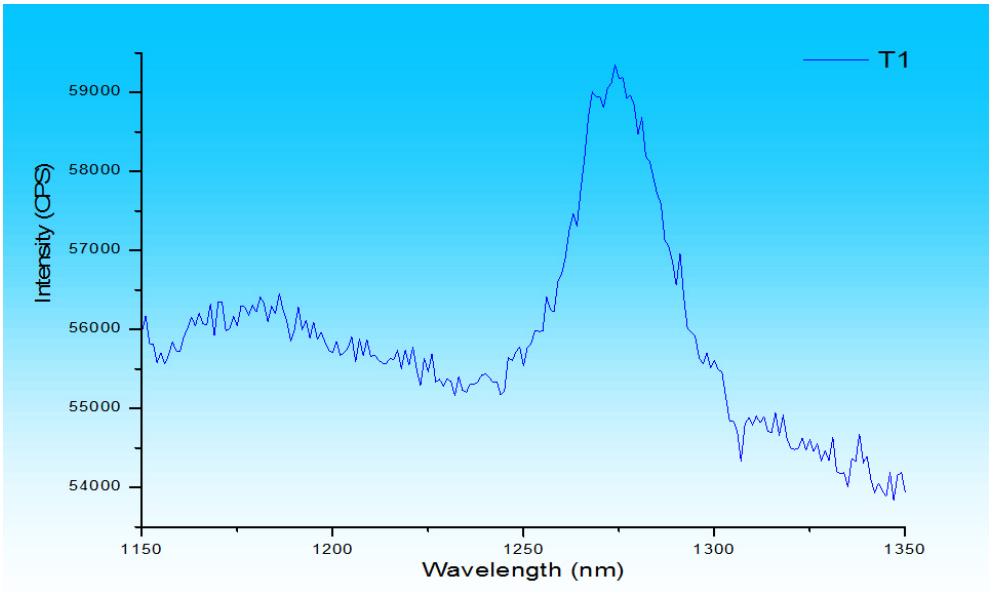

Figure 56. Singlet oxygen phosphorescence with sensitization from compound 33.

Compound **43** was also synthesized in order to prove the working mechanism of the orthogonal BODIPY molecules. As stated before in this thesis, in order for the heavy atom free molecules to work as sensitizers, the molecules assembled to each other must absorb light at the same wavelenght. For instance; compound 33 and compound **37** produced singlet oxygen however, compound **43** did not.

The experiments were performed at the same conditions as compound **33** and compound **37** following the same procedure. DPBF was used as singlet oxygen scavenger and no decrease on the absorbance of the trap molecule was observed. In this case compound **43** presented two different absorbance peaks at higher wavelenghts compared to compounds **33** and **37**. No further experimnts were performed for this compound since no singlet oxygen production was observed.

CHAPTER 5

5. PROGRESS TOWARDS A SINGLET OXYGEN PROBE

5.1 Introduction

Killing cancer is possible with PDT at great extents however; challenges on imaging and detection still prevail. The imaging of cancer cells can be done through several features in the cell itself. The differences in ion concentrations and pH between cancer cells and normal cells have been the greatest asset to imaging and detection. Besides while designing the imaging probes in photodynamic therapy, ICT and PeT are the most commonly used chemical features.

For instance, by attaching a phenyl crown ether on a fluorescent molecule can affect the fluorescence of the same. Here upon excitation, there will be a transfer of electrons from the crown ether to the fluorescent molecule, which will block the fluorescence, but upon binding of an ion to the crown ether, the electron transfer will not be allowed therefore the molecule will be fluorescent. This is known as a Photo-induced electron transfer (PeT) and a detailed explanation in given on the background section of this thesis. The example is given on the illustration on the figure 57.

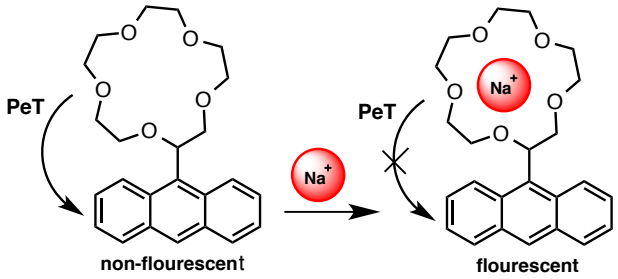

Figure 57. Photo-induced electron transfer example and working principle as sensor.

On the other when a fluorescent molecule's conjugation is extended to an extent by attaching either an electron withdrawing or electron donating group internal charge

transfer (ICT) feature is added to the molecule. For instance, lets take a BODIPY where the conjugation is extended by attaching a pyridine moiety (an electron withdrawing). Upon excitation, the pyridine side of the will be partially negative because it will withdraw electron from the BODIPY molecule. If the withdrawing ability is blocked by an anion then there will be a repulsion that will result in an increase in HOMO-LUMO energy gap. If a cation approaches the negative side of the molecule, then an attraction takes place and this leads to a decrease in the HOMO-LUMO energy gap. Blue shift and red shift take place respectively.

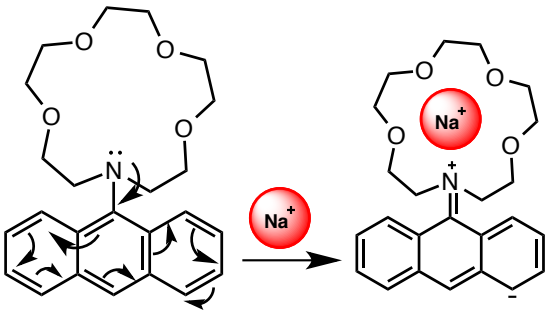

Figure 58. An example of Internal charge transfer with blue shift.

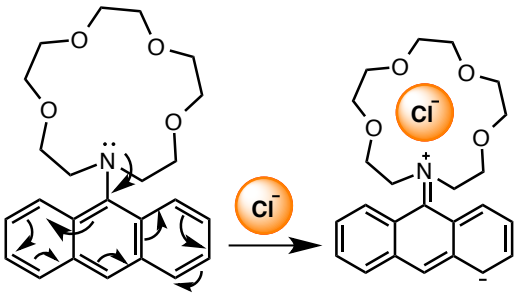

Figure 59. An example of Internal charge transfer with blue shift.

Singlet oxygen is the main and the most important product of photodynamic therapy and so far several instruments have been proposed for its assay. Phosphorescence spectroscopy, UV-vis. and IR spectroscopy are some of such methods. Nevertheless, time-resolved experiments of phosphorescence at 1275 nm are still a challenge for biological systems because singlet oxygen to triplet oxygen phosphorescence quantum yields are typically small around 10^{-6} or smaller. The main reason is the low concentrations of singlet oxygen are usually available. Moreover, IR detectors are no as efficient as UV-vis. optical detectors. As explained on the previous chapter of this

thesis, the PDT experiments are performed using DPBF molecule due to its strong absorbance at 414 nm in DCM solvent. However, DPBF is used for in vitro experiments because of its solubility and the assay would be difficult in vivo.

5.2 Objectives and synthesis of singlet oxygen probe

With all this information in mind, we synthesized an hybrid of a fluorescent molecule and a singlet oxygen scavenger using ICT and PeT features. For our purpose we used BODIPY because it is easy to synthesize and functionalize with good yields. Besides, it is our expertise to functionalize BODIPY molecule for ICT and PeT purposes. To do so, we started with benzoyl chloride reacted with phenol. NaOH was used as a base to remove the acidic proton on phenol group. With 100 % yields hydrozone (**45**) was synthesized to form an imine (**46**) in the next step. The yields of compound **47** were extremely low *ca.* 7%. The same was true for compound **48** with yields around 8%. The idea was to obtain an aldehyde on the DPBF to be able to incorporate BODIPY easily however, due to the low yields only compound **49** was obtained as a crude product.

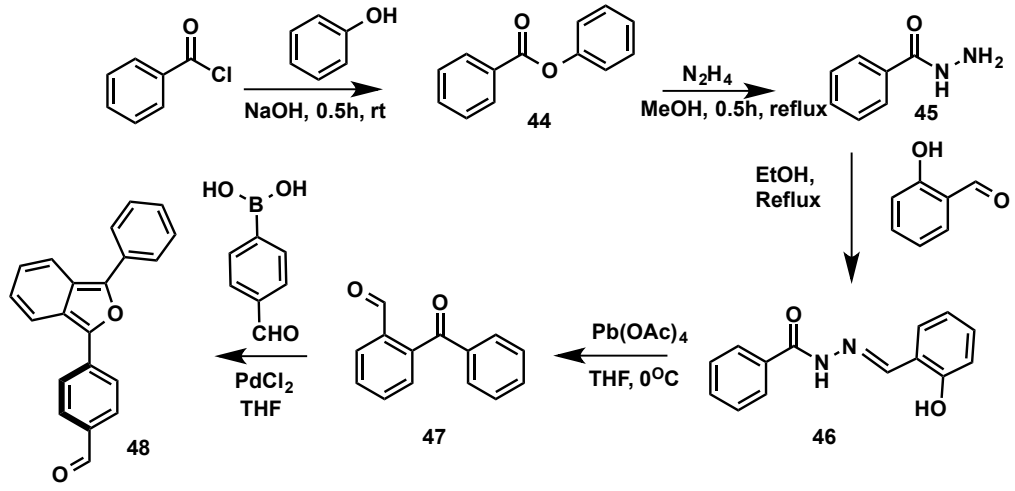

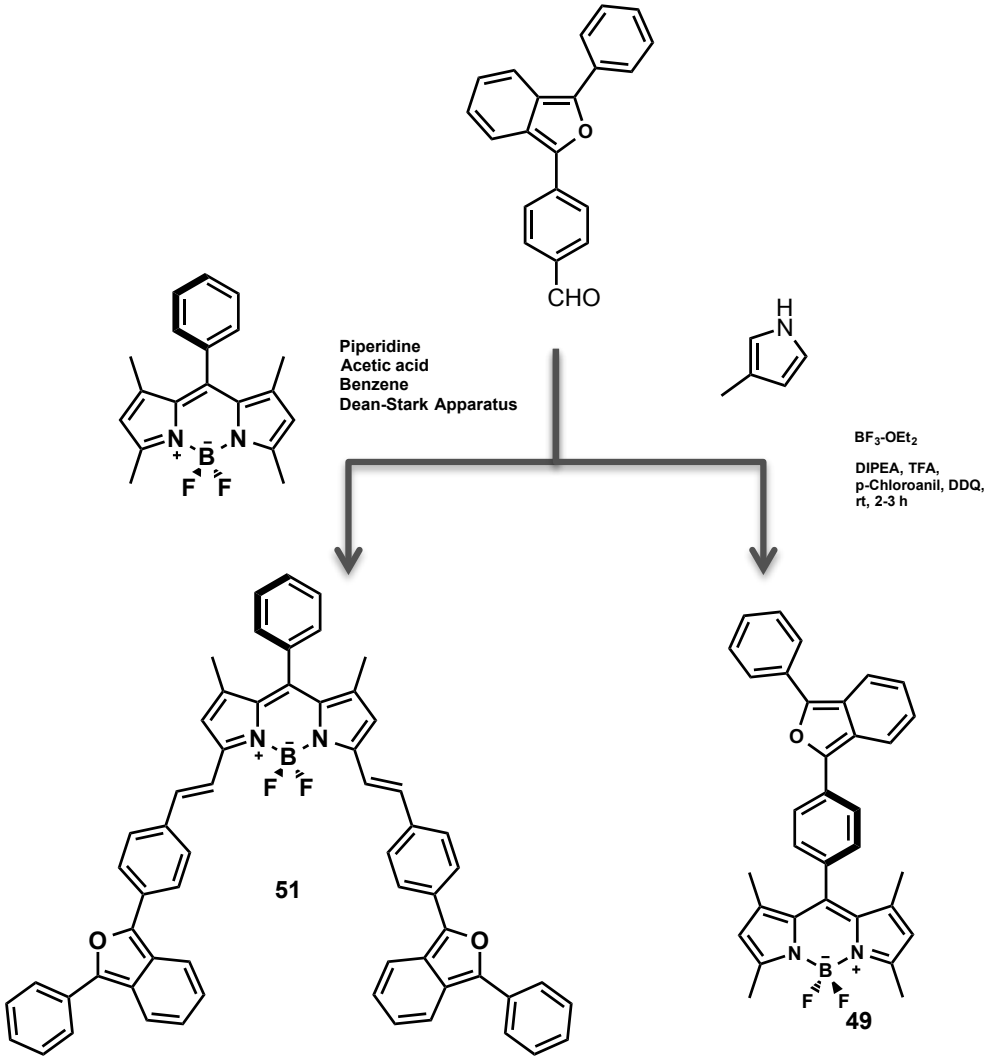

Scheme 1. Representation for the synthesis of compound 49 and 51.

Another problem with this synthesis is that DPBF has a great risk of ring opening even without singlet oxygen but in the presence of light.

In the mass spectroscopy we found out that ring openning takes places slowly as and the formation of electron withdrawing carbonyl groups.

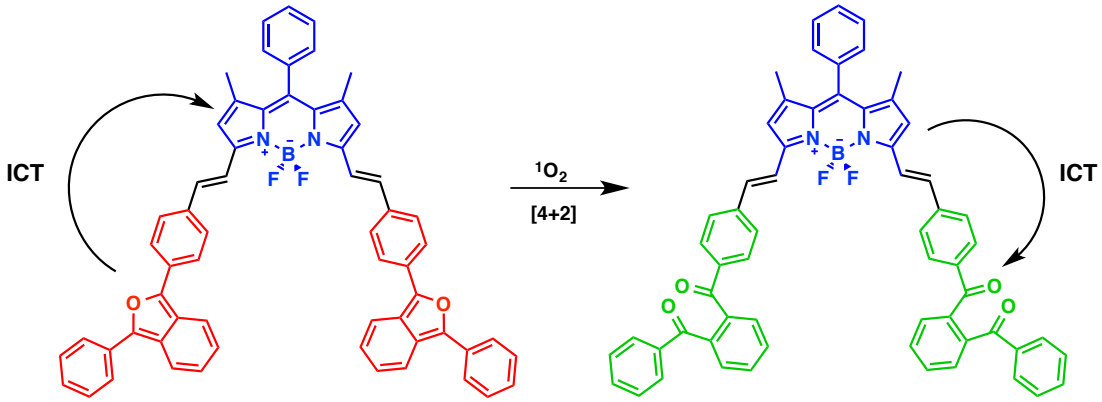

Scheme 2. Expected working mechanism of cmpound 51 upon reaction with singlet oxygen.

In vivo experiments will be performed upon purification of both compounds at higher yields. Oxygen will be bubbled first in dichloromethane, then compound **51** for instance will be added with a sensitizer (Methylene blue). At first, two different absorbance peaks will be observed depending on the photosensitizer used and in this case we propose the use of methylene blue. So one absorption peak will be observed at 666 nm and and the second peak at approximately 550 nm corresponding the singlet oxygen sensor. Upon excitation of the sensitizer, singlet oxygen will be produced which will react with the isobenzofuran forming an endoperoxide. Isobenzofuran acts as an electron donating however, after ring openning will take place we expect carbonyl groups formation that will act as electron withdrawing groups. At this point, we will follow the shift in the absorption peak of the sensor after each excitation. When isobenzofuran is bonded to BODIPY core and it acts as an electron donating group, the BODIPY core will be heavily electron reach and this will cause the BODIPY molecule to absorb at high wavelenghts. Neverheless, when the carbonyl moeities are formed, there will be a drastic decrease in electron density of the BODIPY core and causing it to absorb at lower wavelenghts. Besides, because there is conjugation between BODIPY core and DPBF on compound **51**, upon excitation of the molecule there will be an internat charge transfer from the donating side (DPBF) towards the BODIPY core but the opposite is expected to take place after the carbonyl goup is formed. Meaning that there will be a blue shift. If the decrease is extreme, then even a color change can be observed with a naked eye. However, the presence of a sensitizer (Methylene blue) can somehow block the visibility of this color change since it is as well colorful. As result, the either the

change in color or the shift in the absorption peaks observed on the UV-vis. will prove that the sensor does work as a singlet oxygen sensor. Depending on the photostability of the sensitizer (Methylene blue), a decrease of the absorbance peak with time can also be observed however, the shift absorbance max. of the sensor (compound **51**) is more important.

The design of compound **49** was done such that there is no conjugation possible between compound the BODIPY core and the DPBF. The trick used was; when there are methyl groups on the BODIPY core at position 1,3,5,7 and at position 8 a phenyl group, there will be no rotation possible fort he pheny group because of the steric hindrance cause by the bulky methyl groups. Therefore, if the group bonded to the phenyl group is either and electron donating group or an electron withdrawing group PeT is possible. As stated before, DPBF is expected to work as an electron donating group, so upon excitation of compound 49 in the absence of sensitizer (Methylene blue), a photo-induced electron transfer will take place from the DPBF to the BODIPY core. On the other hand, when the excitation is done in the presence of the sensitizer, the PeT will be blocked because there will be production of singlet oxygen which will react with the DPBF moiety to form carbonyl groups. At this stage, there are two possibilities. First, because of the blocked PeT, a strong increase in flourescence can be observed. The flourescence can be easiliy monitored by flourescence spectroscopy and depending on its intensity, it can be observed with a naked eye. The second possibility can be; to not observe any flourescence increase at all. In this case the possible explanatio would be: because there is a formation of carbonyl groups on the DPBF, reverse PeT would be possible upon excitation. So in this case the excited electron would jump to the nearest upper orbital of the electron withdrawing group as illustrated in **figure 4**.

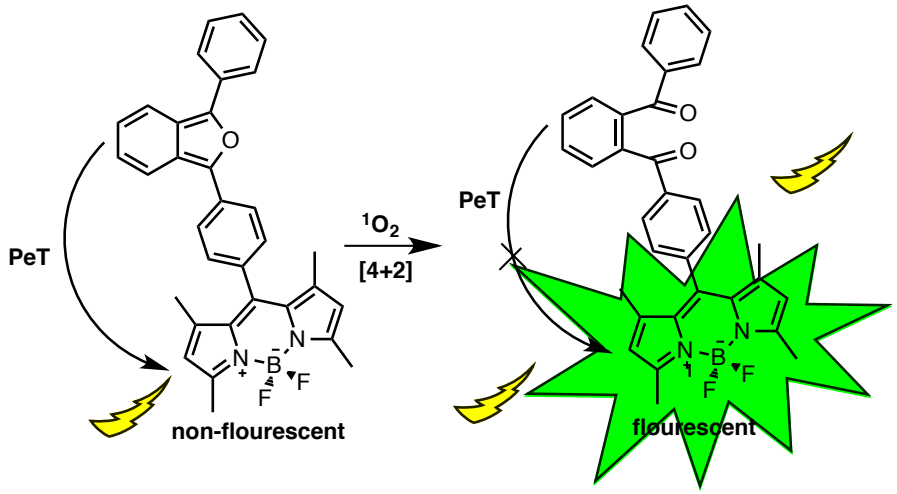

Scheme 3. Expected working mechanism of cmpound 49 upon reaction with singlet oxygen.

5.3 Conclusion

In this thesis we have added two different useful ideas to the PDT research topic. The high triplet quantum yield molecules as desired were designed over the BODIPY core taking advantage of the fact that DS-TR increases the probability of high triplet quantum yields. Orthogonally bonded BODIPY trimmers with absorptions at 507 nm produced singlet oxygen with 0.53 quantum yields. In the future we would like to include water-soluble groups and extend its conjugation in order to bring its use close to the therapeutic window. The second project was the synthesis of a singlet oxygen sensor to be used in vivo in cancer cells. Photo-induced electron transfer and Internal charge transfer are the main mechanisms to be employed by the sensor. High yields were obtained up to a certain extent but the two last steps were of very low yields and the purification of the final product was not possible. Nevertheless, mass spectroscopy and ^{1}H-NMR spectroscopy showed the existence of the desired product. In the future, we hope to successfully purify these compounds with more experiments and different experimental methods. We believe that with a pure product we can easily go on investigating the working principle and mechanism.

Bibliography

1. Stratton, M. R., Campbell, P. J. & Futreal, P. A. The cancer genome. *Nature* **2009**, 458**,** 719–724.

2. Stone, M. J. *et al.* History of the Baylor Charles A. Sammons Cancer Center. *Proc. (Bayl. Univ. Med. Cent).* **2003**, 16**,** 30–58.

3. Korbelik, M. (n.d.). Photodynamic Therapy-Generated Cancer Vaccines. *Methods in Molecular Biology Photodynamic Therapy,* **2012**, 147-153.

4. Rother, K. I. & Harlan, D. M. Science in medicine Challenges facing islet transplantation for the treatment of type 1 diabetes mellitus. *J. Clin. Invest.* **2004**, 114**,** 877–883.

5. Klonisch, T. *et al.* Cancer stem cell markers in common cancers - therapeutic implications. *Trends Mol. Med.* **2008**, 14**,** 450–460.

6. Drucker, B. J. Renal cell carcinoma: Current status and future prospects. *Cancer Treat. Rev.* **2005**, 31**,** 536–545.

7. Shigematsu, H. *et al.* Clinical and biological features associated with epidermal growth factor receptor gene mutations in lung cancers. *J. Natl. Cancer Inst.* **2005**, 97**,** 339–346.

8. Çakmak, Y., & Akkaya, E. (**2008)**. Phenylethynyl-bodipy oligomers: bright dyes and fluorescent building blocks. ANKARA: Middle East Technical university.

9. Su, D. *et al.* Dark to light! A new strategy for large Stokes shift dyes: coupling of a dark donor with tunable high quantum yield acceptors. *Chem. Sci.* **2014**, 5**,** 4812–4818.

10. Ulrich, G., Ziessel, R. & Harriman, A. The chemistry of fluorescent bodipy dyes: Versatility unsurpassed. *Angew. Chemie - Int. Ed.* **2008**, 47**,** 1184–1201.

11. Agostinis, P. et al., Photodynamic therapy of cancer: an update, *CA cancer J. Clin*. **2011**, 61(4), 250-281.

12. Kolemen, S., Cakmak, Y., Kostereli, Z. & Akkaya, E. U. Atropisomeric dyes: Axial chirality in orthogonal bodipy oligomers. *Org. Lett.* **2014**, 16**,** 660–663.

13. Kamholz, a E., Weigl, B. H., Finlayson, B. a & Yager, P. Quantitative analysis of molecular interaction in a microfluidic channel: the T-sensor. *Anal. Chem.* **1999**, 71**,** 5340–5347.

14. Chemosensors, F., Recognition, M., Series, A. C. S. S. & Society, A. C. Fluorescent Chemosensors for Ion and Molecule Recognition. *Instrum. Sci. Technol.* **1994,** 22**,** 405–406.

15. Kölemen, S., Akkaya, E. (**2014**), *fluorescence detection of biological thiols and axially chiral bodipy derivatives & alternative methodologies for singlet oxygen generation for photodynamic action*. ANKARA, Bilkent University.

16. Atkinson, J. K., Cranny, a. W. J., Glasspool, W. V. & Mihell, J. a. An investigation of the performance characteristics and operational lifetimes of multi-element thick film sensor arrays. *Sensors Actuators B*. **1999**, 54**,** 215–231.

17. De Castro, C. S., Sérgio Seixas De Melo, J., Fernández-Lodeiro, A., Núñez, C. & Lodeiro, C. Spectroscopic and photophysical studies of a naphthalene-based emissive probe for metal cations. *Inorg. Chem. Commun.* **2014**, 47**,** 27–32.

18. Putzbach, W. & Ronkainen, N. J. Immobilization techniques in the fabrication of nanomaterial-based electrochemical biosensors: a review. *Sensors (Basel)*. **13,** 4811–4840 (2013).

19. Danuta, F. $ I. *Journal of photochemistry and photobiology* **1988**, 2, 399–408.

20. Andersont, S. R. & Weber, G. Evidence for Preferential Orientation of the Ligand ’. **1969**, 8, 371–377.

21. Shrestha, D., Jenei, A., Nagy, P., Vereb, G. & Szöllősi, J. *Understanding FRET as a Research Tool for Cellular Studies*. *International Journal of Molecular Sciences* **2015**, 16, 6718-6756

22. Kriz, D., Ramstrom, O. & Mosbach, K. Molecular imprinting. New possibilities for sensor technology. *Anal. Chem.* **1997**, 69, 345A–349A.

23. Sudha, B. P., Dixit, N., Moy, V. T. & Vanderkooi, J. M. Reactions of Excited-State Cytochrome-C Derivatives - Delayed Fluorescence and Phosphorescence of Zinc, Tin, and Metal-Free Cytochrome-C at Room-Temperature. *Biochemistry* **1984**, 23, 2103–2107.

24. Venturi, M. The Exploration of Supramolecular Systems and Nanostructures by Photochemical Techniques. *Lect. Notes Chem.* **2012**, 78, 209–225.

25. De Silva, a P., Moody, T. S. & Wright, G. D. Fluorescent PET (photoinduced electron transfer) sensors as potent analytical tools. *Analyst* **2009**, 134, 2385–2393.

26. Valeur, B. Design principles of fluorescent molecular sensors for cation recognition. *Coord. Chem. Rev.* **2000**, 205**,** 3–40.

27. Arimori, S., Bosch, L. I., Ward, C. J. & James, T. D. Fluorescent internal charge transfer (ICT) saccharide sensor. *Tetrahedron lett*. **2001**, 42**,** 4553–4555.

28. Silva, a P. De, Gunaratne, H. N., Lynch, P. L. M., Patty, A. J. & Spence, G. L. (Internal Charge Transfer) Excited States in the Construction of Fluorescent. *Sensors (Peterborough, NH)* (**1993**), 2–7.

29. Lv, Y., Wei, W. E. I. & Xie, Y. A BODIPY-phenol-based sensor for selectively recognizing three basic anions. *J. Chil. Chem. Soc.*, **2015**, 60**,** 2843–2846.

30. Patrice, T., Moan, J. & Peng, Q. An outline in the history of PDT. *Photodyn. Ther.* **2003**, 1–18.

31. Henderson, B. W. & Dougherty, T. J. How does photodynamic therapy work? *Photochem. Photobiol.* **1992**, 55**,** 145–157.

32. Hopper, C. Photodynamic therapy: a clinical reality in the treatment of cancer. (**2000**).

33. Overholt, B. F., Panjehpour, M. & Haydek, J. M. Photodynamic therapy for Barrett ' s esophagus : follow-up in 100 patients. *Gastrointest. Endosc.* **1999**, 49**,** 1–7.

34. O'Connor, A. E., Gallagher, W. M. & Byrne, A. T. Porphyrin and nonporphyrin photosensitizers in oncology: Preclinical and clinical advances in photodynamic therapy. *Photochem. Photobiol.* **2009**, 85**,** 1053–1074.

35. Kotoula, M. G., Tsironi, E. E., Karabatsas, C. H. & Chatzoulis, D. Z. Photodynamic therapy. *Retina* **2005**, 25**,** 102–103.

36. Kamkaew, A. *et al.* BODIPY dyes in photodynamic therapy. *Chem. Soc. Rev.* **2012**, 42, 77–88.

37. Yao, L., Xiao, S. & Dan, F. Boron-fluorine photosensitizers for photodynamic therapy. *J. Chem.* **2013.**

38. Chen, T. C., Huang, L., Liu, C. C., Chao, P. J. & Lin, F. H. Luminol as the light source for in situ photodynamic therapy. *Process Biochem.* **2012**, 47**,** 1903–1908.

39. Ormond, A. B. & Freeman, H. S. Dye sensitizers for photodynamic therapy. *Materials (Basel)*. **2013,** 6, 817–840.

40. Sharma, S., Kumar, D., *Indian J. of Eng. and Mat. Sci.*, **2010**, 17, 231-237.

41. Impert, O. *et al.* Kinetics and mechanism of a fast leuco-Methylene Blue oxidation by copper(II)-halide species in acidic aqueous media. **2003**, 7**,** 348–353.

42. Jockusch, S., Lee, D., Turro, N. J. & Leonard, E. F. Photo-induced inactivation of viruses: adsorption of methylene blue, thionine, and thiopyronine on Qbeta bacteriophage. *Proc. Natl. Acad. Sci. U. S. A.* **1996**, 93, 7446–7451.

43. Chen, Y. *et al.* Apoptosis induced by methylene-blue-mediated photodynamic therapy in melanomas and the involvement of mitochondrial dysfunction revealed by proteomics. *Cancer Sci.* **2003**, 99, 2019–2027.

44. Panzarini, E., Inguscio, V. & Dini, L. Overview of cell death mechanisms induced by rose bengal acetate-photodynamic therapy. *Int. J. Photoenergy* **2011**.

45. Panzarini, E., Inguscio, V., Fimia, G. M. & Dini, L. Rose Bengal Acetate PhotoDynamic Therapy (RBAc-PDT) Induces Exposure and Release of Damage-Associated Molecular Patterns (DAMPs) in Human HeLa Cells. *PLoS One* **2014,** 9, e105778.

46. Ogawa, K. & Kobuke, Y. Nonlinear Absorption by Porphyrin Supramolecules. *210 Nonlinear Opt.* **2004**, 209–224.

47. Matei, C., Tampa, M., Ion, R. M., Neagu, M. & Constantin, C. Photodynamic properties of aluminium sulphonated phthalocyanines in human displazic oral keratinocytes experimental model. *Dig. J. Nanomater. Biostructures* **2012**, 7, 1535–1547.

48. Contakes, S. M., Complexes of phthalocyanines and metallophthalocyanines. *Organometallics* **2000**, 19**,** 4767–4774.

49. Josefsen, L. B. & Boyle, R. W. Photodynamic therapy and the development of metal-based photosensitisers. *Met. Based. Drugs* **2008**.

50. Agostinis, P., Vantieghem, A., Merlevede, W., & Witte, P. (n.d.). Hypericin in cancer treatment: More light on the way. *The International Journal of Biochemistry & Cell Biology,* **2002**, 34, 221-241.

51. Article, R., Abdelhamid, S. & Youssef, T. 2 . Spectroscopic study of water soluble conjugates of hypericin with polyvinylpyrrolidone. *Recent Res. Devel. Photochem. Photobiol,* 9, **2014**,25-34**.**

52. Kubin, A., et. al. Hypericin- the facts about a controversial agent, (**n.d**.), 21, 233-253

53. Buttermeck, V. *et. al*., Long-term efects of st. johns wort and hypericin on monoamine levels in rat hypothalamus and hippocampus, **2002**, 930, 21-29.

54. Bergh, H. and Ballini, J.-P., Principles of photodynamic therapy, Swiss Federal Institute of Technology EPFL, LPAS, CH - 1015 Lausanne, Switzerland. *Mitochondrion,* **2004,** 1–27.

55. Feix, J. B., Anderson, M. S. & Kalyanaraman, B. Enhancement of merocyanine 540 uptake and photodynamic cell killing by salicylates. *Cancer Res.* **1994**, 54**,** 3474–3478.

56. Pervaiz, S. Reactive oxygen-dependent production of novel photochemotherapeutic agents. *FASEB J.* **2001**, 15, 612–617.

57. Dasgupta, S., *Libration, M. M., Microwave, R., Absorption, E., X-ray, V. F. L. & Electron, A. Spectroscopy Techniques and information content*, **2000**.

58. Mehranfar, F., Bordbar, A. & Amiri, R. In Vitro Cytotoxic Activity and Binding Properties of Curcumin in the Presence of β -Casein Micelle Nanoparticles. **2015**, 1, 69–79.

59. Kumar, A. et. al., Photophysics and photochemistry of organometallic rhenium diimine complexes, Top. *Organomet. Chem.* **2010**, 29, 1-35.

60. Derosa, M. C. & Crutchley, R. J. Photosensitized singlet oxygen and its applications. *Coordination Chem. Rev*. **2002,** 351-371**.**

61. Lee, S. *et al.* In vivo PDT dosimetry : singlet oxygen emission and photosensitizer fluorescence, **2011**.

62. Hamblin, Michael R.; Hasan, T. Photodymamic therapy: a new antimicrobial approach to infectious disease? *Photochem Photobiol Sci.* **3,** 436–450 (2014).

63. Flyen, A. Photosensitization. *Diseases of Sheep,* **2007,** 338-342.

64. Question, E. 28-4 The Pauli Exclusion Principle. **1958**, 10–11.

65. Duffey, G. Quantum Mechanical Operators. *A Development of Quantum Mechanics,* **1946,** 143-172.

66. Wilkinson, F. (1962). Transfer Of Triplet State Energy And The Chemistry Of Excited States. *J. Phys. Chem.,* **1962**, 66, 2569-2574.

67. Yersin, H. & Finkenzeller, W. J. *Triplet Emitters for Organic Light-Emitting Diodes: Basic Properties*. *Highly Efficient OLEDs with Phosphorescent Materials*, **2008**.

68. Steffen, A. et al. Fluorescence in rhoda- and iridacyclopentadienes neglecting the spin-orbit coupling of the heavy atom: the ligand dominates. *Inorg. Chem.* **2014**, 53, 7055-7069

69. Coupling of Angular Momentum and Spectroscopic Term Symbols. (n.d.). Retrieved July 28, **2015**.

70. Dillingham, I., Dykes, J. & Wood, J. City Research Online. *City Res. Online - City Univ. London* **2012**, 14–16.

71. Kuemmeth, F., SPIN STATES AND SPIN-ORBIT COUPLING IN NANOSTRUCTURES. (**2008)**, Cornell University, PhD dissertation.

72. Parnis, M. *Spin-Orbit Coupling and Atomic State (Term) Symbols.* Trent University, website:www.trentu.ca/chemistry/documents/termsymbols.pdf

73. Islam,D.-M. and Osamu I., Solvent effects on rates of photochemical reactions of rose bengal triplet state studied by nanosecond laser photolysis, *J. of Phot. and Photobiol.* **1999**, 123, 53-59

74. Cakmak, Y. *et al.* Designing excited states: Theory-guided access to efficient photosensitizers for photodynamic action. *Angew. Chemie - Int. Ed.* **2011**, 50, 11937–11941.

75. O. Berndt, F. Bandt, I. Eichwurzel and H. Stiel, Picosecond transient absorption of xanthene dyes, *A CTA PHYSICA POLONICA A,* **1999**, 95, 207-220.

76. Kearvell, a. & Wilkinson, F. Fluorescence Quenching and External Spin-Orbit Coupling Effects. *Mol. Cryst.* **1968**, 4, 69–81.

77. Korol, N. V, Klimenko, V. G., Kir, T. A., Serov, S. A. & Gastilovich, E. A. Internal heavy-atom effect on spin – orbit and vibronic – spin – orbit coupling : n p) phosphorescence of 9 , 10-anthraquinone haloderivatives. *Chem. Phys*. **1999,** 248, 233-246 .

78. Atilgan, S., Kutuk, I., & Ozdemir, T. (n.d.). A near IR di-styryl BODIPY-based ratiometric fluorescent chemosensor for Hg(II). *Tetrahedron Letters,* **2010**, 892-894.

79. Gabe, Y., Urano, Y., Kikuchi, K., Kojima, H. & Nagano, T. Highly sensitive fluorescence probes for nitric oxide based on boron dipyrromethene chromophore-rational design of potentially useful bioimaging fluorescence probe. *J. Am. Chem. Soc.* **2004**, 126**,** 3357–3367.

80. Atilgan, S., Ekmekci, Z., Dogan, A., Guc, D., & Akkaya, E. (n.d.). Water soluble distyryl-boradiazaindacenes as efficient photosensitizers for photodynamic therapy. *Chem. Commun.,* **2006**, 42, 4398-4398.

81. Awuah, S. G. & You, Y. Boron dipyrromethene (BODIPY)-based photosensitizers for photodynamic therapy. *RSC Adv.* **2012**, 2, 11169.

82. Komatsu, T. *et al.* Rational design of boron dipyrromethene (BODIPY)-based photobleaching-resistant fluorophores applicable to a protein dynamics study. *Chem. Commun. (Camb).* **2011**, 47, 10055–10057.

83. Berezin, M., & Achilefu, S. (2010). Fluorescence Lifetime Measurements and Biological Imaging. *Chemical Reviews Chem. Rev.,* **2010**, 110, 2641-2684.

84. Yu-Tzu Li, E., Jiang, T.-Y., Chi, Y. & Chou, P.-T. Semi-quantitative assessment of the intersystem crossing rate: an extension of the El-Sayed rule to the emissive transition metal complexes. *Phys. Chem. Chem. Phys.* **2014**, 16**,** 26184–26192.

85. Webster, S. *et al.* Near-unity quantum yields for intersystem crossing and singlet oxygen generation in polymethine-like molecules: Design and experimental realization. *J. Phys. Chem. Lett.* **2010**, 1**,** 2354–2360.

86. Ramirez, M. A. *et al.* Novel linear and V-shaped D-π-A+-π-D chromophores by Sonogashira reaction. *Arkivoc* **2011,** 140–155.

87. Matile, S., Berova, N., Nakanishi, K., Fleischhauer, J. & Woody, R. W. Structural studies by exciton coupled circular dichroism over a large distance: Porphyrin derivatives of steroids, dimeric steroids, and brevetoxin B. *J. Am. Chem. Soc.* **1996**, 118**,** 5198–5206.

88. Bruhn, T. *et al.* Axially Chiral BODIPY DYEmers: An Apparent Exception to the Exciton Chirality Rule. *Angew. Chemie Int. Ed.* **2014**, 53**,** 14592–14595.

89. Yagai, S., Iwai, K., Karatsu, T. & Kitamura, A. Photoswitchable exciton coupling in merocyanine-diarylethene multi-chromophore hydrogen-bonded complexes. *Angew. Chemie - Int. Ed.* **2012**, 51**,** 9679–9683.

90. Wang, H. *et al.* Multifunctional TiO2 nanowires-modified nanoparticles bilayer film for 3D dye-sensitized solar cells. *Optoelectron. Adv. Mater. Rapid Commun.* **2010**, 4**,** 1166–1169.

91. Benniston, A., Copley, G., Harriman, A., Howgego, D., Harrington, R., & Clegg, W. (2010). Cofacial Boron Dipyrromethene (Bodipy) Dimers: Synthesis, Charge Delocalization, and Exciton Coupling. *The Journal of Organic Chemistry J. Org. Chem.,* **2010**, 75, 2018-2027.

92. Matile, S., Berova, N. & Nakanishi, K. Porphyrins: Powerful chromophores for structural studies by excitation-coupled circular dichromism, *J. Am. Chem. Soc.* **1995**, 1**,** 7021–7022.

93. Jiménez-hoyos, C. A. & Gustavo, E. fullerene molecules : An ab initio non-collinear Hartree – Fock study. **2014**, 1–41

94. Ito, O. & D'Souza, F. Recent Advances in Photoinduced Electron Transfer Processes of Fullerene-Based Molecular Assemblies and Nanocomposites. *Molecules* **2012**, 17**,** 5816–5835.

95. Huang, L., Yu, X., Wu, W. & Zhao, J. Styryl Bodipy-C 60 dyads as efficient heavy-atom-free organic triplet photosensitizers. *Org. Lett.* **2012**, 14**,** 2594–2597.

96. Bracher, P. J. & Schuster, D. I. Electron Transfer in Functionalized Fullerenes by. *Fullerenes From Synth. to Optoelectron. Prop.* **2002,** 163-212.

97. Dubacheva, G. V, Liang, C. & Bassani, D. M. Functional monolayers from carbon nanostructures – fullerenes , carbon nanotubes , and graphene – as novel materials for solar energy conversion. *Coord. Chem. Rev.* **2012**, 256**,** 2628–2639.

98. Kim, H. J. & Kim, J. S. BODIPY appended cone-calix[4]arene: selective fluorescence changes upon Ca2+ binding. *Tetrahedron Lett.* **2006**, 47**,** 7051–7055.

99. Erten-Ela, S. *et al.* A panchromatic boradiazaindacene (BODIPY) sensitizer for dye-sensitized solar cells. *Org. Lett.* **2008**, 10**,** 3299–3302.

100. Hecht, M., Kraus, W. & Rurack, K. A highly fluorescent pH sensing membrane for the alkaline pH range incorporating a BODIPY dye. *Analyst* **2012**, 325–332.

101. Cakmak, Y. & Akkaya, E. U. Phenylethynyl-BODIPY oligomers: Bright dyes and fluorescent building blocks. *Org. Lett.* **2009**, 11**,** 85–88.

102. Coskun, A., Baytekin, B. T. & Akkaya, E. U. Novel fluorescent chemosensor for anions via modulation of oxidative PET: A remarkable 25-fold enhancement of emission. *Tetrahedron Lett.* **2003**, 44**,** 5649–5651.

103. Ekmekci, Z., Yilmaz, M. D. & Akkaya, E. U. A monostyryl-boradiazaindacene (BODIPY) derivative as colorimetric and fluorescent probe for cyanide ions. *Org. Lett.* **2008**, 10**,** 461–464.

104. Li, L., Nguyen, B. & Burgess, K. Functionalization of the 4,4-difluoro-4-bora-3a,4a-diaza-s-indacene (BODIPY) core. *Bioorganic Med. Chem. Lett.* **2008**, 18**,** 3112–3116.

105. Schmitt, A., Hinkeldey, B., Wild, M. & Jung, G. Synthesis of the core compound of the BODIPY dye class: 4,4'-difluoro-4-bora-(3a,4a)-diaza-s-indacene. *J. Fluoresc.* **2009**, 19**,** 755–758.

106. Atilgan, S., Ekmekci, Z., Dogan, a L., Guc, D. & Akkaya, E. U. Water soluble distyryl-boradiazaindacenes as efficient photosensitizers for photodynamic therapy. *Chem. Commun. (Camb).* **2006**, 4398–4400.

107. Galletta, M. *et al.* Absorption spectra, photophysical properties, and redox behavior of ruthenium(II) polypyridine complexes containing accessory dipyrromethene-BF 2 chromophores. *J. Phys. Chem. A* **2006**, 110, 4348–4358.

108. Zhu, S. *et al.* Highly water-soluble BODIPY-based fluorescent probes for sensitive fluorescent sensing of zinc(ii). *J. Mater. Chem. B* **2013**, 1**,** 1722.

109. Li, L., Han, J., Nguyen, B. & Burgess, K. Syntheses and spectral properties of functionalized, water-soluble BODIPY derivatives. *J. Org. Chem.* **2008**, 73**,** 1963–1970.

110. Songlin, N. Advanced water soluble BODIPY dyes : Synthesis and application. **2011**., Strasbourg, University of Strasbourg.

111. Fan, G., Yang, L. & Chen, Z. Water-soluble BODIPY and aza-BODIPY dyes: synthetic progress and applications. *Front. Chem. Sci. Eng.* **2014**, 8, 405–417.

112. Alemdaroglu, F. E. *et al.* Poly(BODIPY)S: A new class of tunable polymeric dyes. *Macromolecules* **2009**, 42**,** 6529–6536.

113. Jameson, L. P. & Dzyuba, S. V. Aza-BODIPY: Improved synthesis and interaction with soluble Aβ1-42 oligomers. *Bioorganic Med. Chem. Lett.* **2013**, 23**,** 1732–1735.

APPENDIX A - NMR SPECTRA

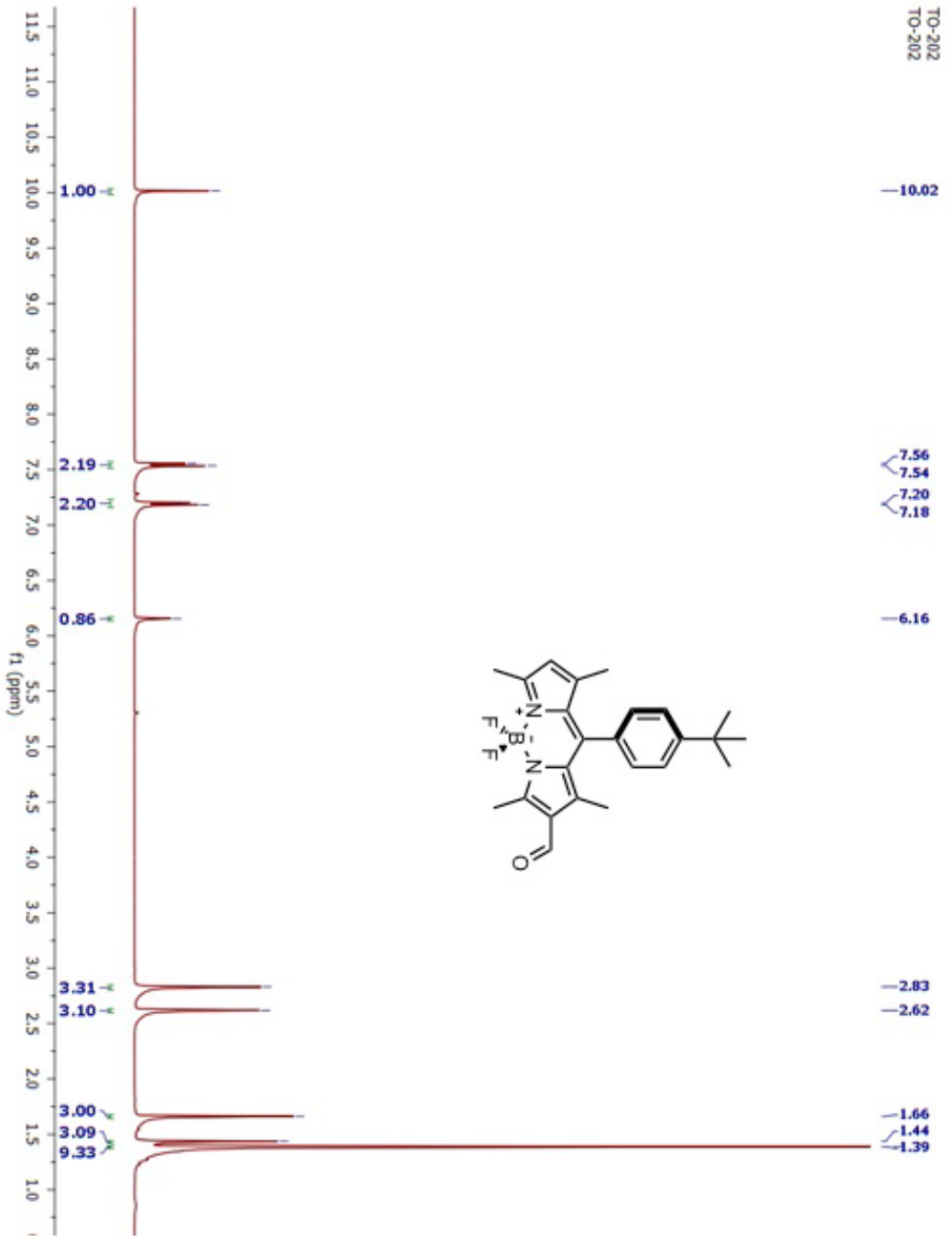

Figure 60. ^{1}H-NMR of compound 31

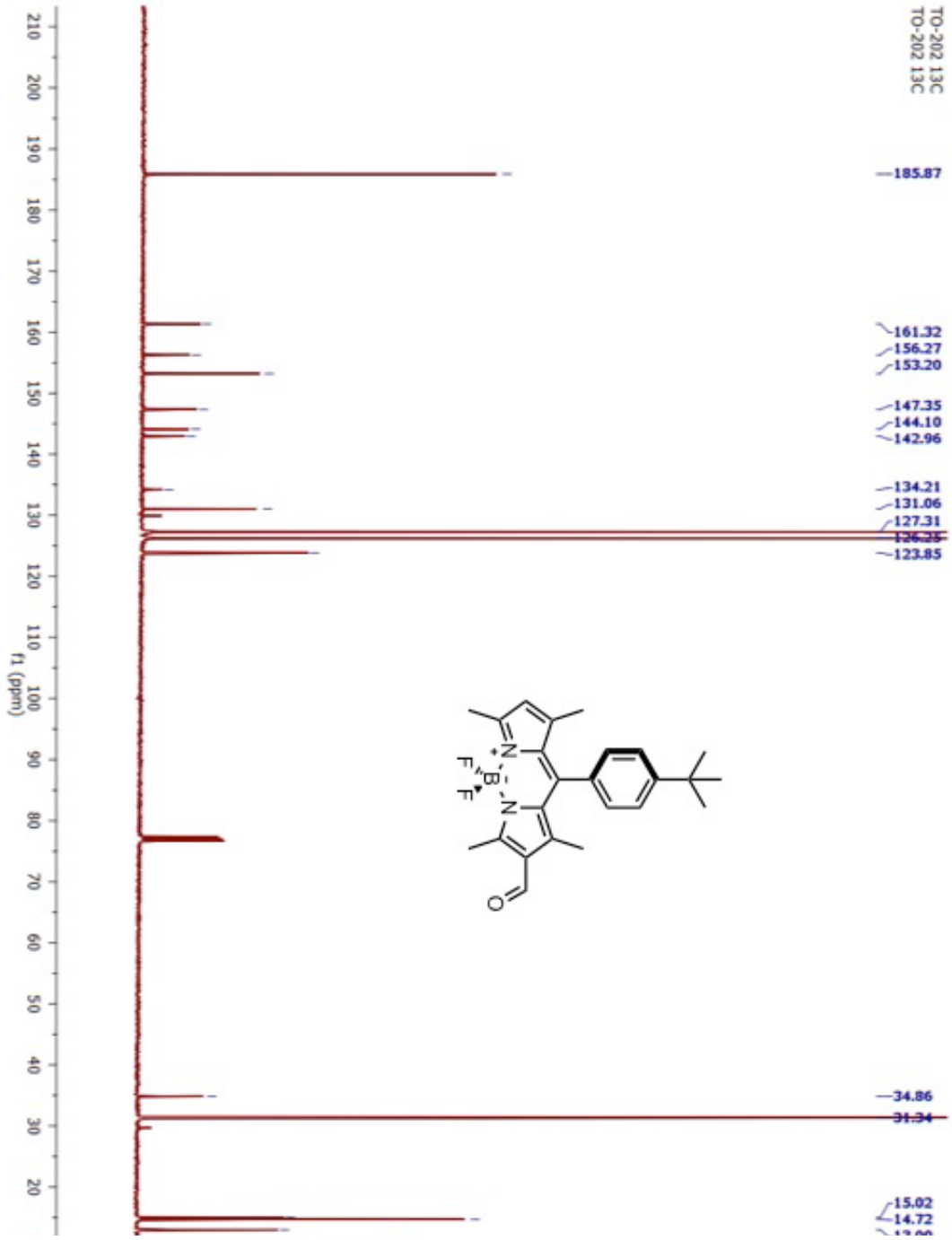

Figure 61. ^{13}C-NMR of compound 31

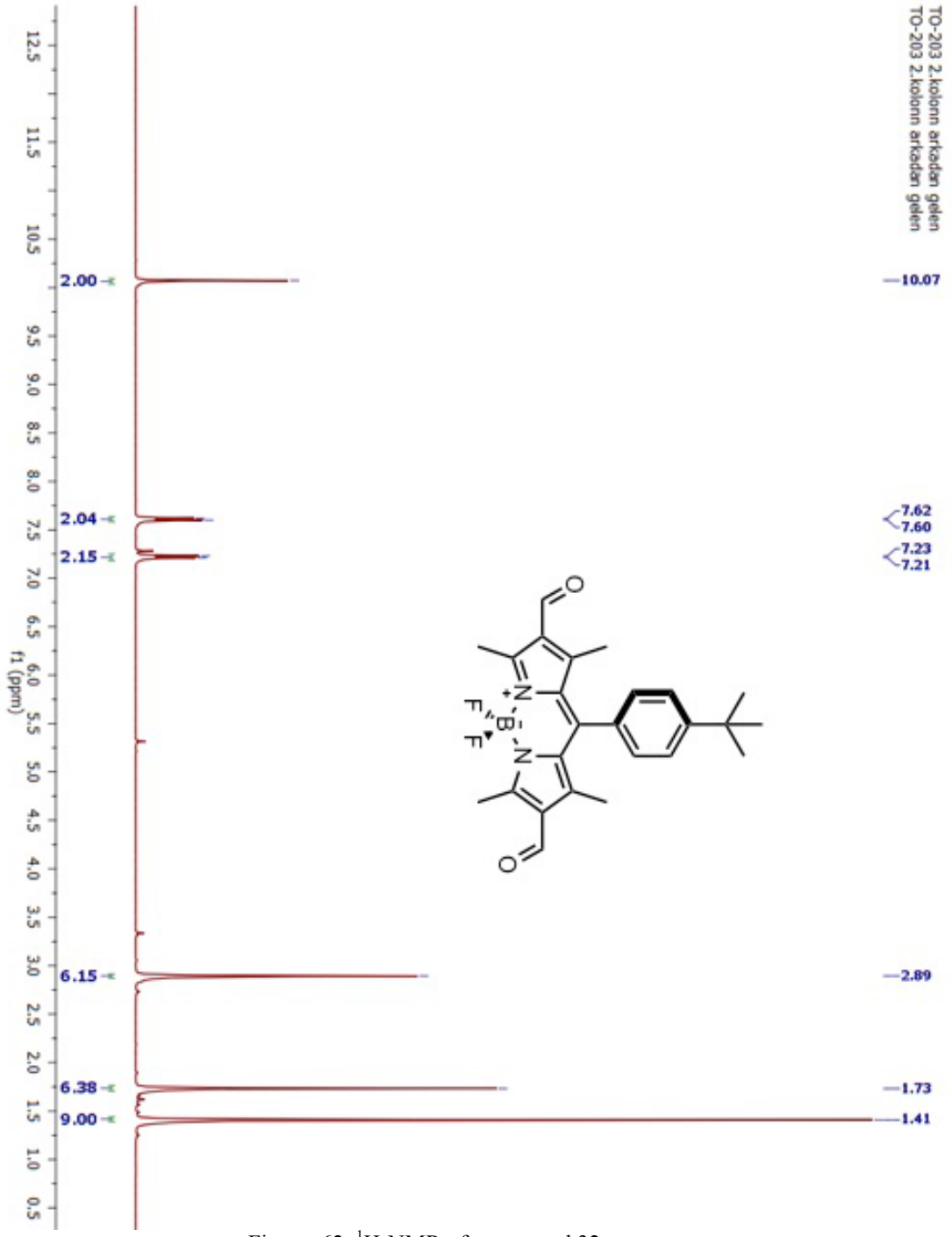

Figure 62. ^{1}H-NMR of compound 32

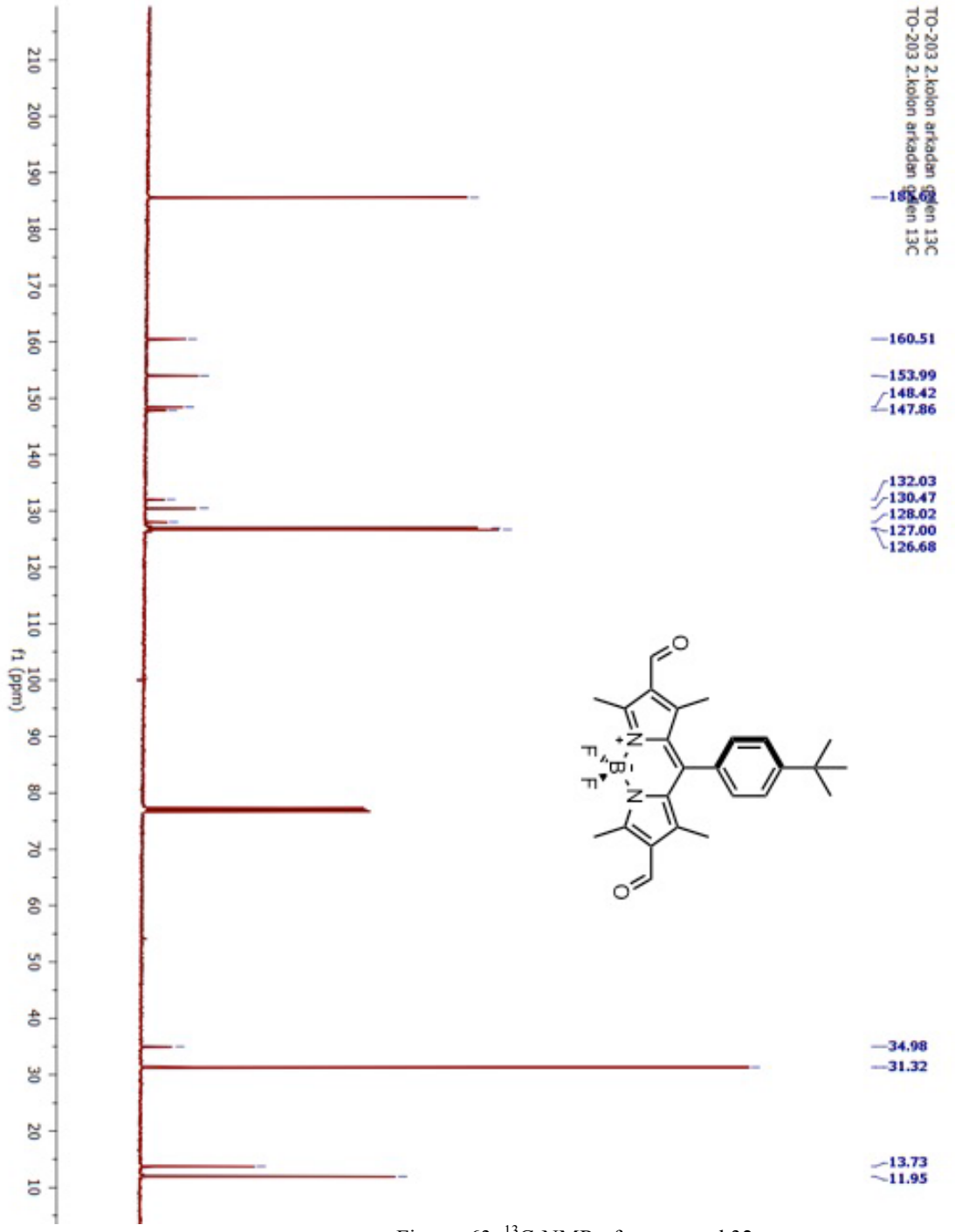

Figure 63. ^{13}C-NMR of compound 32

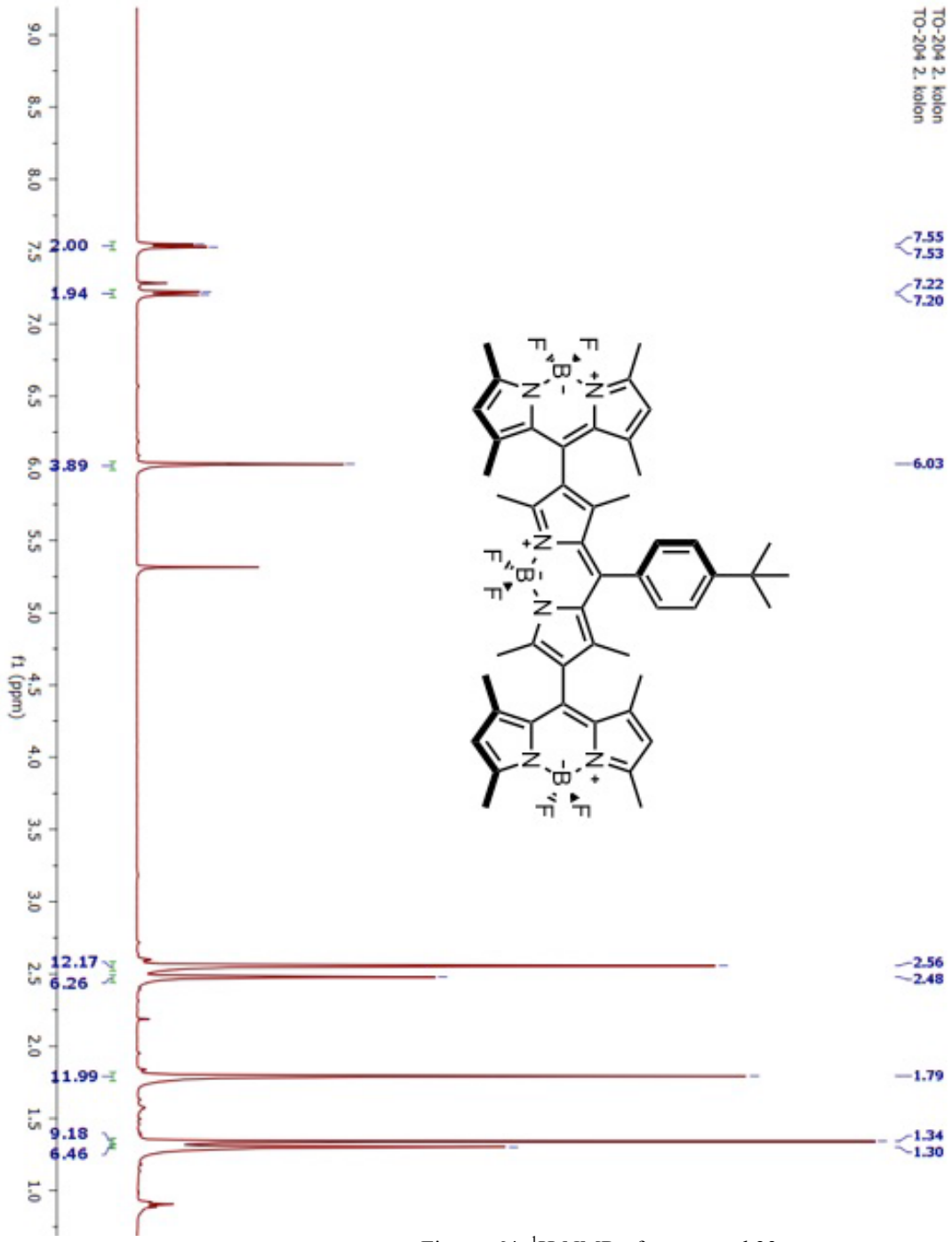

Figure 64. ^{1}H-NMR of compound 33

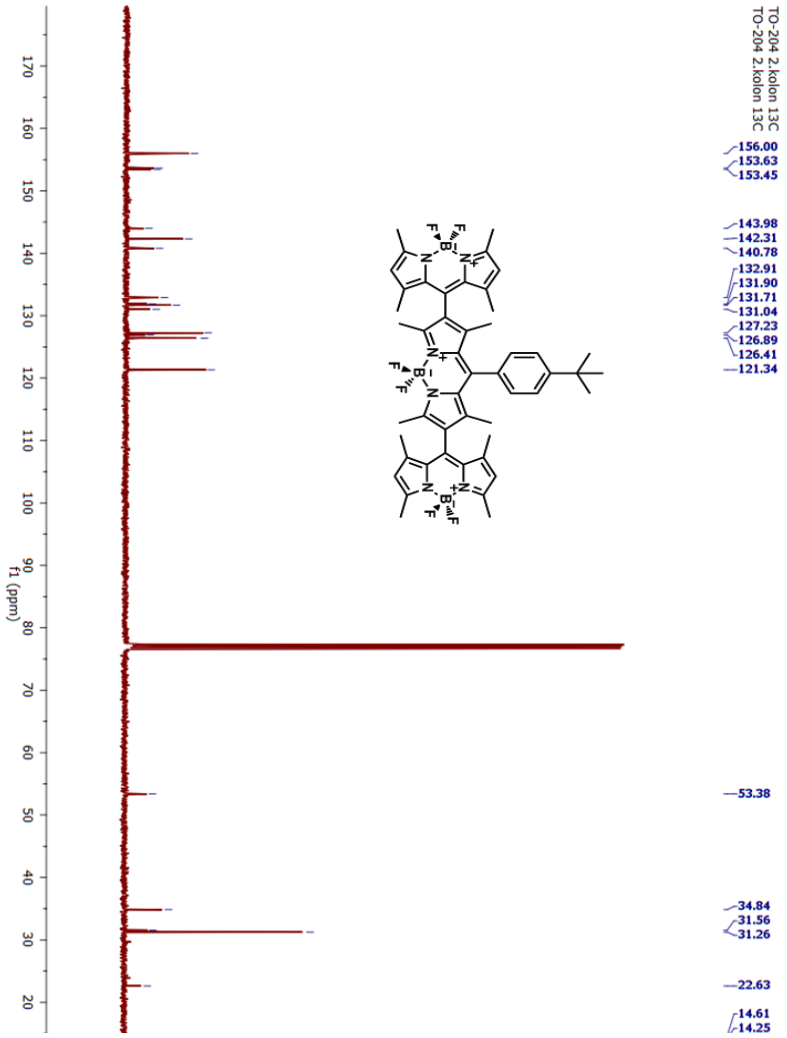

Figure 65. ^{13}C-NMR of compound 33

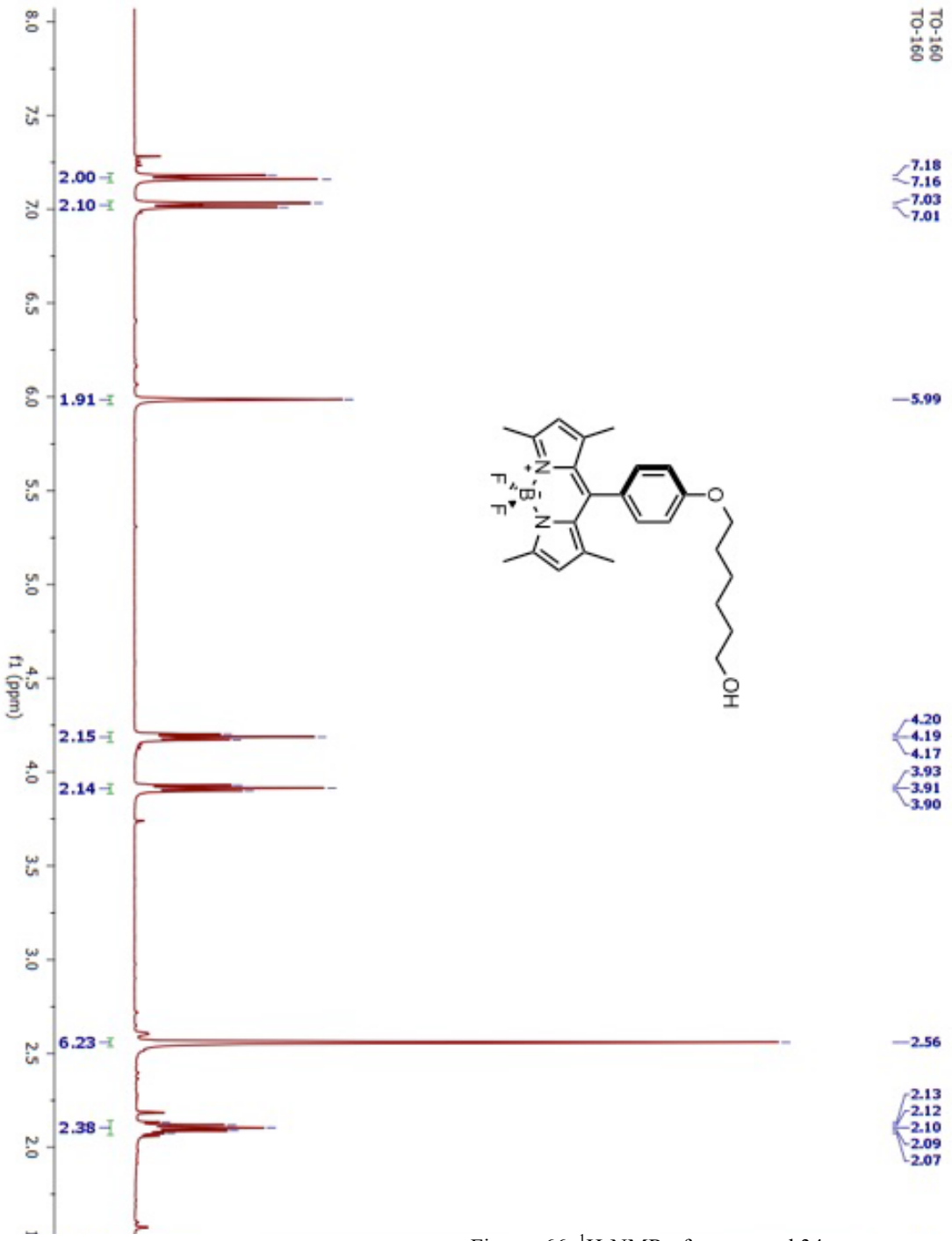

Figure 66. ^{1}H-NMR of compound 34

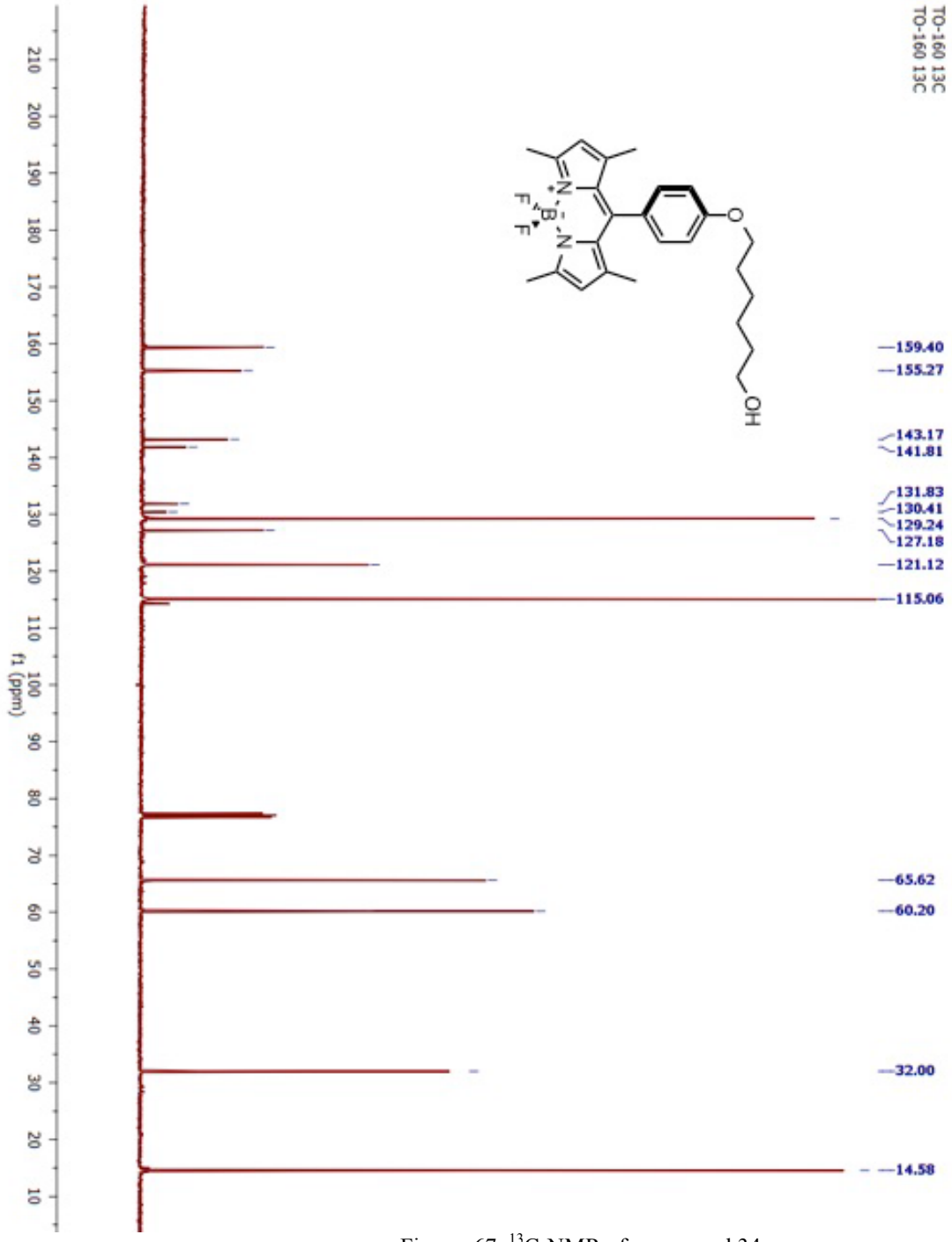

Figure 67. ^{13}C-NMR of compound 34

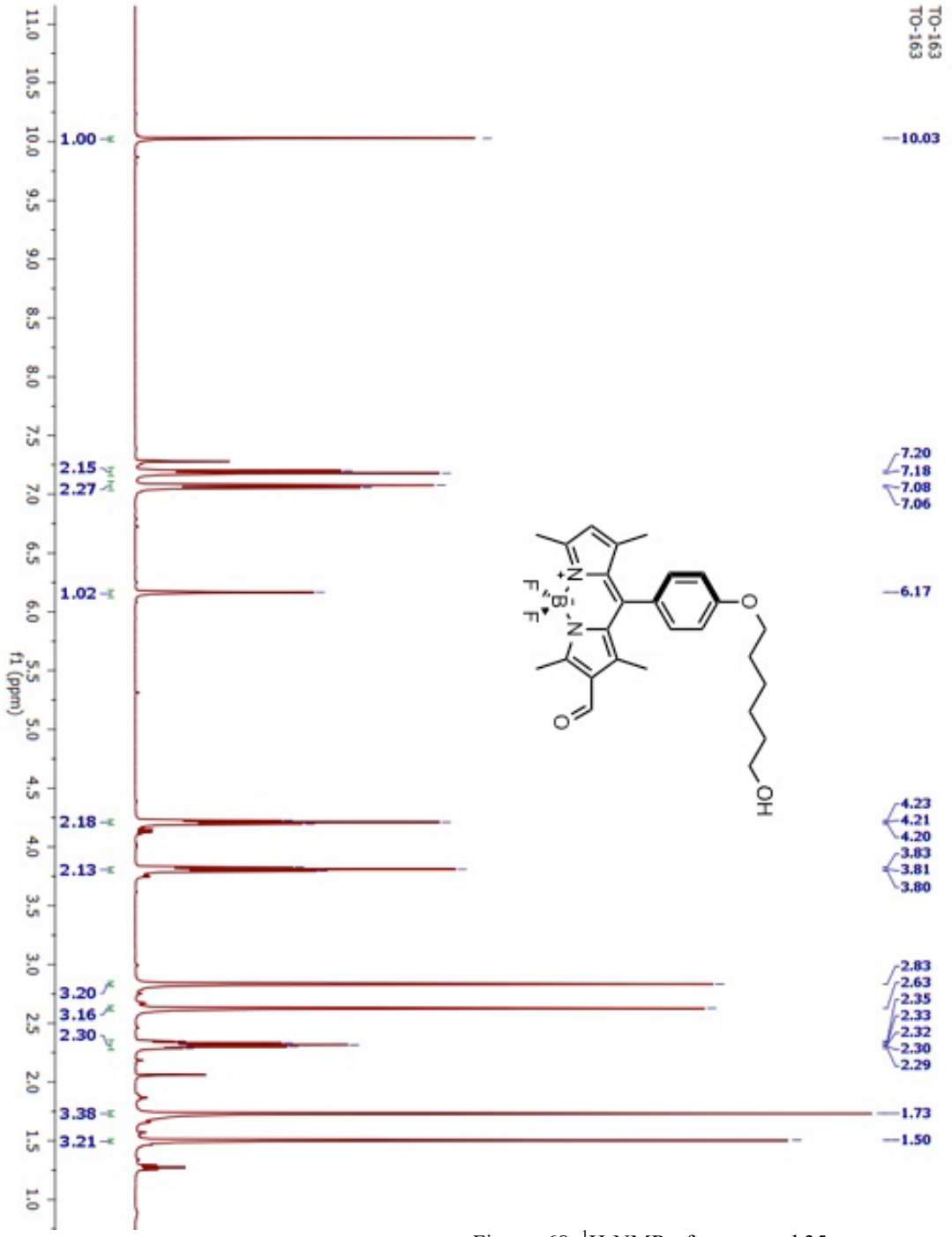

Figure 68. ^{1}H-NMR of compound 35

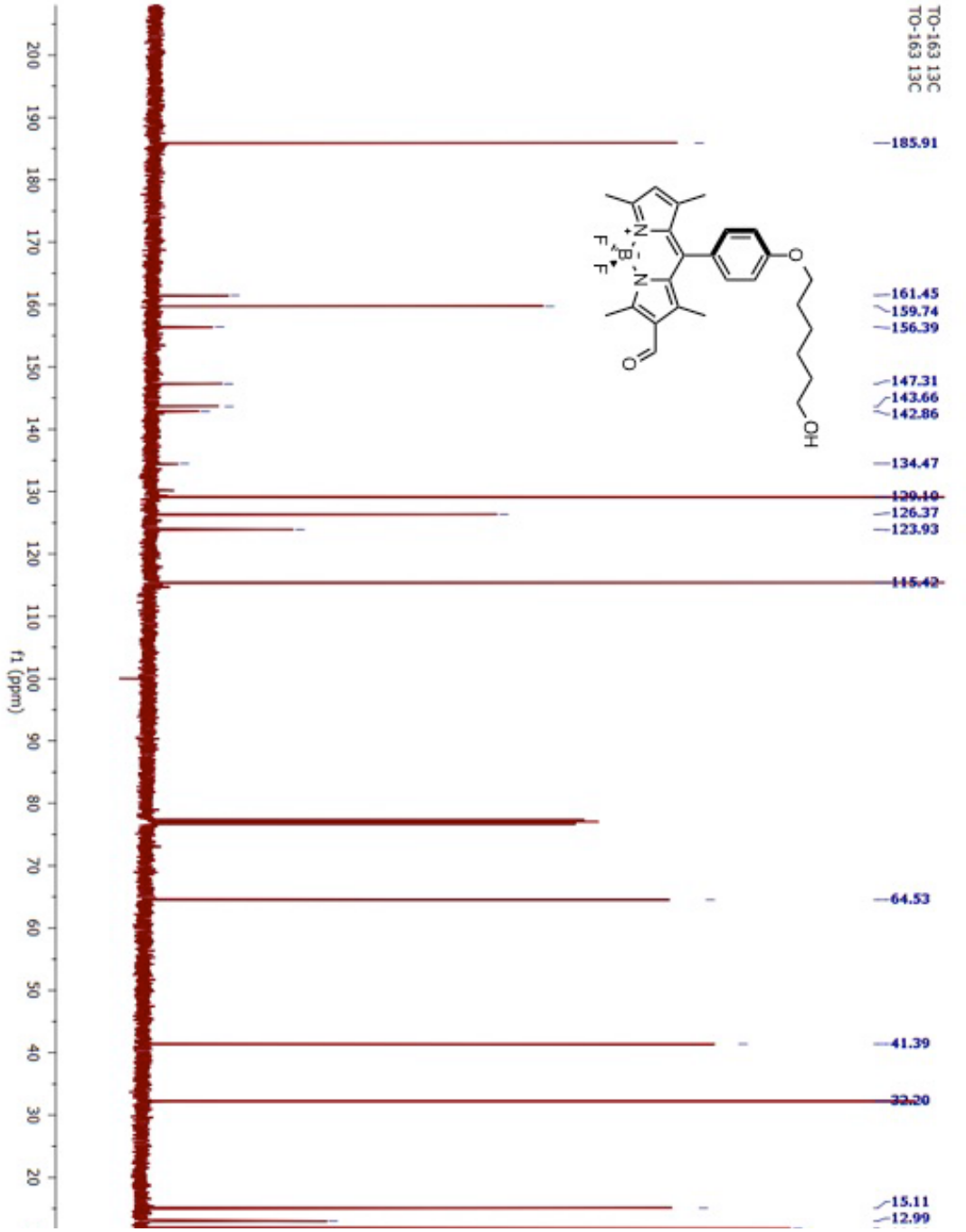

Figure 69. ^{13}C-NMR of compound 35

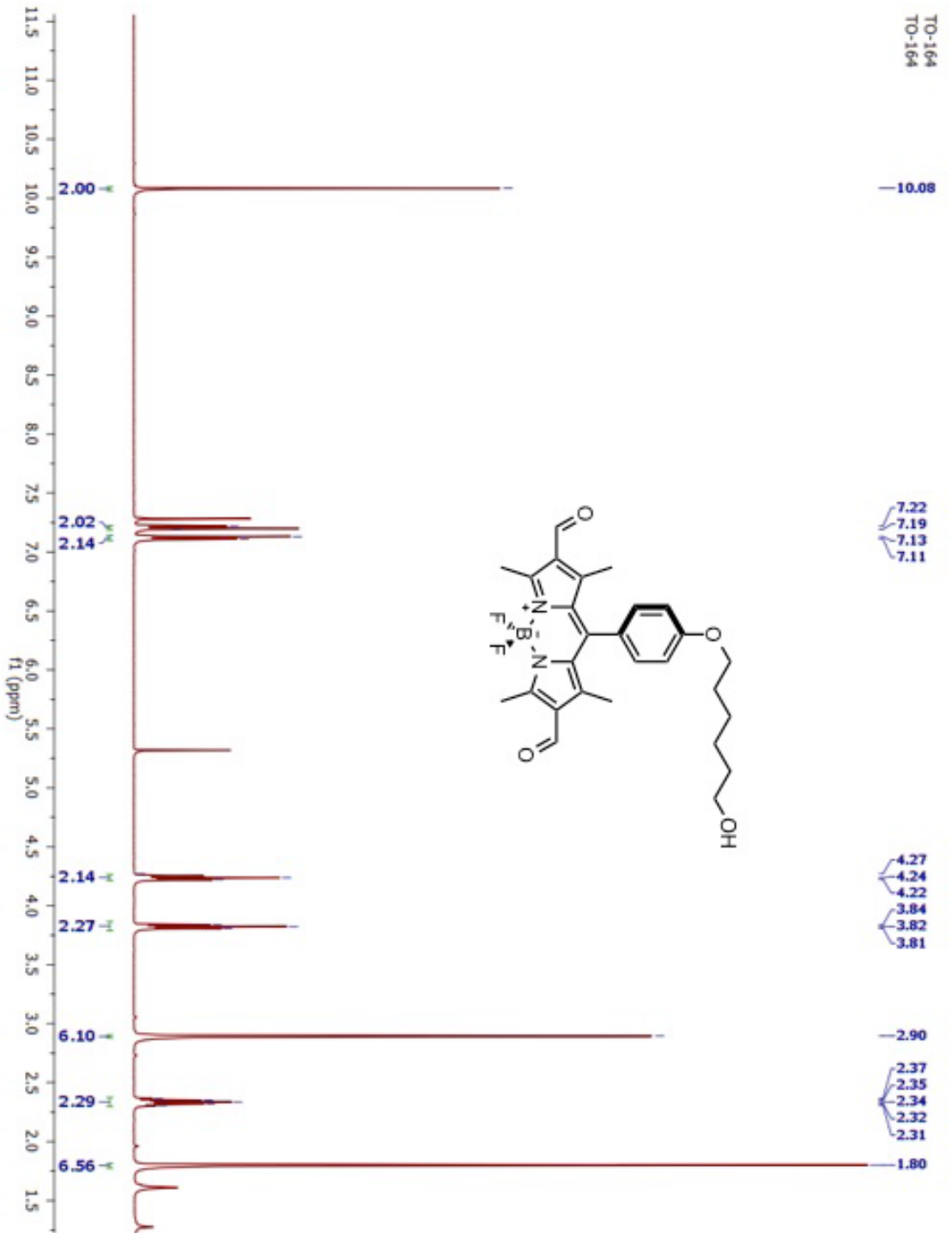

Figure 70. ^{1}H-NMR of compound 36

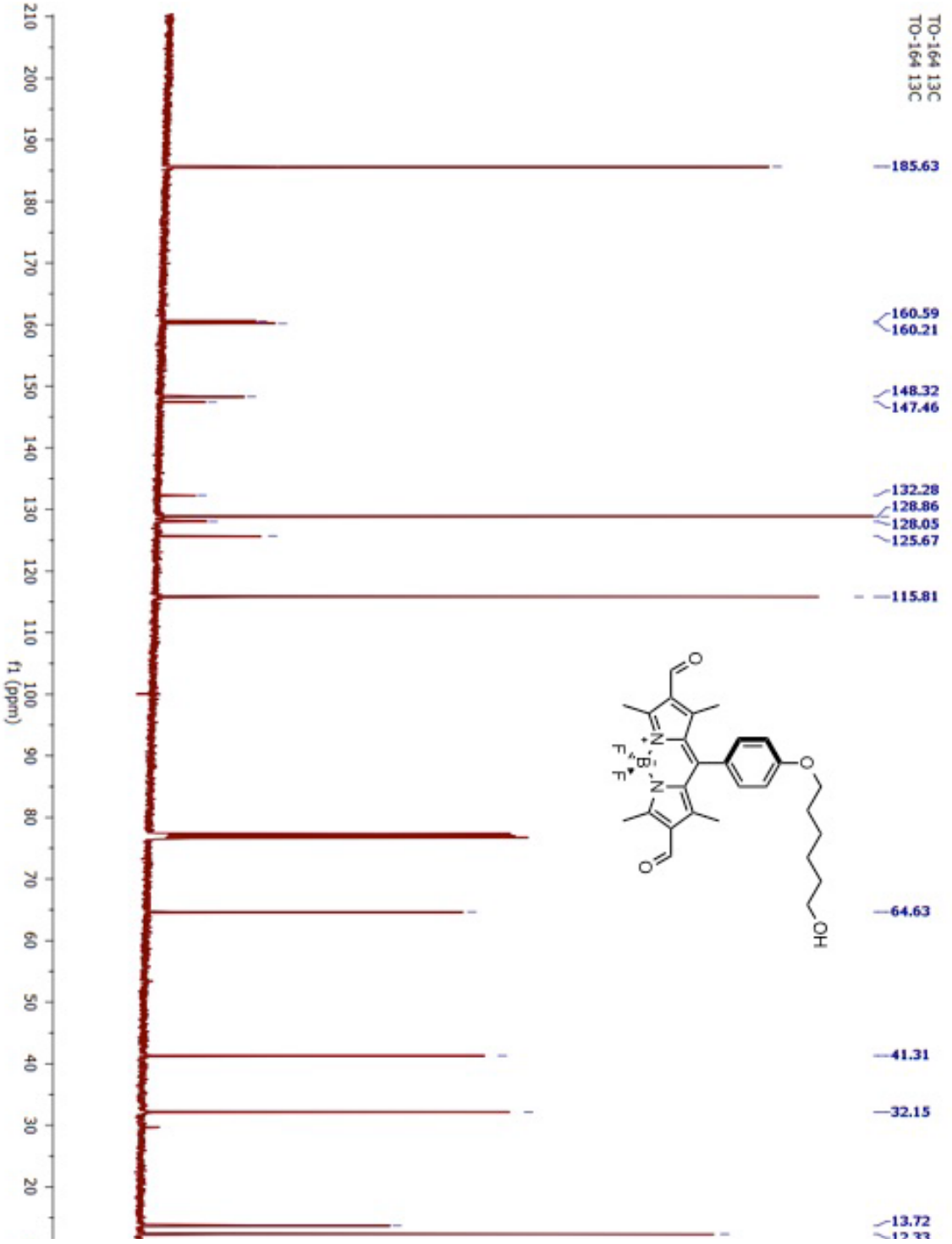

Figure 71. ^{13}C-NMR of compound 36

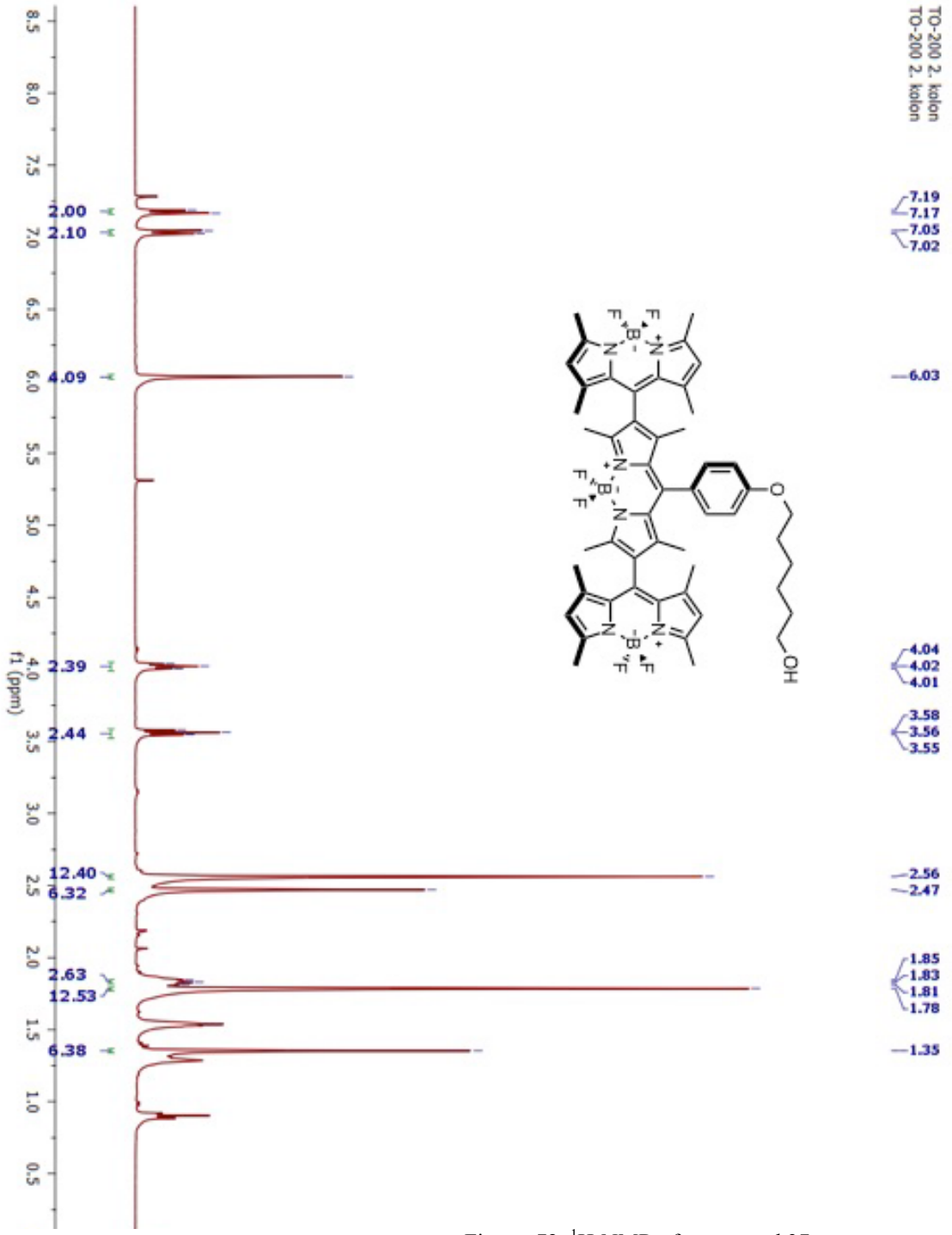

Figure 72. ^{1}H-NMR of compound 37

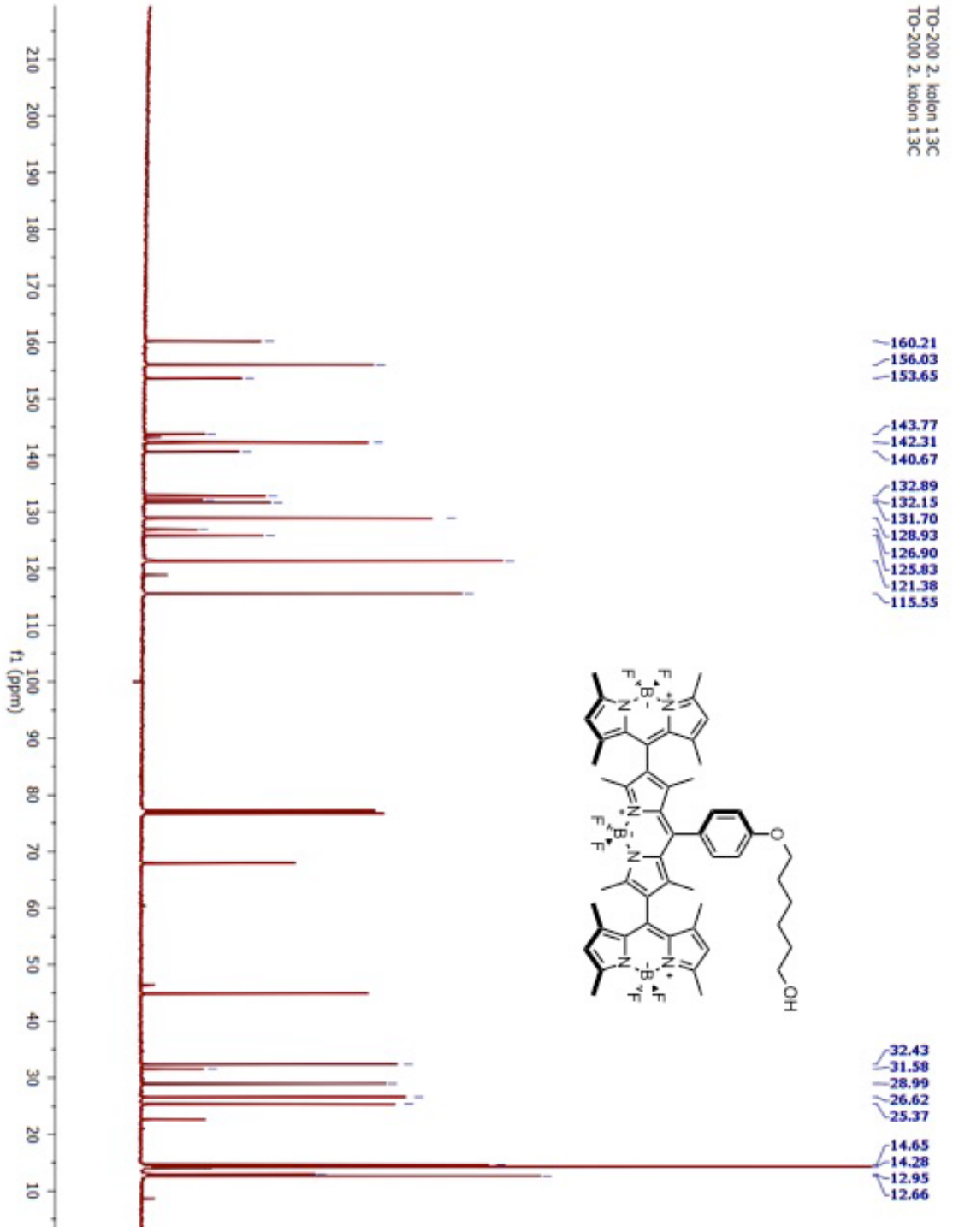

Figure 73. ^{13}C-NMR of compound 37

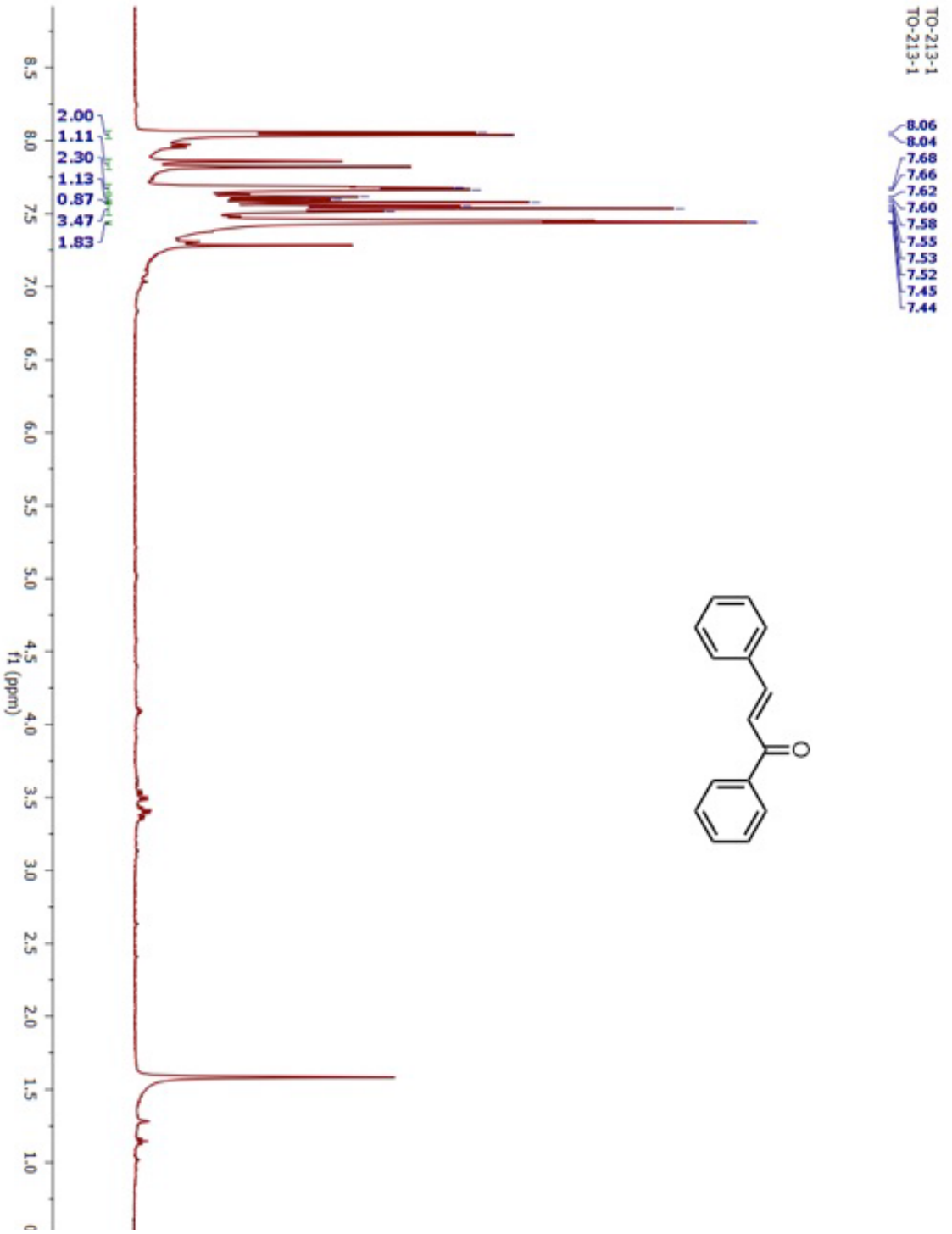

Figure 74. ^{1}H-NMR of compound 38

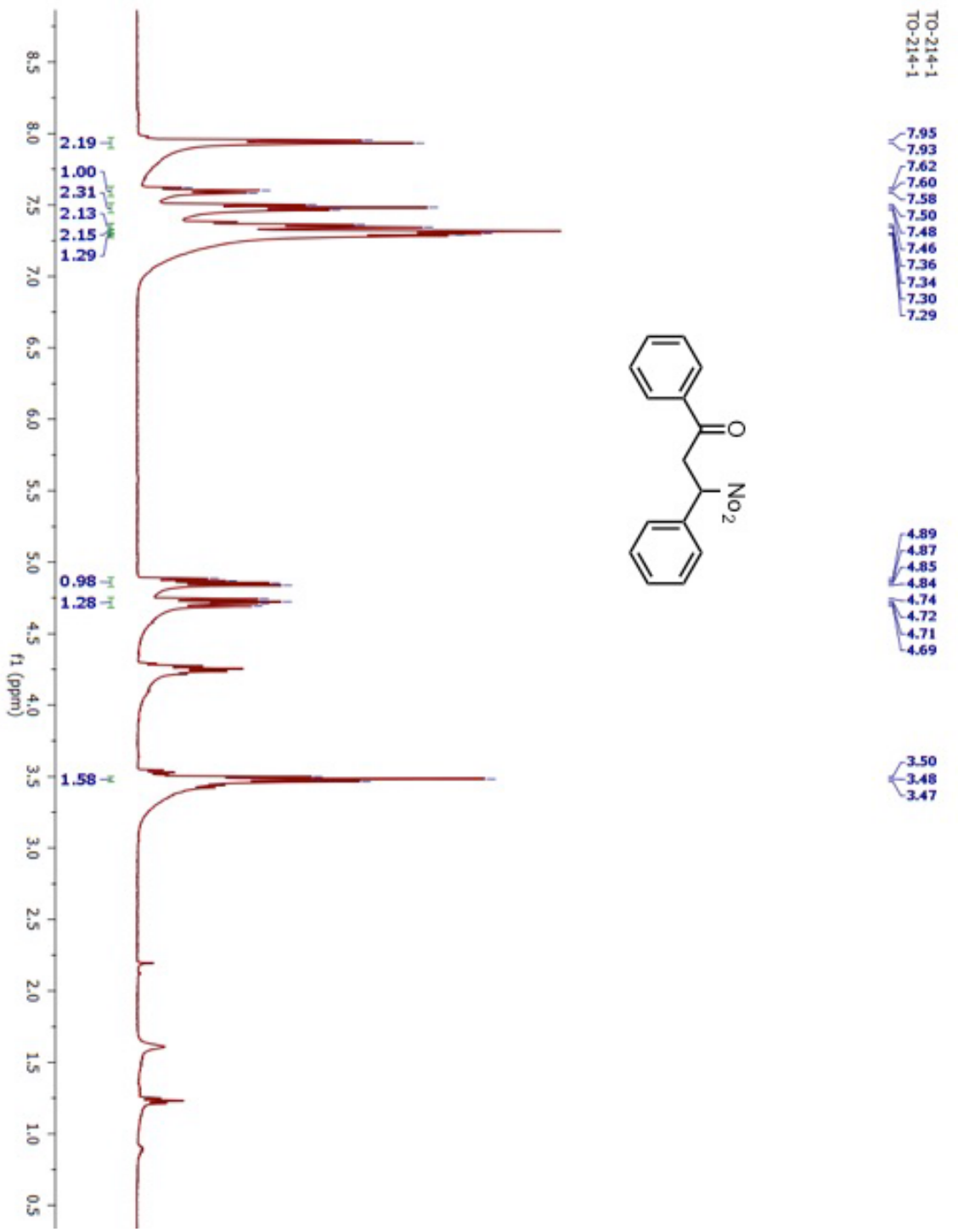

Figure 75. ^{1}H-NMR of compound 39

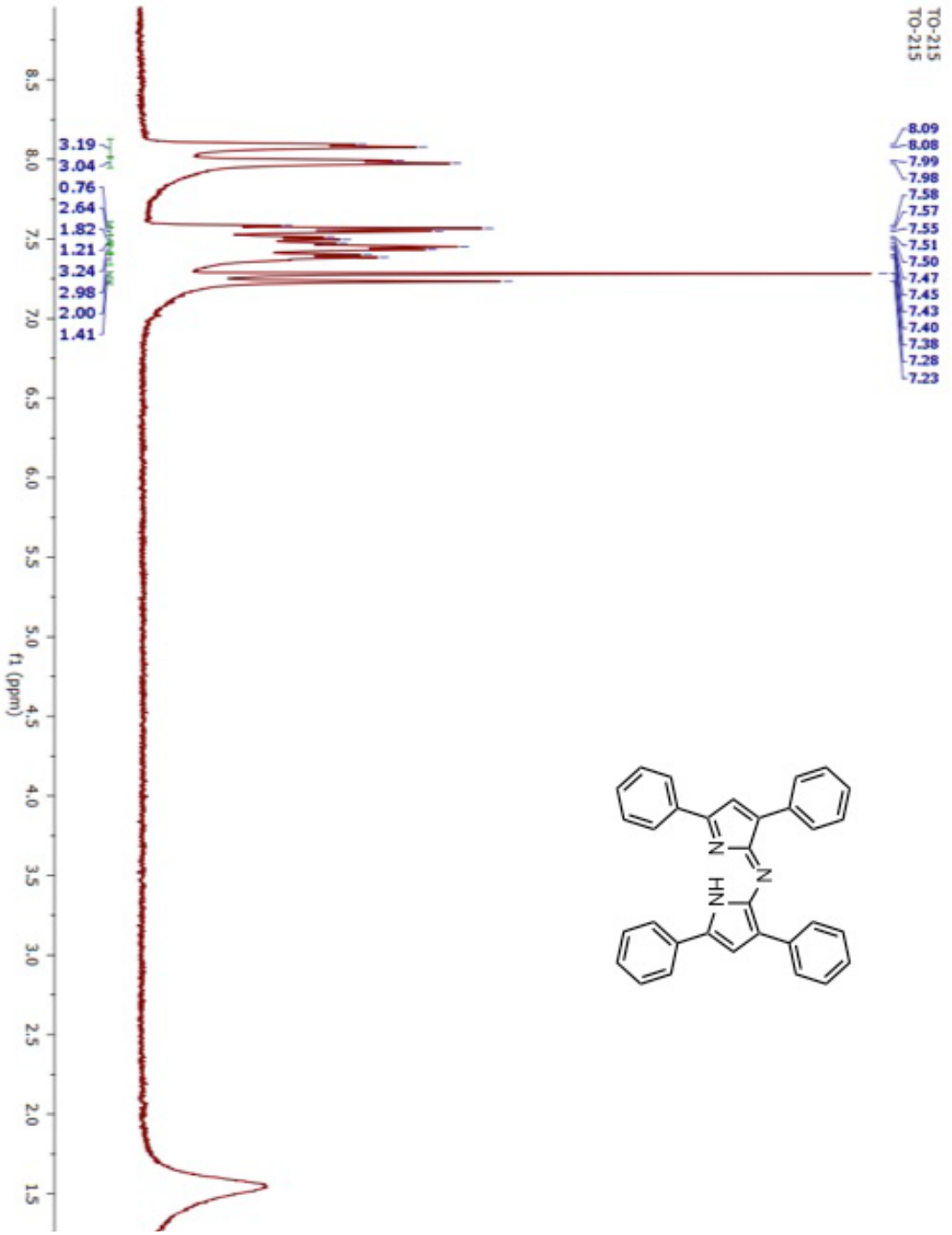

Figure 76. ^{1}H-NMR of compound 40

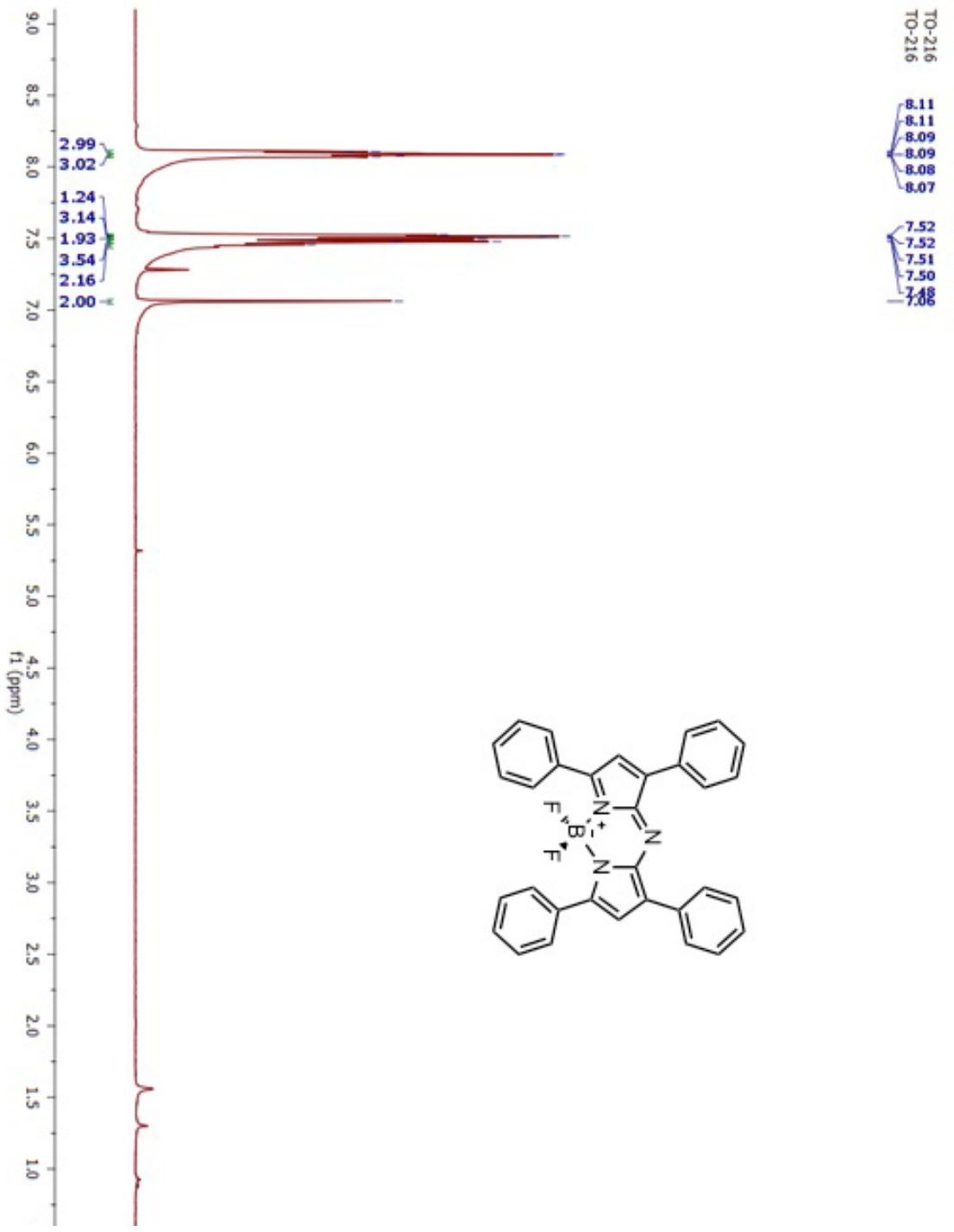

Figure 77. ^{1}H-NMR of compound 40

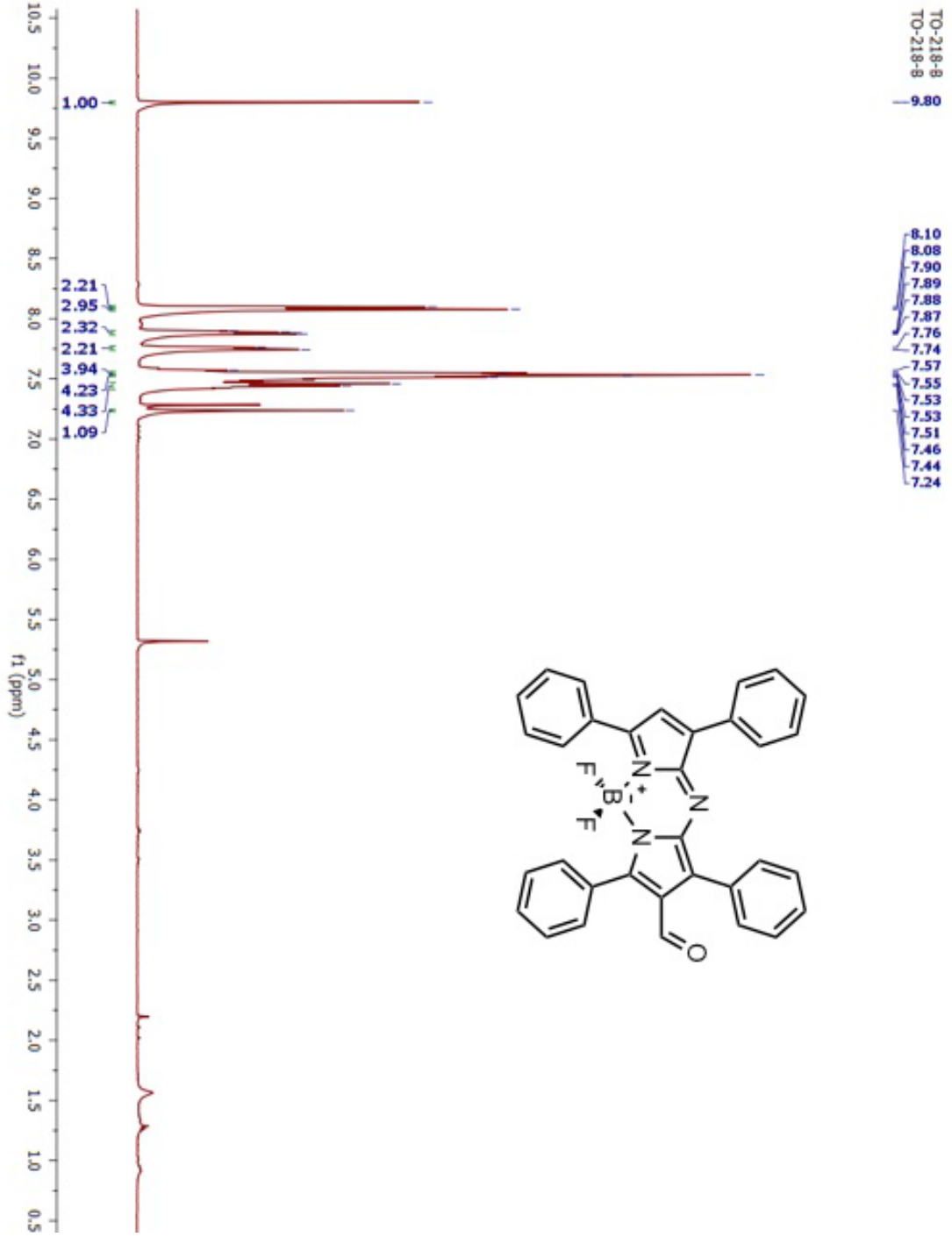

Figure 78. ^{1}H-NMR of compound 41

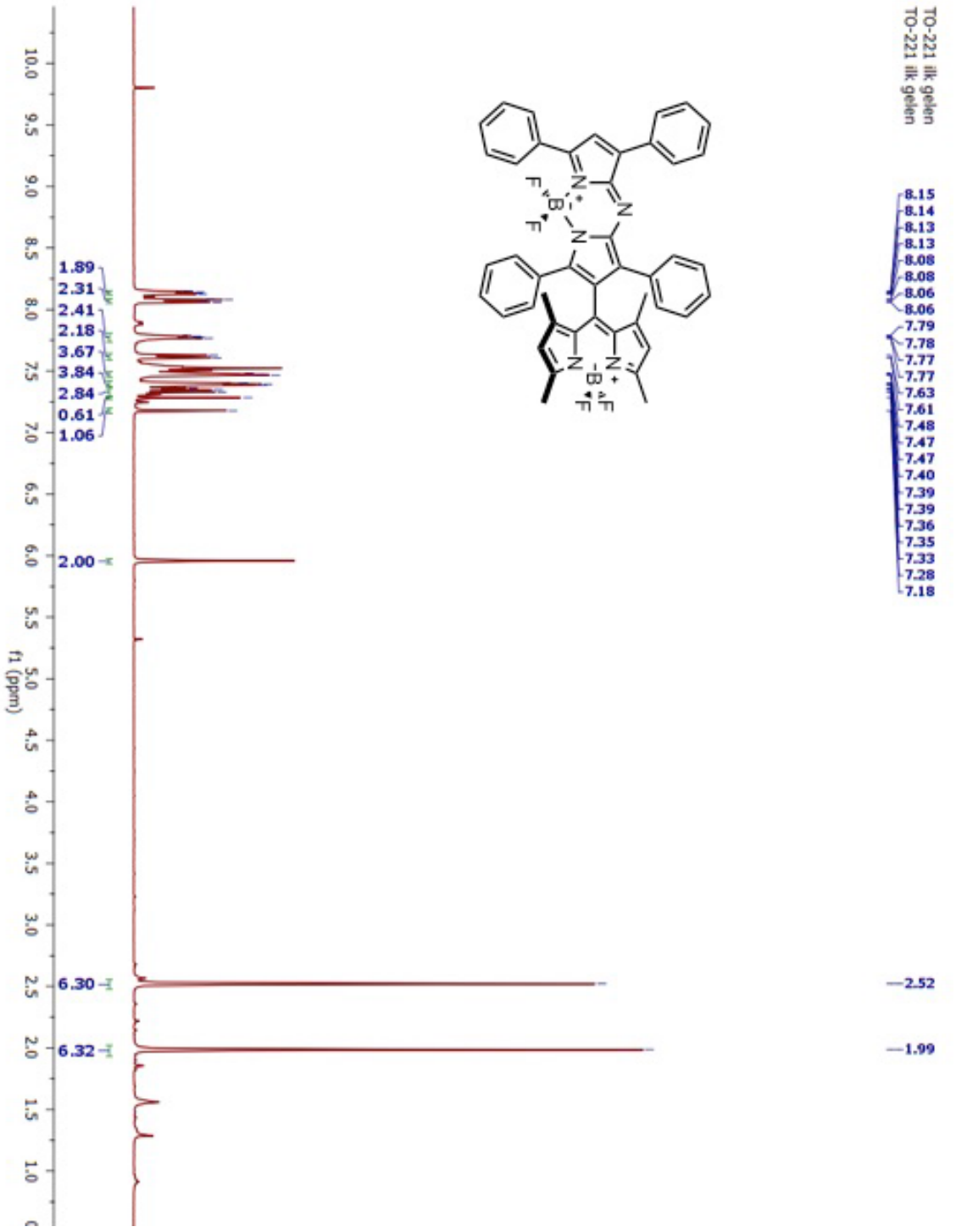

Figure 79. ^{1}H-NMR of compound 43

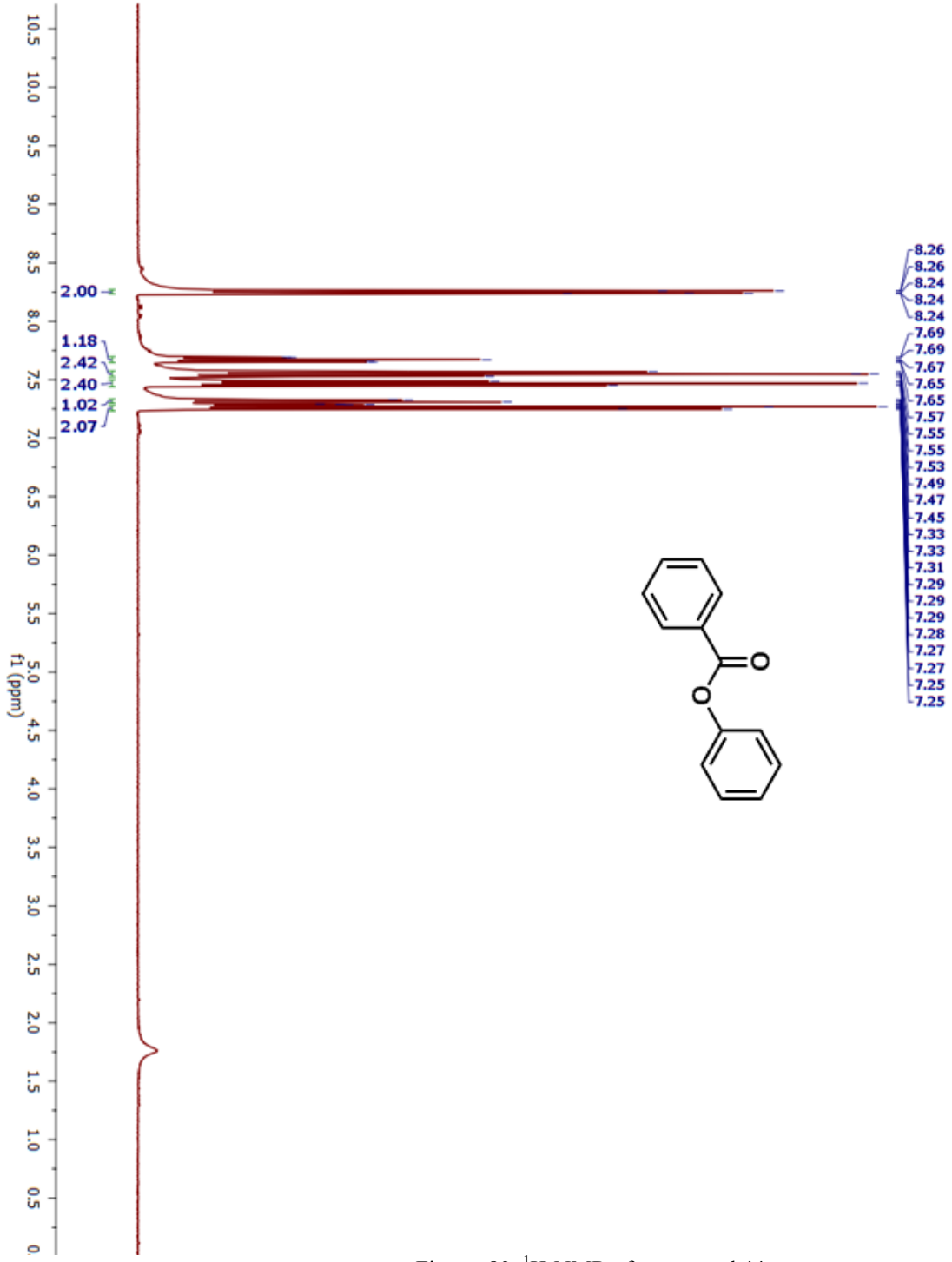

Figure 80. ^{1}H-NMR of compound 44

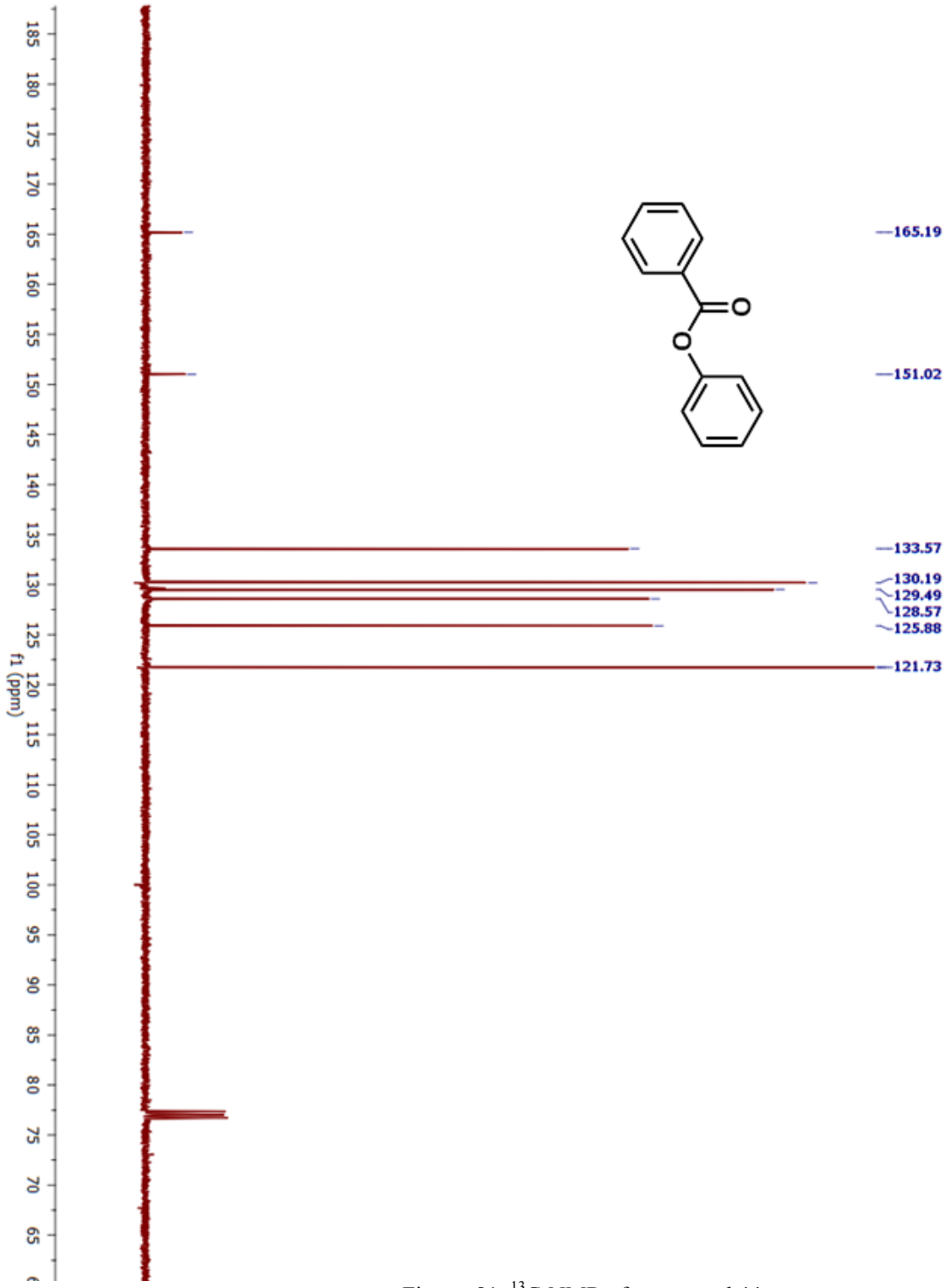

Figure 81. ^{13}C-NMR of compound 44

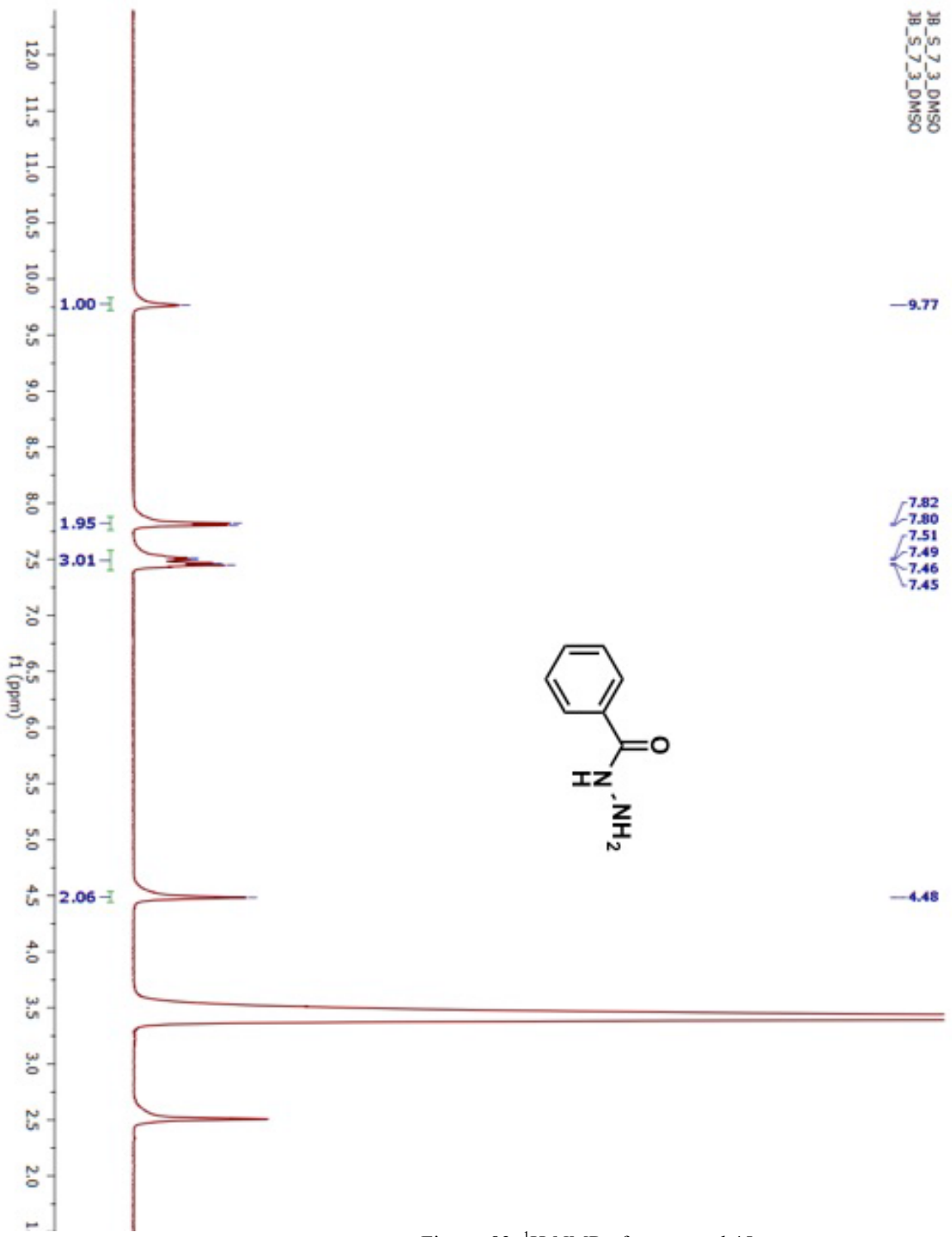

Figure 82. ^{1}H-NMR of compound 45

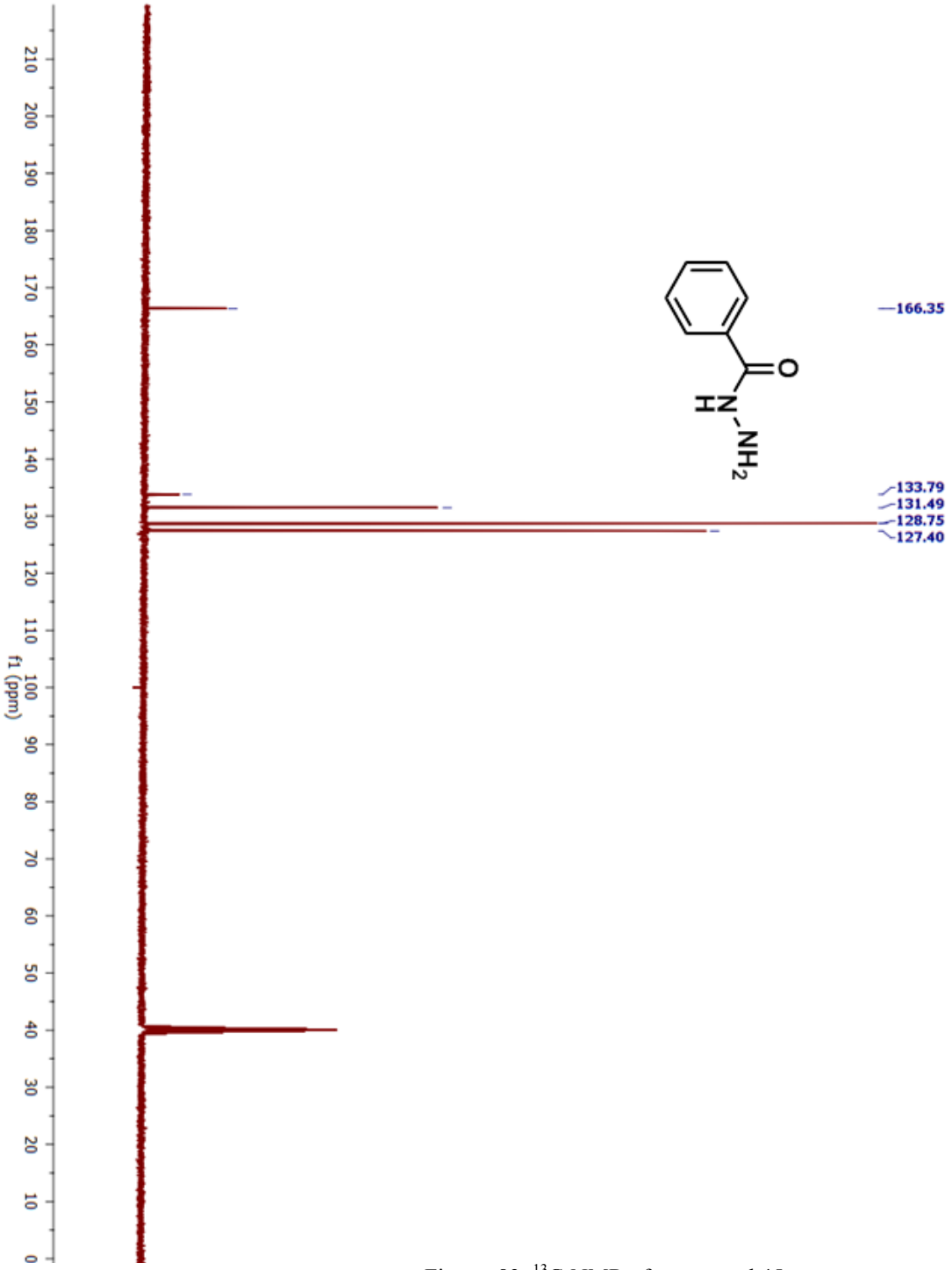

Figure 83. ^{13}C-NMR of compound 45

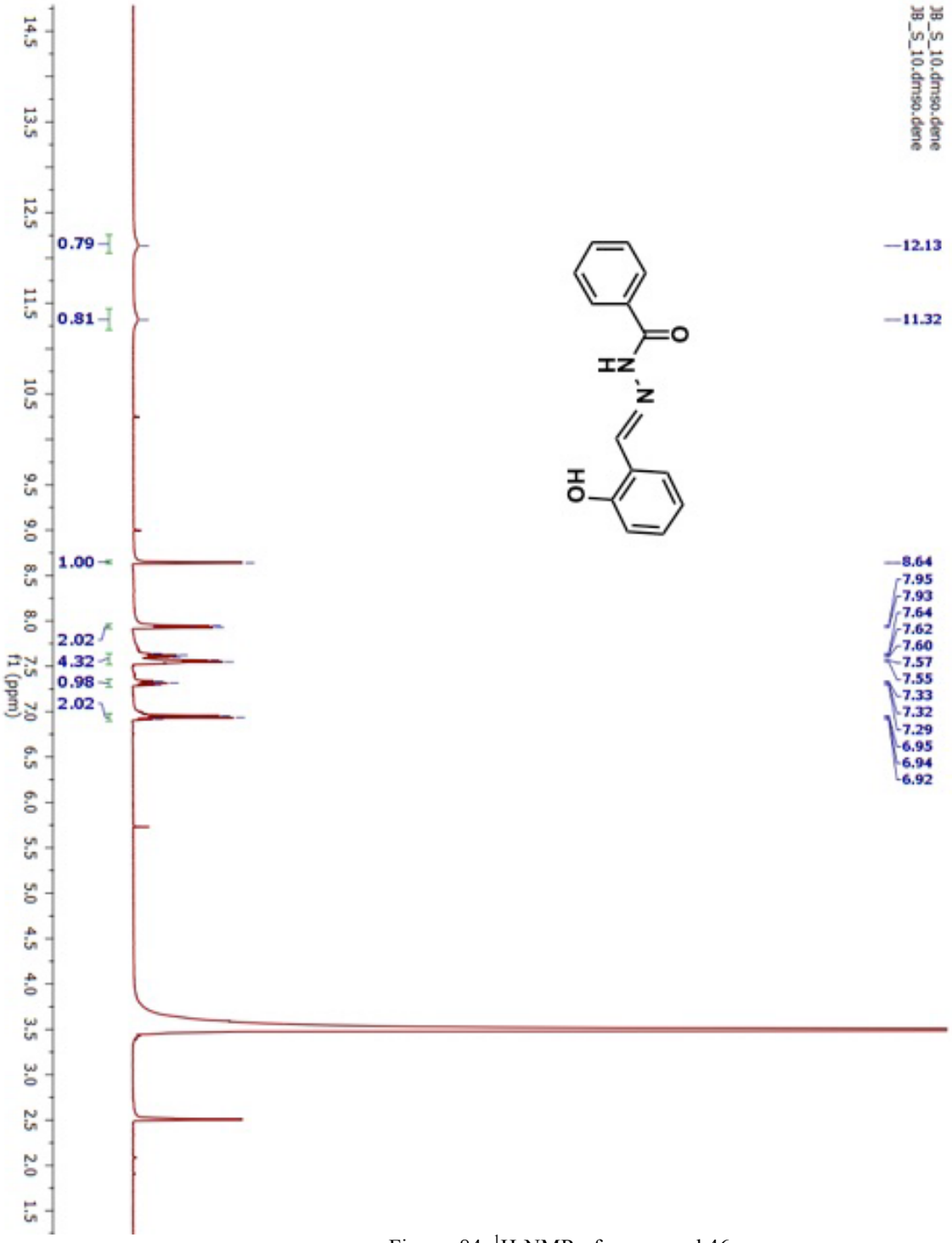

Figure 84. ^{1}H-NMR of compound 46

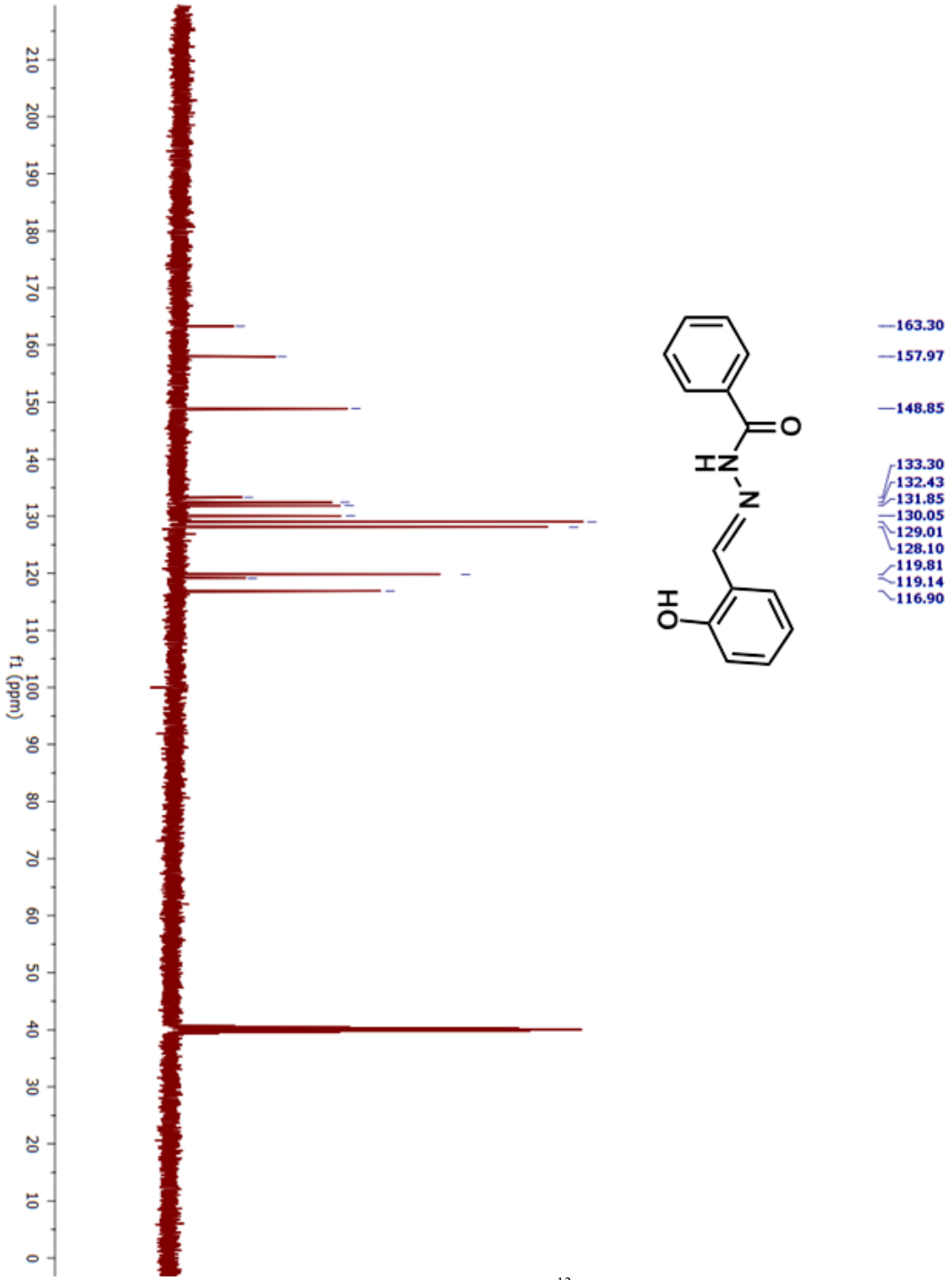

Figure 85. ^{13}C-NMR of compound 46

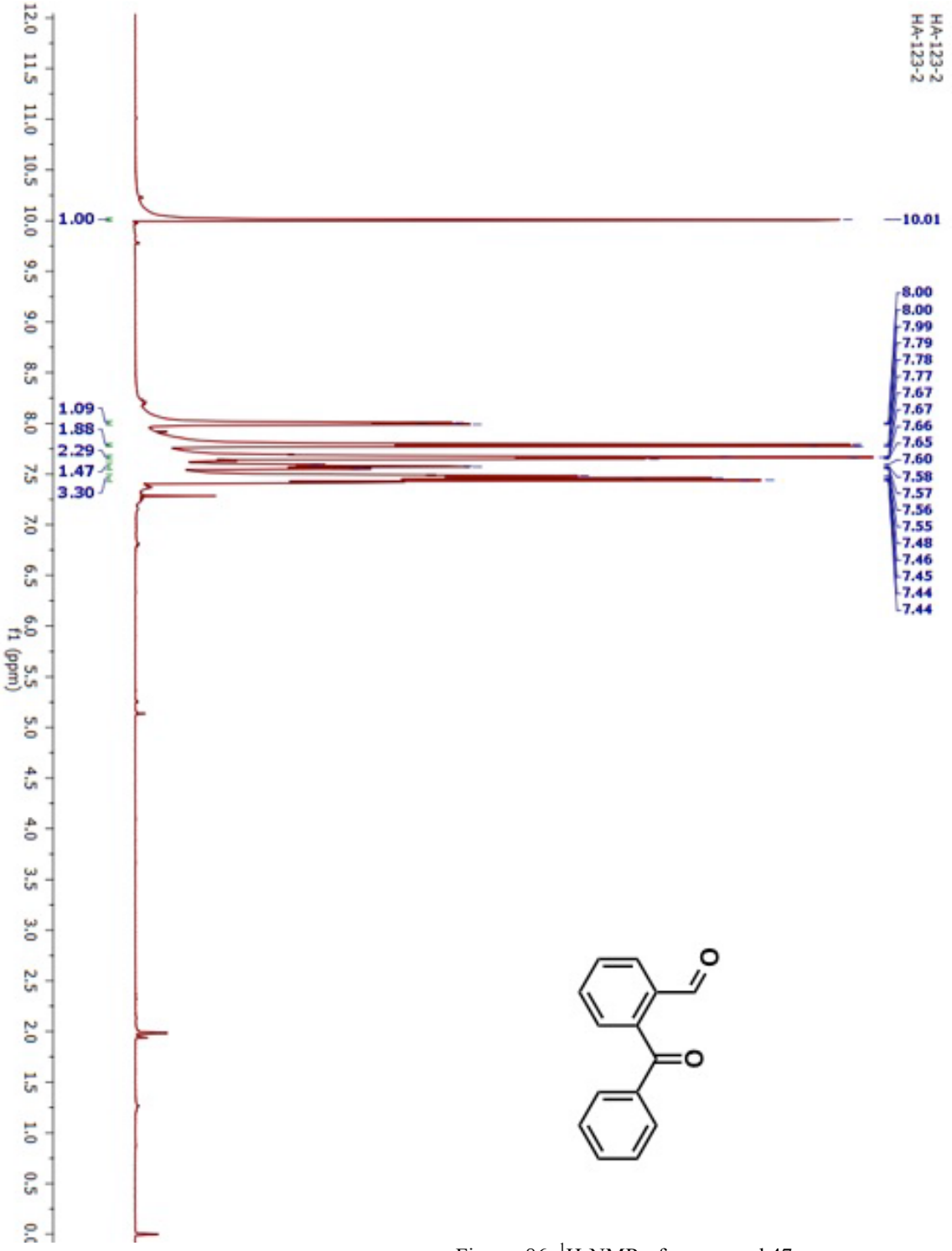

Figure 86. ^{1}H-NMR of compound 47

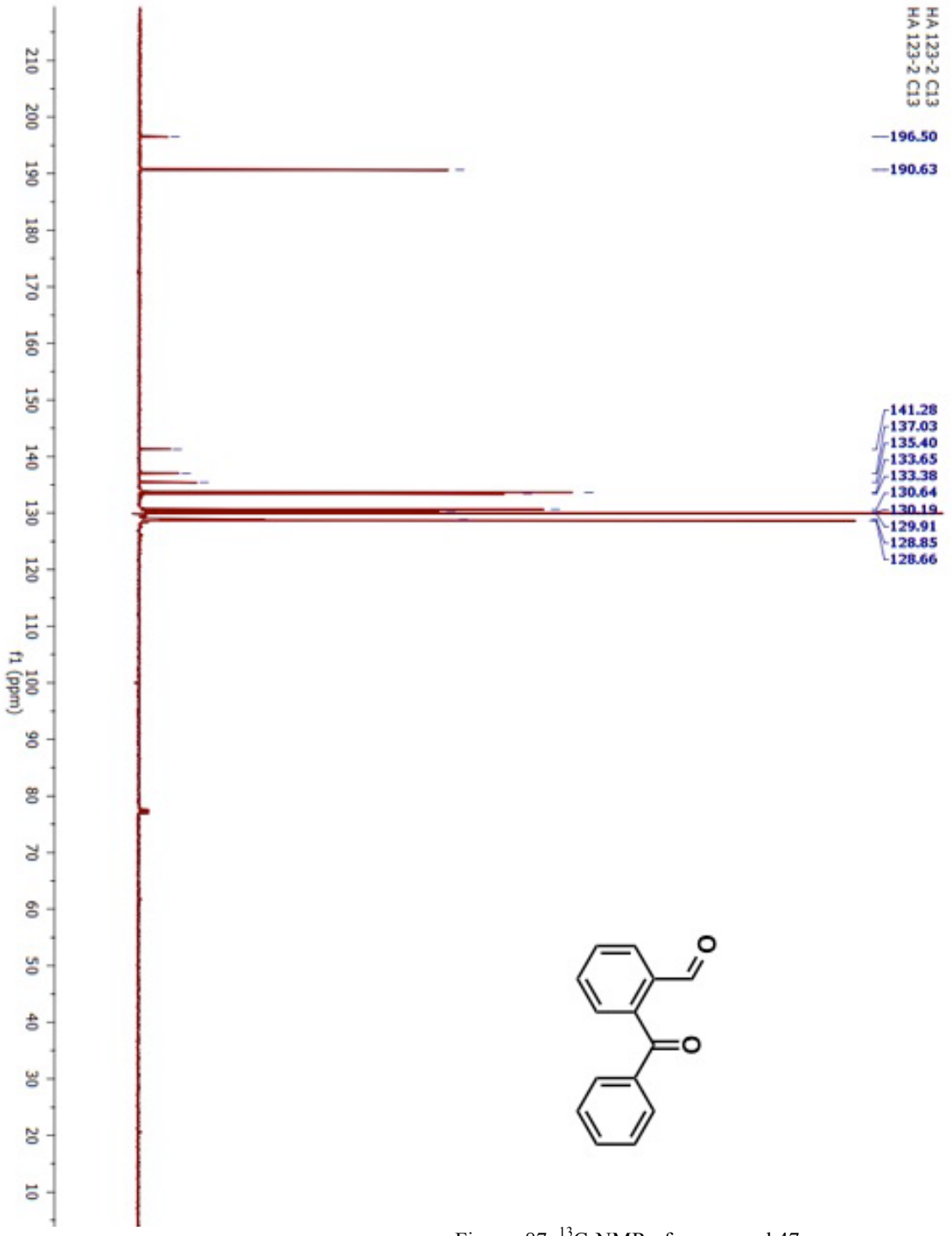

Figure 87. ^{13}C-NMR of compound 47

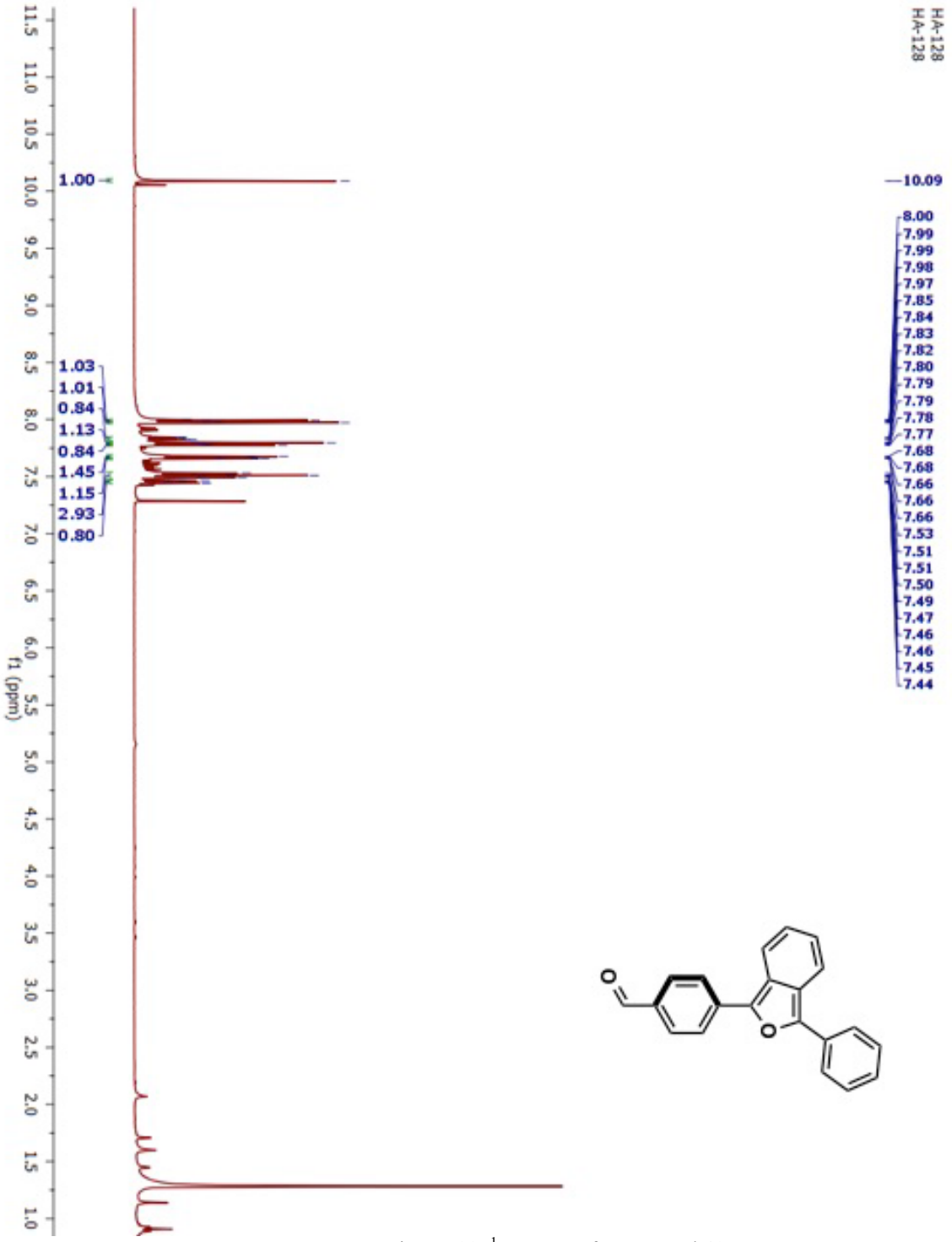

Figure 88. ^{1}H-NMR of compound 48

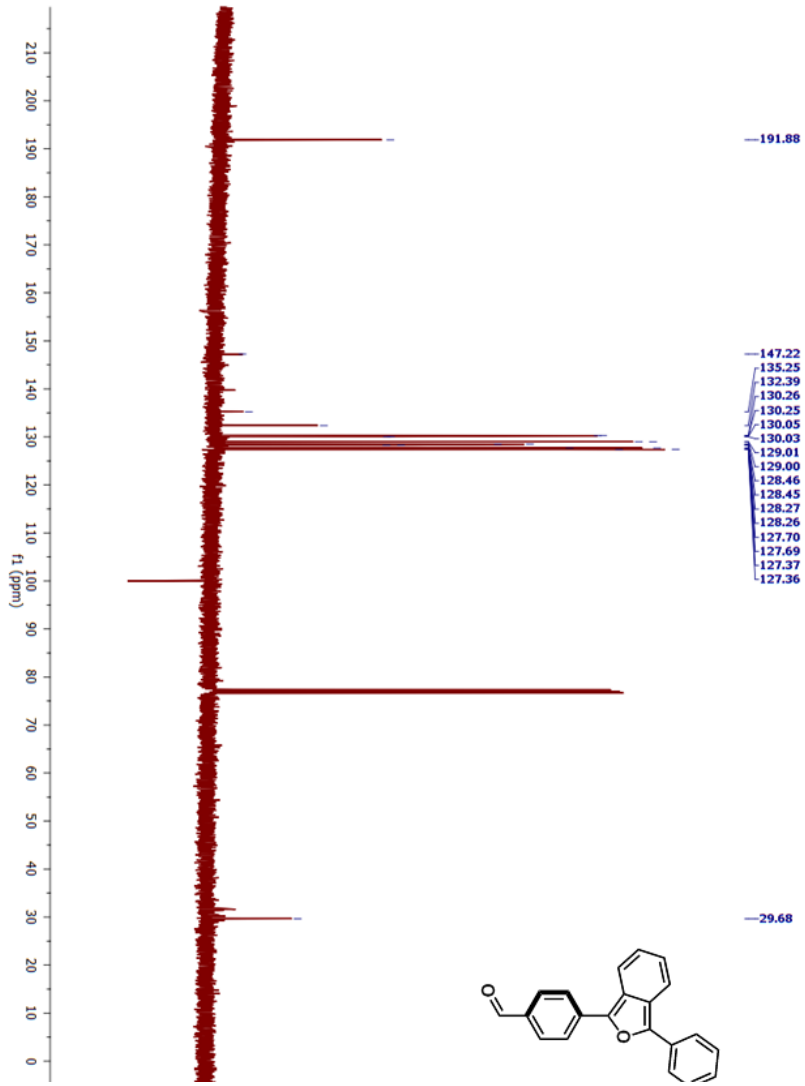

Figure 89. ^{13}C-NMR of compound 48

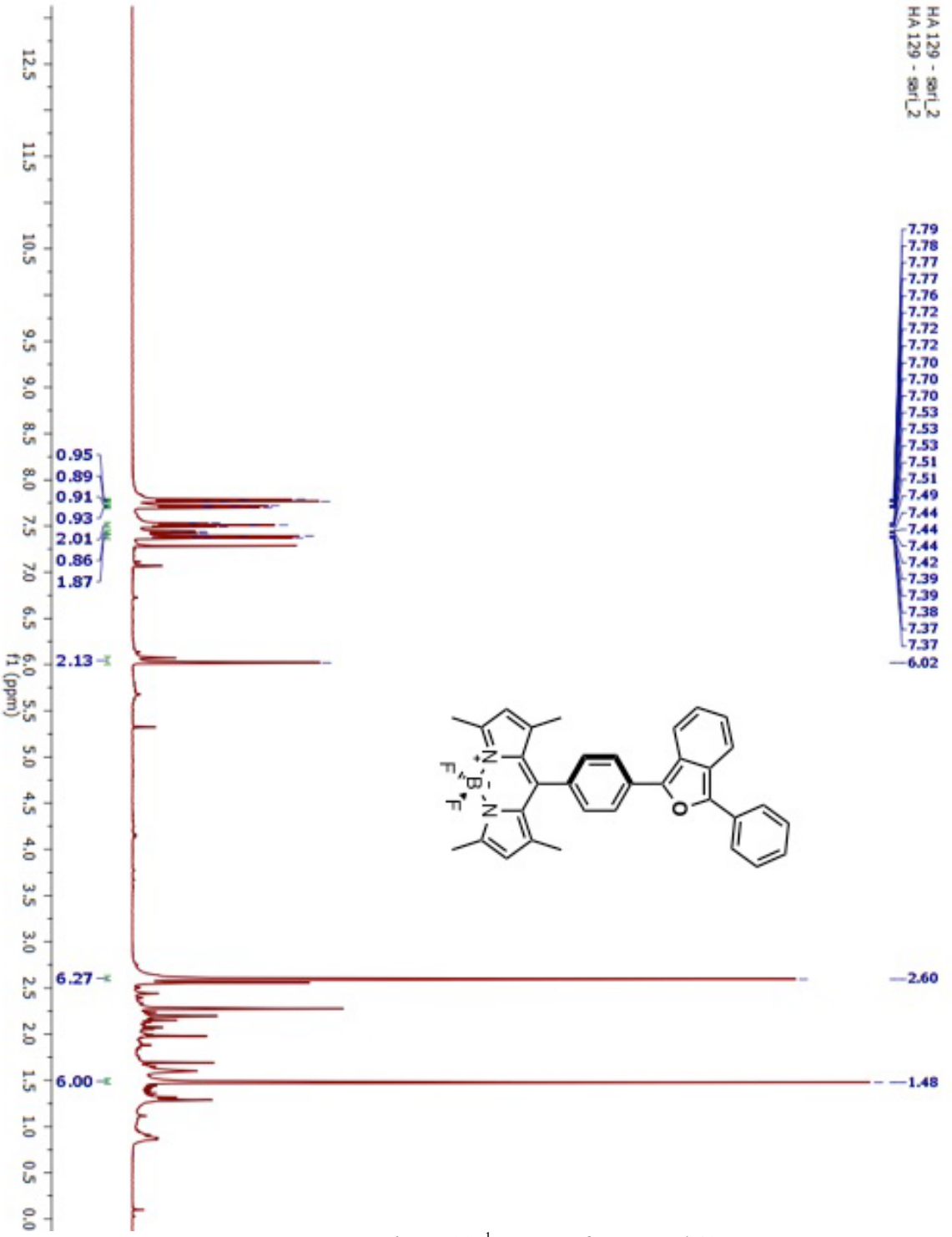

Figure 90. ^{1}H-NMR of compound 49

APPENDIX B MASS SPECTRA

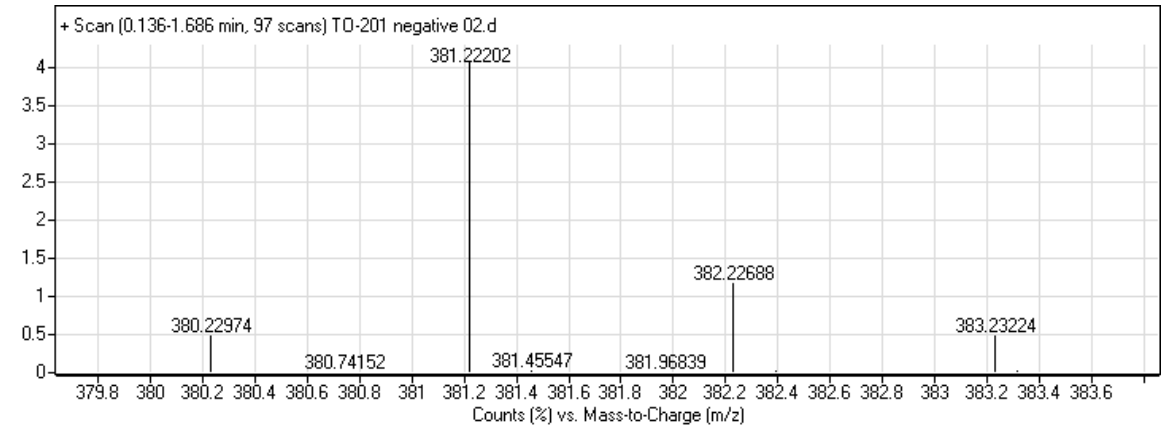

Figure 91. Mass spectrum of compound 30

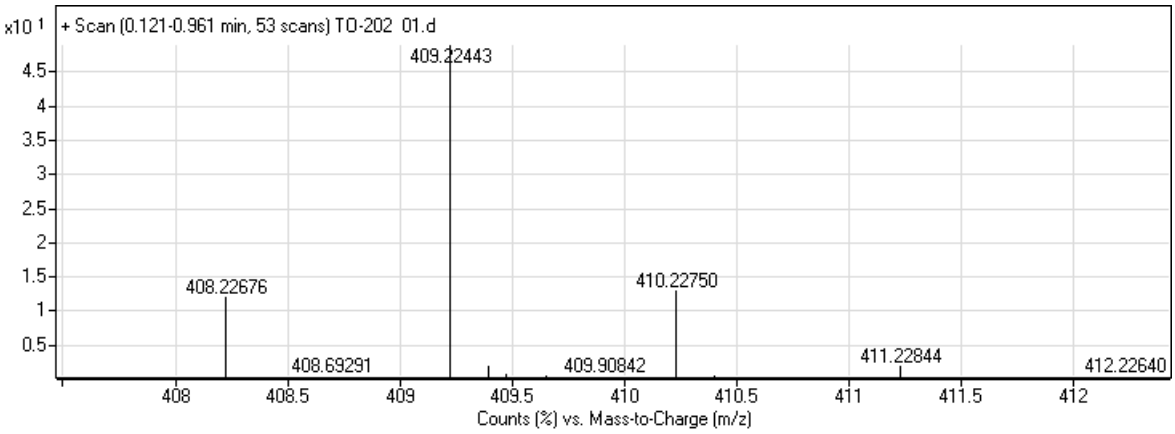

Figure 92. Mass spectrum of compound 31

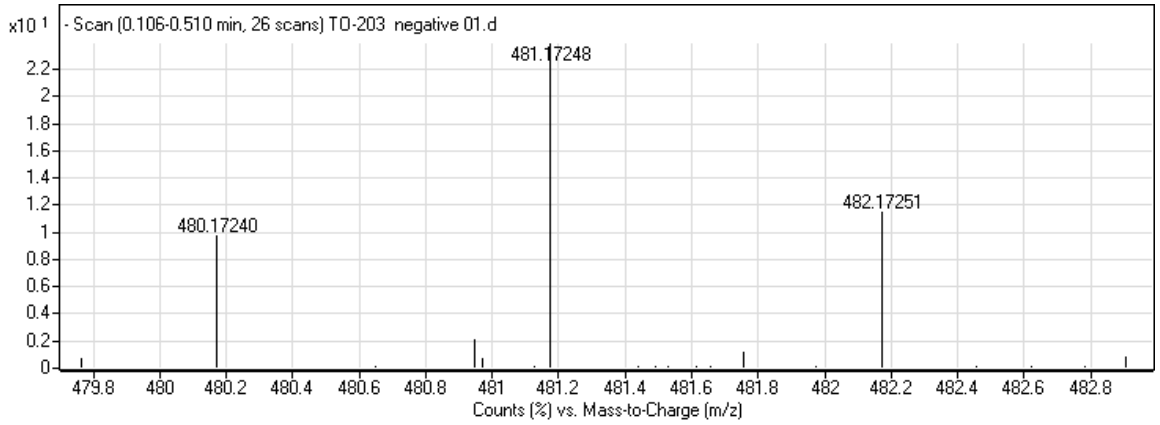

Figure 93. Mass spectrum of compound 32

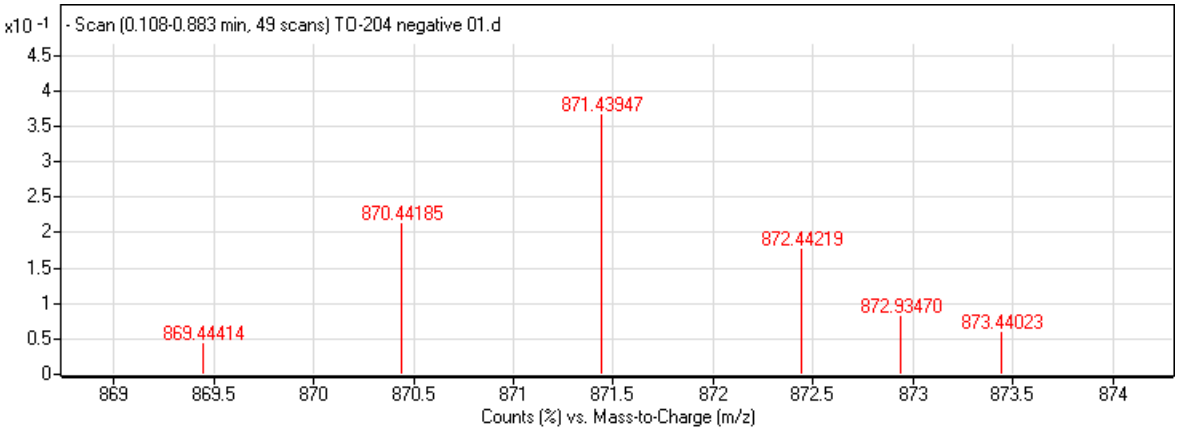

Figure 94. Mass spectrum of compound 33

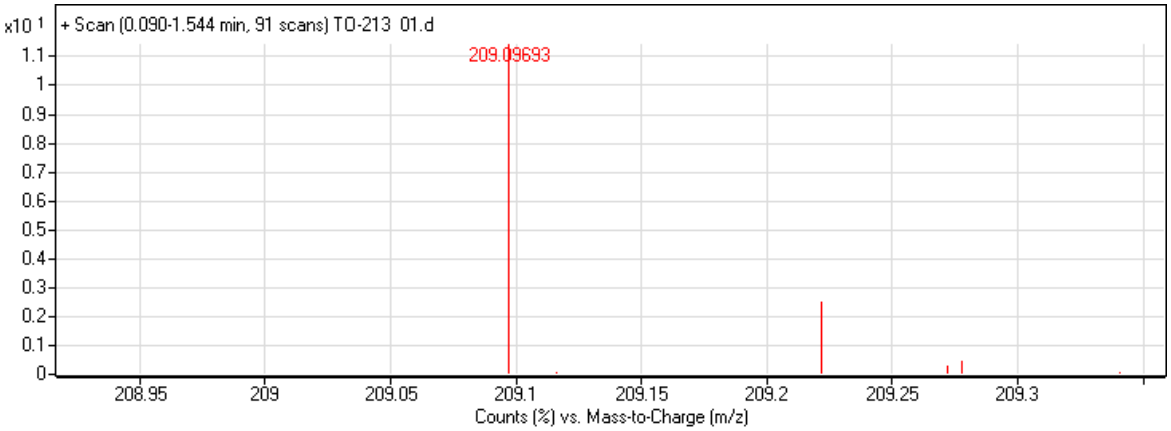

Figure 95. Mass spectrum of compound 38

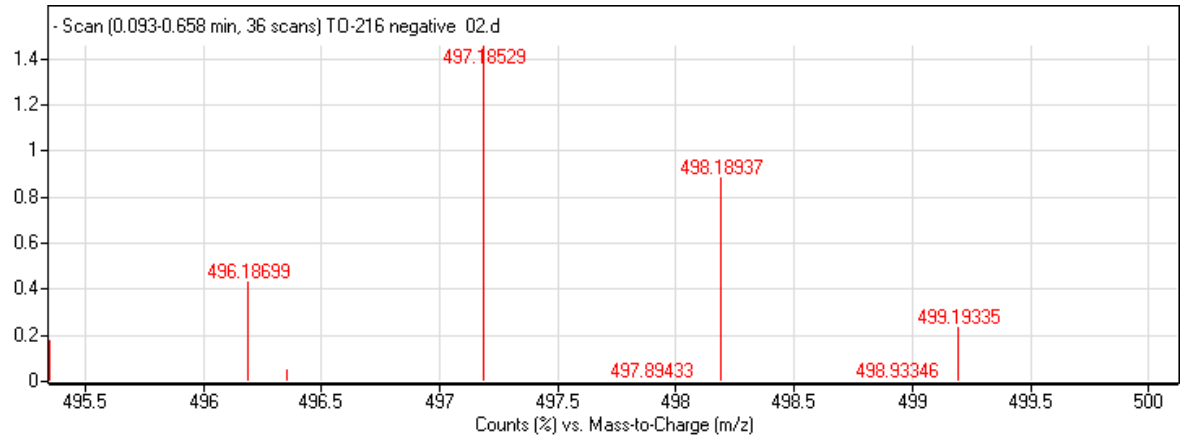

Figure 96. Mass spectrum of compound 42

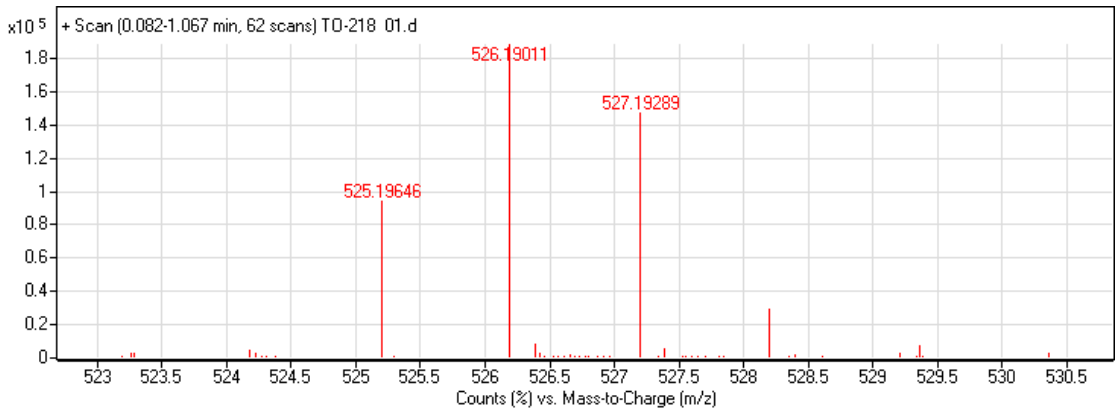

Figure 97. Mass spectrum of compound 41

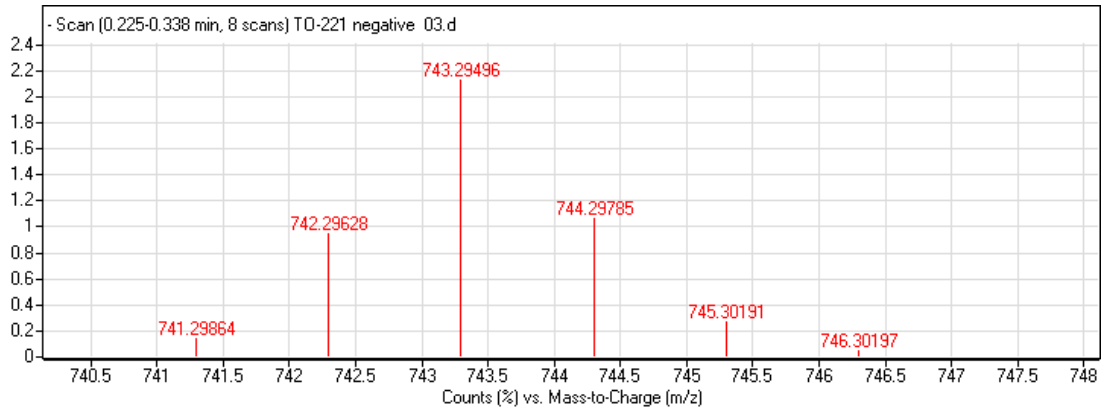

Figure 98. Mass spectrum of compound 43

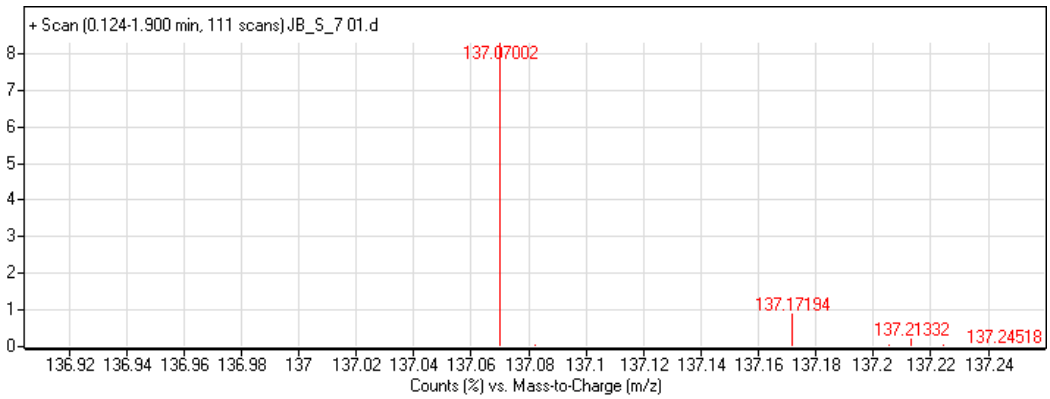

Figure 99. Mass spectrum of compound 45

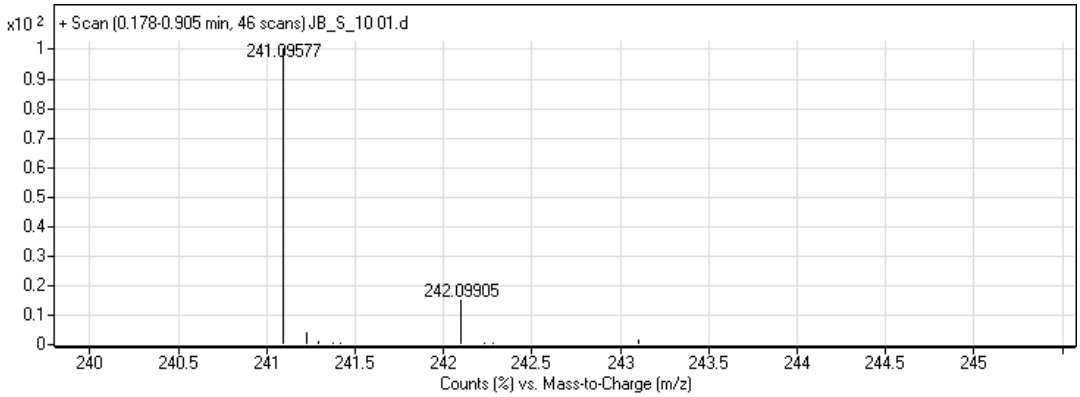

Figure 100. Mass spectrum of compound 46

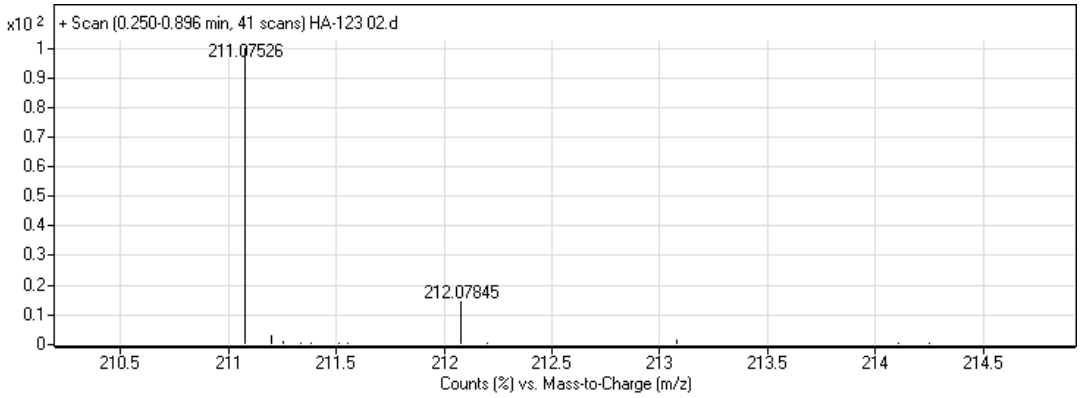

Figure 101. Mass spectrum of compound 47

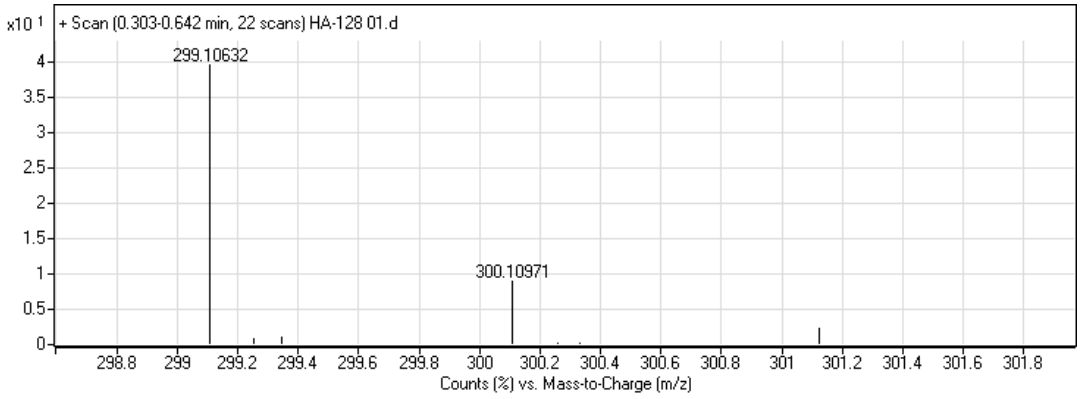

Figure 102. Mass spectrum of compound 48